# Chapter 13

# GEOTECHNICAL SEISMIC HAZARDS

## GEOTECHNICAL DESIGN MANUAL

*January 2022*

## Table of Contents

## List of Tables

## List of Figures

# CHAPTER 13

# GEOTECHNICAL SEISMIC HAZARDS

## 13.1 INTRODUCTION

The screening, identification, and evaluation of geotechnical seismic hazards at a project site are integral parts of geotechnical seismic engineering. The effects of these hazards must be taken into consideration during the design of geotechnical structures such as bridge foundations, ERSs, and embankments. Geotechnical seismic hazards can generally be divided into those that are associated with losses in soil shear strength and stiffness; seismic ground shaking (i.e., accelerations and inertial forces); and, seismic induced lateral ground movements and settlement. Losses in the soil shear strength in South Carolina are primarily due to cyclic liquefaction of loose cohesionless soils and secondarily due to cyclic softening of plastic cohesive soils. Seismic accelerations and inertial forces can create instability due to increased driving forces as a result of increased static active soil pressures. Seismic induced lateral ground movement can occur in sloping ground conditions where the increased driving forces can exceed the soil shear strength. Seismic settlement can be either the result of cyclic liquefaction of cohesionless soils or densification/compression of unsaturated soils and compacted fill materials.

The procedures for analyzing soil Shear Strength Loss (SSL) and associated geotechnical seismic hazards such as flow slide failure and seismic slope instability are provided in this Chapter. Methods of computing horizontal seismic accelerations based on peak ground accelerations (PGA) and seismic displacements are also provided in this Chapter. Finally, procedures for evaluating seismic settlement due to either cyclic liquefaction or densification/compression of unsaturated and saturated soils are presented in this Chapter. Methods of computing seismic active and passive soil pressures on ERSs and bridge abutments are provided in Chapter 14.

SCDOT recognizes that the methods presented in this Manual may not be the only methods available, particularly since geotechnical seismic engineering is developing at a very rapid pace as seismic events around the world contribute to the study and enhancement of analytical methods for geotechnical seismic hazard evaluation. Because geotechnical seismic engineering in South Carolina (and CEUS) is at the very early stages of development, the overall goal of this Chapter is to establish a state-of-practice that can evolve and be enhanced as methodologies improve and regional (CEUS) experience develops. Methods other than those indicated in this Manual may be brought to the attention of the OES/GDS for consideration on a specific project or for consideration in future updates of this Manual.

Geotechnical seismic hazards such as fault rupturing and flooding (tsunami, seiche, etc.) are not addressed in this Chapter since current views suggest that the potential for these types of hazards in the CEUS is very low. If there is any evidence of faults traversing a project site that have been active within the Holocene epoch (10 thousand years ago to present day) it should be brought to the attention of the OES/GDS.

South Carolina geology and seismicity, discussed in Chapter 11, will have a major impact on the evaluation of soil SSL and should be well understood when evaluating geotechnical seismic hazards. Seismic shaking parameters will have a direct effect on the amount and extent of the

deformations caused by geotechnical seismic hazards. Seismic shaking parameters such as the $M_w$, R, $D_{a5\text{-}95}$, PGV, and PGA must be determined based on the design seismic event (FEE or SEE) under evaluation as described in Chapter 12. Geotechnical seismic hazards that may affect the design of transportation structures are described in the following Sections and analytical methods are presented to evaluate the potential for, and magnitude of displacement. The effects of geotechnical seismic hazards on the geotechnical design of bridge foundations, abutment walls, ERSs, and other miscellaneous structures are discussed in Chapter 14.

## 13.2 GEOTECHNICAL SEISMIC HAZARD FAILURE MODES

In order to evaluate the potential for the various geotechnical seismic hazards to occur at a project site, it is important to understand the various modes of failure that have been documented through case histories. Geotechnical seismic hazard modes of failure can be generally categorized as: Seismic Acceleration Hazards (seismic stability) or Global Hazards (flow failure). These geotechnical seismic hazard categories are discussed in the following Sections and are also summarized in Table 13-1.

**Seismic Stability** - Instability due to seismic inertial driving forces and static gravitational driving forces either with or without soil SSL.

**Flow Failure** - Instability due to static gravitational driving forces and soil SSL without seismic inertial driving forces.

**Table 13-1, Global Hazard Instability Cases**

| Contributors to Instability | Instability Types | | |
|---|---|---|---|
| | Seismic Stability | | Flow Failure |
| Seismic Inertial Driving Forces | X | X | N/A |
| Static Gravitational Driving Forces | X | X | X |
| Soil SSL | N/A | X | X |

### 13.2.1 Seismic Acceleration Hazards

Seismic Acceleration Hazards consist of seismically-induced global instability and lateral spreading that can occur at bridge abutments, roadway embankments, bridge approach fills, natural cut slopes, and at ERSs. This geotechnical seismic hazard occurs as a coherent sliding soil mass (assumes that soil mass stays together as a block) moves along a critical shear failure surface. The triggering mechanism for slope instabilities is the seismic horizontal acceleration that induces inertial driving forces in addition to the initial static driving stresses that already exist within the slope. Lateral spreading is caused by a combination of seismic inertial driving forces, static gravitational driving stresses and soil SSL. Lateral spreading will typically end once the seismic inertial driving forces cease. Typically seismic instability failures are characterized by translational or rotational slope failure that occurs during seismic shaking and are evaluated using conventional limit-equilibrium pseudo-seismic slope stability methods with appropriate soil shear strengths (accounting for soil SSL) and seismic acceleration coefficients. Deformations are typically evaluated using Newmark's rigid sliding block displacements method. Seismic inertial loads can cause damage as described below:

- Static active earth pressures plus seismic inertial loads can increase lateral earth pressures on ERSs which can result in failure due to deformations that exceed the performance limits or structural capacity of the ERS. Failure may manifest itself in the form of lateral translations, rotations, overturning, or structural failure. Failure of tie-back systems (soil anchors or soil nails) may jeopardize the integrity of the whole structure. Increased bearing loads at the toe of shallow foundations may exceed the bearing capacity of the soil causing rotational displacement or bearing failure.
- Static passive earth pressure resistance to lateral loads can be reduced due to seismic inertial loads that can result in failure of the ERS by allowing forces from either seismic active soil pressures or inertial forces from the structure to cause large translational displacements.
- Global limit-equilibrium instability of the structure resulting in rotational or translational deformations that may exceed the ERS performance limits or structural capacity.
- Volumetric strain and accompanying ground settlement (Section 13.15) that results from the seismic shaking. The settlement can be due to either seismic densification/compression of unsaturated soils or fills and/or seismic densification resulting from excess pore water pressure relief of and rearrangement of cohesionless soils that have undergone cyclic liquefaction. There may be ground surface manifestations in the form of sand-boils as excess pore water pressure dissipates to the ground surface during cyclic liquefaction. Alternatively, water may get trapped under non-liquefiable soil layers above the cyclic liquefiable soils that will affect the rate of soil subsidence and may trigger other hazards due to soil SSL at these interfaces.

### 13.2.2 Global Hazards

Global hazards are those failures that result in large-scale site instability in the form of translational/rotational instability and/or flow failure sliding. Displacements associated with global hazards (flow failure) are the result of static gravitational driving forces combined with soil SSL.

Flow slide failures are the most catastrophic form of ground failures. Sites susceptible to flow failure typically are continuous over large areas of soils that are contractive and susceptible to cyclic liquefaction (Section 13.6.1 – Sand-Like Soil). These failures result from instability when the resisting force available from soils that undergo soil SSL is less than the static gravitational driving force of the soil mass. Flow slide failure potential is typically characterized by screening for contractive soils that are susceptible to soil SSL, evaluating triggering of soil SSL, and then evaluating instability by using conventional limit-equilibrium static slope stability methods.

## 13.3 GEOTECHNICAL SEISMIC HAZARD EVALUATION PROCESS

The effects of geotechnical seismic hazards must be considered in the design of all bridges, ERSs, embankments, and other transportation structures where poor performance could endanger the lives and safety of the traveling public. The effectiveness of highways in South Carolina depends on the proper evaluation of the geotechnical seismic hazards and designs to meet the performance requirements established in Chapter 10 for embankments, and ERSs.

The geotechnical seismic hazard evaluation begins with an evaluation of the seismic shaking parameters that are used to define the intensity and duration of the seismic event at the project

site. A summary of the seismic shaking parameters that will be used for geotechnical seismic hazard evaluation is presented in Section 13.3.1.

The geotechnical seismic hazard evaluation process then proceeds to screening and identification of the subsurface soils that have the potential to experience soil SSL. The soil SSL evaluation process is presented in Section 13.3.2. Once the potential for soil SSL has been identified, the potential failure modes of the geotechnical seismic hazards presented in Section 13.2 can be evaluated.

The effects of the geotechnical seismic hazards on the stability and performance of embankments and slopes are addressed in this Chapter. The seismic design of bridge foundations, bridge abutments, and ERSs is addressed in Chapter 14.

Provided in Appendix J are a series flow charts of the geotechnical seismic hazard evaluation process upon which this Chapter is based. The processes presented in this Manual are meant to serve as a guide in the evaluation and assessment of geotechnical seismic hazards. It is by no means the only approach that can be used; at a minimum, it should serve as a point of reference to understand the layout of the following Sections in this Chapter.

### 13.3.1 Seismic Shaking Evaluation Process

Geotechnical seismic hazards are triggered by the intensity and duration of the seismic shaking at the project site. The intensity and duration of the seismic shaking is primarily dependent on the size and location of the seismic events and the characteristics of the site. Chapters 11 and 12 provide the methodology for the assessment of the seismic shaking at a project site. The seismic shaking can be quantitatively assessed by the seismic $M_w$, R, $T'_o$, $T_{NH}$, PGV, $D_{a5\text{-}95}$, PGA, $S_{DS}$ and $S_{D1}$. Project sites that are closer to the seismic source experience higher levels of shaking; therefore, more damage can occur from geotechnical seismic hazards when compared to project sites further away.

### 13.3.2 Soil Shear Strength Loss Hazard Evaluation Process

Soil SSL that is induced by seismic shaking can produce severe damage as a result of the various geotechnical seismic hazard failure mechanisms described in Section 13.2. The soil SSL hazard evaluation process has three components: (1) Evaluating soil SSL susceptibility at the project site; (2) Evaluating soil SSL triggering potential of the seismic shaking; and (3) Evaluating the effects of soil SSL on the design parameters used to evaluate the geotechnical seismic hazard.

The soil SSL evaluation process begins by screening for soils that are susceptible to soil SSL for the design seismic events (FEE or SEE) under evaluation. The screening criteria (Section 13.6) consist of 3 soil categories that are susceptible to soil SSL: Sand-Like soils, Normally Sensitive (NS) Clay-Like soils, and Highly Sensitive (HS) Clay-Like soils. The screening criteria uses site conditions (i.e., water table); in-situ testing; and standard laboratory index testing and soil shear strength testing to determine if soils are susceptible to soil SSL. If the soils are found not to be susceptible to soil SSL during the screening process, then no further analysis is required to determine the triggering of soil SSL and an evaluation of geotechnical seismic hazard evaluation can proceed. Soils found to be susceptible to soil SSL during the screening process shall be further evaluated for soil SSL triggering. An exception to this is, if the PGA is less than or equal

to 0.2g (PGA $\leq$ 0.2g); the Seismic Design Category (SDC) is A (see Seismic Specs for definition); and the slope is 2H:1V or flatter, then neither screening nor soil SSL triggering analysis will be required for bridge embankments. However, if the slope is steeper than 2H:1V or an ERS is located within the bridge embankment, then either screening or soil SSL triggering analysis will be required. In addition, the screening or triggering analysis may be required by either SCDOT or if in the opinion of the GEOR it is required. The GEOR shall document why SSL is required in the BGER.

Determining whether soil SSL triggering occurs during the seismic shaking or after the seismic shaking is very complex and beyond the scope of the methodology that will be used in the design of typical bridges and typical roadway structures. Therefore, the effects of cyclic liquefaction and cyclic softening (soil SSL) shall be assumed to occur during the seismic shaking and will continue into the post-seismic period, to allow for the evaluation of soil SSL-induced geotechnical seismic hazards. Soil SSL shall be assumed to occur instantaneously throughout the full thickness of the soil layer and shall be assumed to occur at the beginning of shaking. These fundamental assumptions must be used when selecting soil shear strengths in accordance with Section 13.10.

The main contributor to catastrophic damage and poor performance of structures has in past case histories been attributed to cyclic liquefaction-induced seismic geotechnical hazards shown in Figure 13-1. Soil SSL due to cyclic liquefaction of Sand-Like soils (Section 13.6.1) has the potential to cause the most damage in the Coastal Plain of South Carolina as evident from the cyclic liquefaction case histories presented in Section 13.5.3.

Soils that are identified as being susceptible to losses in soil shear strength need to be evaluated to determine if the seismic shaking can trigger (or initiate) soil SSL. Soil SSL triggering for Sand-Like soils and Clay-Like soils is dependent on the site conditions (i.e., soil in-situ strength; soil composition including grain-size and moisture-plasticity relationship and location of ground water surface). The soil SSL triggering of Clay-Like soils is applicable to both NS Clay-Like soils and HS Clay-Like soils. The overall method for analyzing soil SSL triggering for Sand-Like soils and Clay-Like soils consists of determining if the cyclic stress ratio (CSR) induced by the design seismic event (FEE or SEE) and any initial static shear stresses ($\tau_{static}$) in the soil (CSR = Demand, D) are greater than the soil's cyclic resistance ratio (CRR = Capacity, C) based on a specified margin of safety (on-set of soil SSL resistance factor, $\varphi_{SL}$), see Equation 13-1. If the soil SSL resistance ratio, $(D/C)_{SL}$, is greater than $\varphi_{SL}$, the soil under evaluation has the potential for soil SSL and a reduced shear strength shall be used in the evaluation of geotechnical seismic hazards.

$$\left(\frac{D}{C}\right)_{SL} = \frac{CSR^{*}_{eq}}{CRR^{*}_{eq}} \leq \varphi_{SL} \qquad \textbf{Equation 13-1}$$

Where,

$CRR^{*}_{eq}$ = Corrected, magnitude weighted and normalized CRR (Section 13.9).
$CSR^{*}_{eq}$ = Magnitude weighted and equivalent-seismically induced CSR (Section 13.8).

Initial static shear stress ($\tau_{Static}$) reduces the soil's capacity (C) to resist the soil SSL. If the triggering of soil SSL is indicated at the site, then a flow failure analysis as described in Section

13.11 shall be conducted. If the flow failure resistance ratio, $(D/C)_{Flow}$ is greater than $\varphi_{Flow}$, then a displacement analysis is required as described in Section 13.14. The triggering of soil SSL in Clay-Like soils (NS and HS) can also occur due to an increase in static shear stresses similar to that which occurs when Sand-Like soils experience cyclic liquefaction. Soil SSL in NS Clay-Like soils causes the soils to have cyclic softened residual shear strength ($\tau_{rs}$) and in HS Clay-Like soils causes the soils to have remolded soil shear strength ($\tau_{remolded}$).

The selection of soil shear strength properties for soils with and without the potential for soil SSL is performed during the geotechnical seismic hazard evaluation. The overall process for evaluating soil SSL is shown in Appendix J.

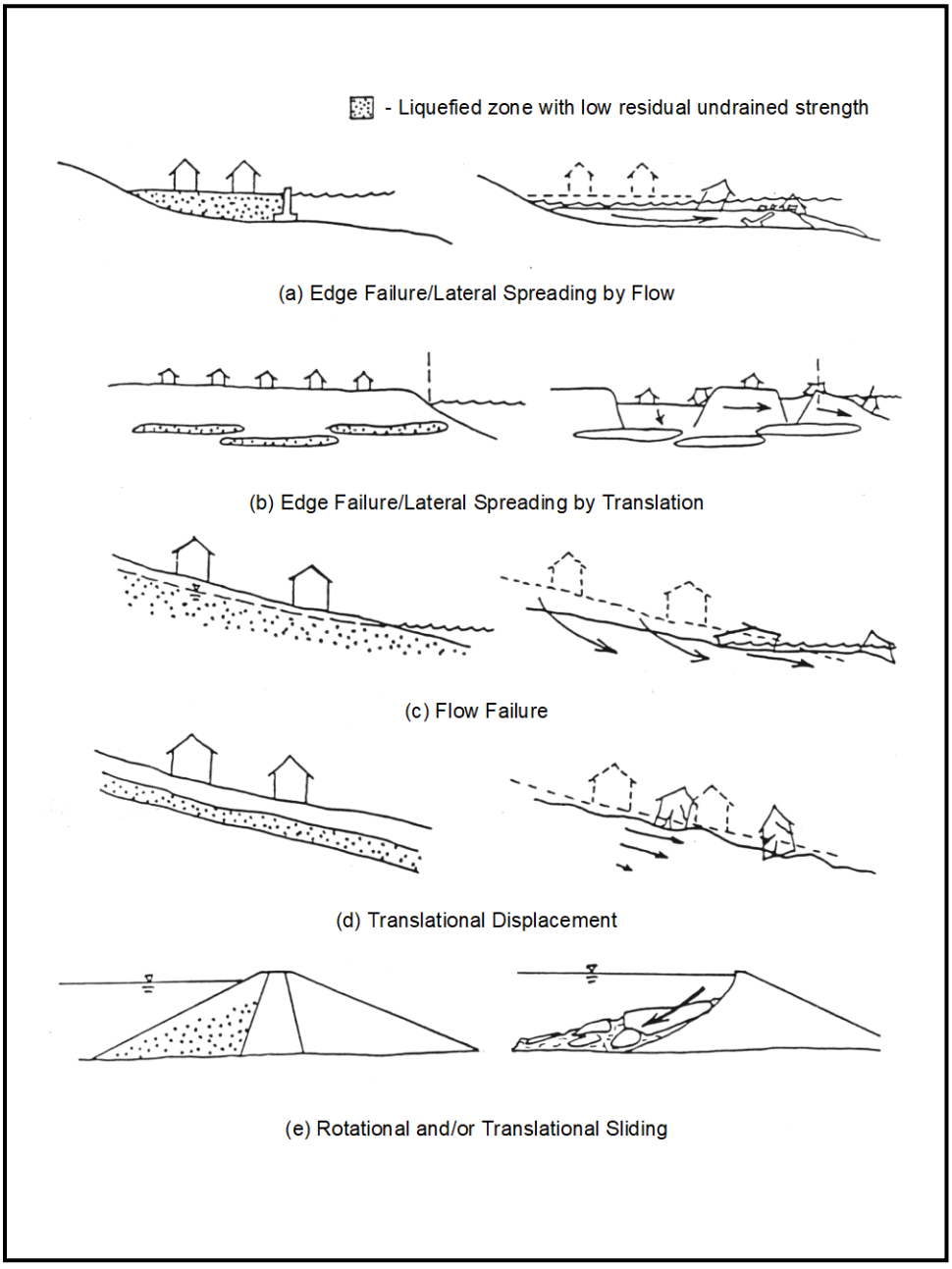


**Figure 13-1, Cyclic Liquefaction-Induced Seismic Geotechnical Hazards (Seed, et al. (2003))**

## 13.4 GEOTECHNICAL SEISMIC HAZARD ANALYTICAL METHODOLOGIES

The methodologies presented in this Chapter for evaluating and assessing the impact of the geotechnical seismic hazards on transportation structures are based primarily on general limit-equilibrium (GLE) (see Chapter 17 for definition) methods of analyses and empirical/semi-empirical analytical methods that are easily performed and are currently within the state-of-practice of geotechnical seismic engineering. References for the design methodologies used in this Manual have been listed to allow the designer the opportunity to become more thoroughly familiar with the methodology, its applicability, and its limitations. Within the scope of this Manual, it is not possible to provide sufficient detail and caveats to preclude any misuse of the methods. When necessary, several methods of analyzing the geotechnical seismic hazard have been provided in order to allow for variance in analytical methodologies and to identify trends in results or performance. Several of the methods presented are empirical/semi-empirical and their applicability to the project site is dependent on the limits of the database used to develop the analytical basis of the method. Therefore, it is the responsibility of the GEOR to know the applicability and limitations of these methods. This Chapter does not address numerical analyses (e.g., finite element, finite difference, etc.), because these methods are typically not performed in the design of typical bridges or typical transportation structures. If numerical analyses are required for a project, contact the OES/GDS for design requirements, review and acceptance of the proposed methods.

## 13.5 SOIL SHEAR STRENGTH LOSS MECHANISMS

The mechanism of soil SSL is very complex and has been the subject of much confusion in literature. This is particularly due to the lack of standardization of terminology and the fact that research efforts are still ongoing. Additional confusion has occurred when the method of soil SSL triggering (static stresses, cyclic loads, etc.) has been used as a means of categorizing the soil SSL mechanism. Current understanding of soil SSL failure mechanisms is based on the study of case histories and laboratory experimentation. One of the problems in the evaluation of field case histories is that more than 1 geotechnical seismic hazard is typically responsible for the observed failures. For example, this problem can occur when lateral spread movements trigger flow failures and the resulting final deformations observed reflect the influence of all geotechnical seismic hazard failure modes (lateral spread, flow failure, and seismic settlement). Laboratory testing has provided much insight into the mechanisms that trigger soil SSL under a controlled laboratory environment. Laboratory experimentation has limitations in that sampling disturbance of the in-situ soil structure (i.e., cementation, layering, etc.) can significantly affect the initial and residual soil shear strength results. Another limitation is that laboratory testing can be very complex and routinely not within the standard-of-practice for design of typical bridge structures. Detailed explanation of the mechanisms of soil SSL based on field and laboratory observations can be obtained from Robertson and Wride (1997), Kramer and Elgamal (2001), and Idriss and Boulanger (2008). Although the term liquefaction has been used widely in literature (Kramer (1996) and Robertson and Wride (1997)) to describe several mechanisms of soil SSL, the term liquefaction as used in this Manual will only be applicable to discussions of Sand-Like soil SSL that results from cyclic loading.

The predominant soil behavior (i.e., cohesionless or cohesive) is used in this Manual to evaluate the soil's SSL susceptibility (Section 13.6) and to determine the most appropriate soil SSL triggering evaluation method for use in geotechnical seismic design. Field case histories and

laboratory testing have demonstrated that the predominant soil SSL behavior for the majority of soils can be grouped into either Sand-Like soils (i.e., cohesionless) that are subject to cyclic liquefaction failure mechanisms or Clay-Like soils (i.e., cohesive) that are subject to cyclic softening failure mechanisms. A description of these soil failure mechanisms is provided in the following Sections.

### 13.5.1 Cyclic Liquefaction of Sand-Like Soils

Cyclic liquefaction of Sand-Like soils is typically responsible for the most damaging geotechnical seismic hazards that affect transportation infrastructure. Potential damage to transportation facilities due to cyclic liquefaction includes loss of bearing capacity, lateral spread, flow failure, excessive settlements, and reduced lateral and vertical carrying capacity of deep foundations. Even though cyclic liquefaction can be triggered by non-seismic loadings such as low amplitude vibrations produced by rail traffic/construction equipment or by static loads, such as those that might be caused by rapid drawdown, this Manual will focus on liquefaction triggered by seismic shaking. Non-seismic cyclic liquefaction triggers are not covered by this Manual. Cyclic liquefaction occurs in Sand-Like soils that are nonplastic, saturated, and have been deposited during the Quaternary Period (past 1.6 million years) in a loose state and are subject to strain softening. Typically, the more recent soil deposits have the greatest susceptibility for cyclic liquefaction. Cyclic liquefaction typically begins during a seismic event when the in-situ soil pore water pressure ($u_o$) increases ($+\Delta u$). As the increased pore water pressure ($u = u_o + \Delta u$) approaches the total overburden stress ($\sigma_{vo}$), the effective overburden stress ($\sigma'_{vo} = \sigma_{vo} - u$) will approach zero causing a reduction in grain-to-grain contact and a significant decrease in soil shear strength. The reduction in grain-to-grain contacts cause a redistribution of soil particles resulting in densification. As indicated previously it is assumed that pore pressures increase to the total overburden stress instantaneously within a Sand-Like soil layer at the beginning of the seismic event and continues into the post-seismic period. Further it is assumed that the entire Sand-Like soil layer experiences soil SSL across the full soil layer thickness at the same time.

Significant lateral soil deformation may occur as a result of reduced soil shear strength of the liquefied soil zone combined with the seismic inertial forces and/or initial static driving forces. Other surface manifestations of cyclic liquefaction are often associated with the upward flowing of pore water that generates sand boils at the ground surface. Evidence of sand boils occurring at the ground surface have been found throughout the South Carolina Coastal Plain as indicated in Section 13.5.3. The absence of sand boils is not an indication that cyclic liquefaction has not occurred. Sand boils will not always occur during or after cyclic liquefaction, especially if the drainage paths are restricted due to overlying less permeable layers, i.e.,, the sand is immediately beneath a less permeable soil. Seismic settlement at the ground surface may occur from cyclic liquefaction induced volumetric strain that develops as seismically induced pore water pressures dissipate.

The determination of the onset of cyclic liquefaction either during shaking or post-seismic is a very complex analytical problem and beyond the scope of typical SCDOT projects. Several case histories have documented that liquefaction can both occur during shaking or after shaking has occurred (Seed (1986), Kramer and Elgamal (2001)). The onset and manifestation of cyclic liquefaction is primarily dependent on the magnitude, duration, and proximity of the seismic event, the depth of the liquefied soil zone, stratification and relative permeability of the soil layers above and below the liquefied soil zone, and the susceptibility of the soils to liquefy. Consequently

liquefaction will conservatively be assumed to occur at the beginning of the seismic shaking and continues into the post-seismic time.

### 13.5.2 Cyclic Softening of Clay-Like Soils

Cyclic softening refers to soil SSL and deformations in Clay-Like soils. Clay-Like soils are typically moist, plastic clays. Cyclic softening occurs when the seismic-induced cyclic shear stresses exceed the soil's cyclic shear resistance, causing an accumulation of deformations that result in soil SSL in cohesive soils that exhibit strain softening. Cyclic softening of Clay-Like soils typically results in soil SSL that is dependent on the soil's sensitivity (Chapter 7). Soil deformations may occur as a result of reduced soil shear strength of Clay-Like soils combined with the inertial forces and/or initial static driving forces. The limited case histories in South Carolina have not documented cyclic softening of Clay-Like soils. Field evidence of cyclic softening of Clay-Like soils is difficult to document because it does not manifest itself as sand boils at the ground surface as has been documented for cyclic liquefaction of Sand-Like soils. As with Sand-Like soils, it will be conservatively assumed that cyclic softening occurs at the beginning of the shaking and that the entire layer softens at the same time.

### 13.5.3 SC Historical Cyclic Liquefaction

There is significant evidence that cyclic liquefaction has historically occurred in the CEUS. Soil liquefaction has been found to have occurred as a result of seismic events in New Madrid, Missouri 1811–1812 and in Charleston, South Carolina 1886. The 1886 Charleston seismic event caused the manifestation of large sand boils as a result of cyclic liquefaction. Sand boils were created as the soil pore water, carrying soil particles, was expelled from the ground, collapsing the surface and forming craters at the ground surface. Figure 13-2 shows a sand boil crater that appeared during the 1886 Charleston seismic event.

**Figure 13-2, Sand Boil Crater - 1886 Charleston, SC Seismic Event (McGee, et al. (1986))**

Hayati and Andrus (2008) developed a liquefaction potential map of Charleston, South Carolina based on the 1886 seismic event. The geologic map of the Charleston Peninsula and Drum Island originally developed by Weems, et al. (1997) was used by Hayati and Andrus (2008) to indicate locations of liquefaction and ground deformations as shown in Figure 13-3. For a description of the near surface geologic units and a description of the Cases (indicated on the map as 1 – 27) of cyclic liquefaction evidence and permanent ground deformation see Hayati and Andrus (2008).

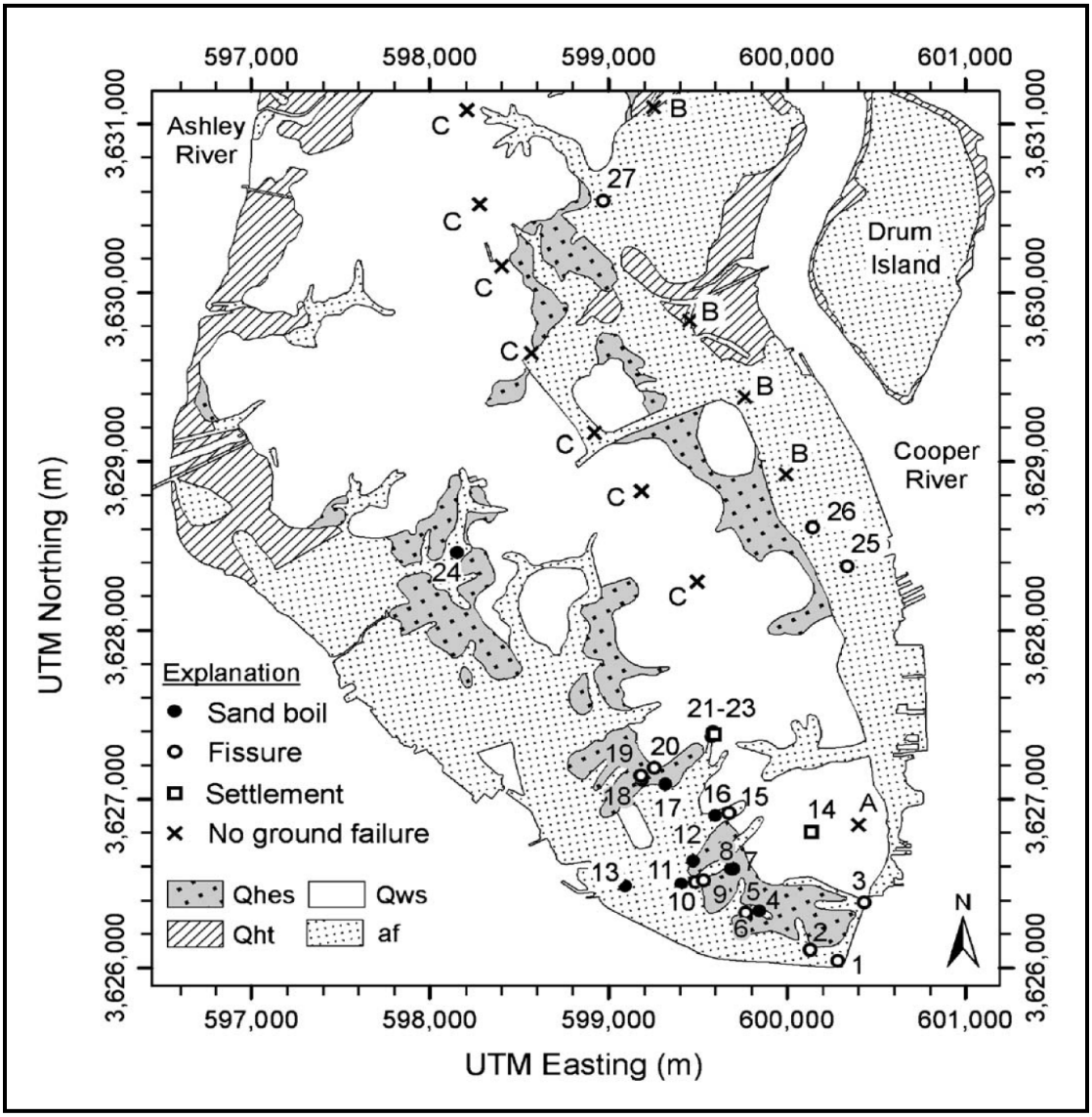


**Figure 13-3, 1886 Liquefaction and Ground Deformations Sites (Weems, et al. (1997), Hayati and Andrus (2008) with permission from ASCE)**

Paleoliquefaction studies in South Carolina conducted since the mid-1980s have indicated that at least 7 episodes of paleoliquefaction have occurred in the past 6,000 years. The seismic events in the Charleston, SC area appear to have magnitudes greater than 7 and the seismic event cycle suggests a recurrence interval of 500-600 years (Talwani and Schaffer, 2001). Paleoliquefaction study site locations in the South Carolina Coastal Plain are shown in Figure 13-4.

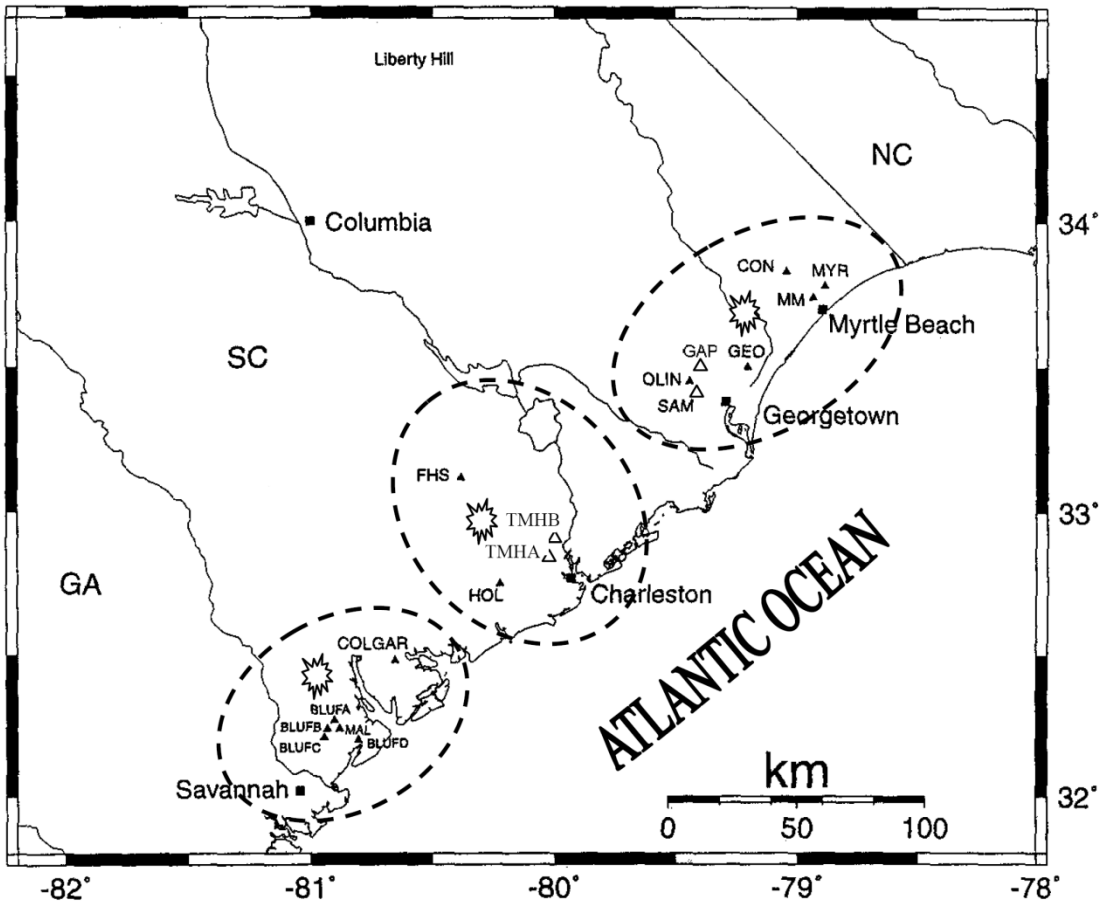


**Legend**:

- Dashed lines enclose three zones of paleoliquefaction along the South Carolina Coastal Plain. The explosion symbols represent three possible inferred epicentral locations.
- Triangles show the locations of sandblows in South Carolina Coastal Plain. Reports of liquefaction features extend to Columbia and Georgetown and to Sand Hills near Liberty Hill.
- Open triangles indicate the locations of in-situ engineering tests for this study.
- Abbreviations are as follows: Bluffton, BLUF; Colony Gardens, COLGAR; Conway, CON; Four Hole Swamp, FHS; Gapway, GAP; Georgetown, GEO; Hollywood, HOL; Malpherous, MAL; Martin Marietta, MM; Myrtle Beach, MYR; Sampit, SAM; and Ten Mile Hill, TMH

**Figure 13-4, Coastal Plain Paleoliquefaction Study Sites (adapted from Talwani and Schaffer (2001)).**

Figure 13-5 shows a map, prepared by the USGS, of the liquefaction features in South Carolina. The shaded area on the map indicates areas of potential Quaternary and historic liquefaction. The USGS maintains a database of published reports of Quaternary faults, liquefaction and tectonic features in the CEUS. The USGS database for South Carolina contains the following 3 sites with liquefaction features: 2657, Charleston, SC; 2658, Bluffton, SC; and 2659, Georgetown, SC. Liquefaction feature 2657 has geologic evidence of the 1886 Charleston seismic event. Liquefaction features 2658 and 2659 have geologic evidence of prehistoric liquefaction that occurred during the late Quaternary Period (Holocene, <10,000 years ago).

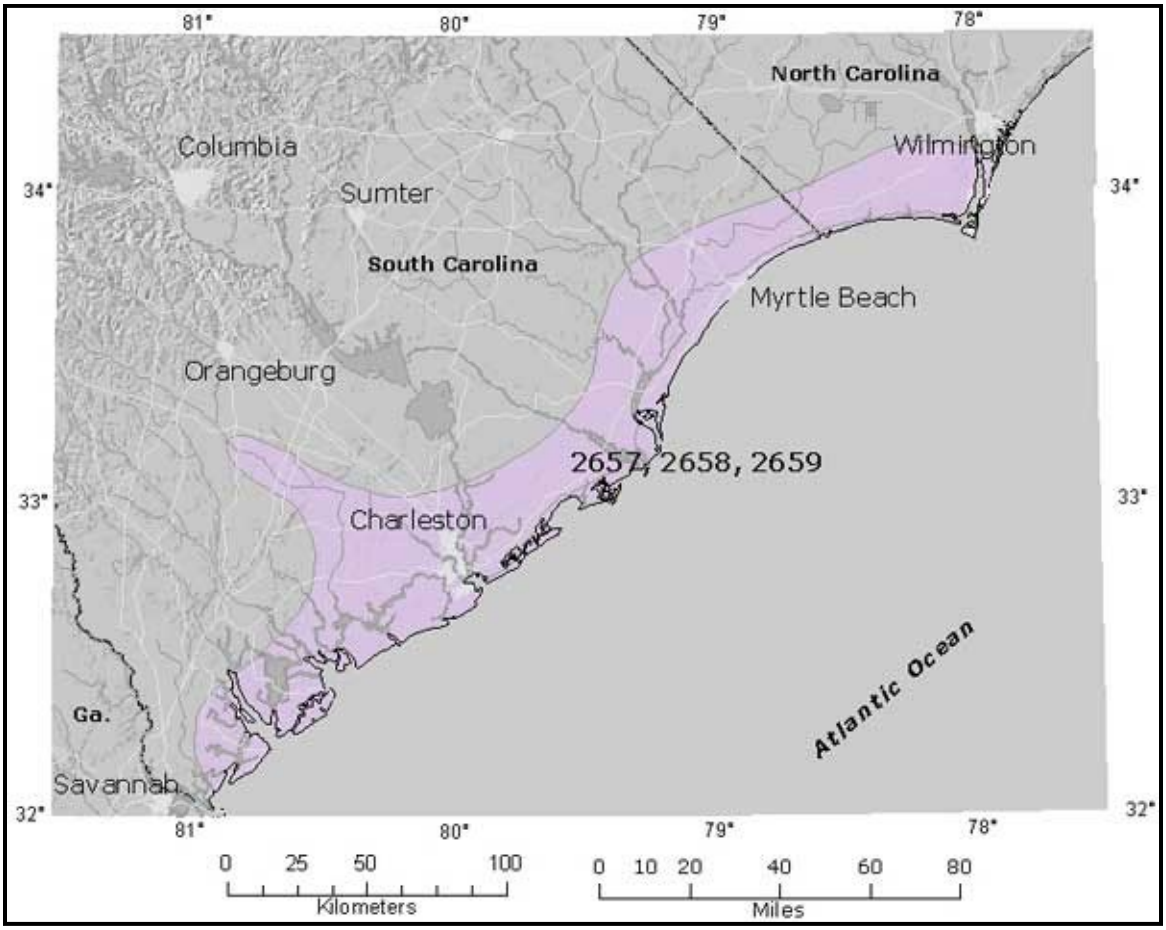


**Figure 13-5, SC Quaternary Liquefaction Areas (USGS Website)**

Even though liquefaction has occurred in the CEUS, a limited number of the liquefaction case histories have been evaluated, since most seismic events with moment magnitudes, $M_w$, greater than 6.5 occurred more than 100 years ago. Liquefaction evaluation in the CEUS and consequently in South Carolina, is relatively more complex than in other areas where liquefaction has occurred in the more recent past. The deep vertical soil column (up to 4,000 feet) encountered in the Atlantic Coastal plain, lack of recorded large seismic events, and uncertainty of the mechanisms and subsequent motions resulting from intraplate seismic events make liquefaction evaluation difficult (Schneider and Mayne (1999)). Nevertheless, historical soil liquefaction studies in the CEUS (Schneider and Mayne (1999)) indicate that current methods to evaluate cyclic liquefaction are in general agreement with predictions of cyclic liquefaction.

## 13.6 SOIL SHEAR STRENGTH LOSS SUSCEPTIBILITY SCREENING CRITERIA

Screening criteria is based on laboratory and in-situ test properties of soils that experience soil SSL in seismic hazard case histories. It has been observed that the potential for cyclic liquefaction decreases as FC and PI of the soils increase and as the *w* decreases below the LL.

Screening for seismic-induced soil SSL has traditionally been focused on cyclic liquefaction of cohesionless soils. Recent studies (Seed, et al. (2003), Boulanger and Idriss (2004 and 2007); Bray and Sancio (2006), Idriss and Boulanger (2008)) have stressed the need to evaluate soil

SSL in other soil types, such as cyclic liquefaction of low plasticity silts and cyclic softening of plastic clays. Seed, et al. (2003) proposed the liquefaction susceptibility chart for fine grained soils shown in Figure 13-6 that is based on soil plasticity. The chart is divided into 3 zones of varying soil SSL susceptibility. Zone A has the highest potential for loss in shear strength resulting from cyclic liquefaction. Zone B was considered a transition area where soils could be subject to soil SSL and would require laboratory cyclic load testing for confirmation of soil shear strength susceptibility. Soils located in Zone C (the Zone not covered by Zones A or B) were not susceptible to cyclic liquefaction induced soil SSL but can be susceptible to soil SSL due to cyclic softening of sensitive cohesive soils.

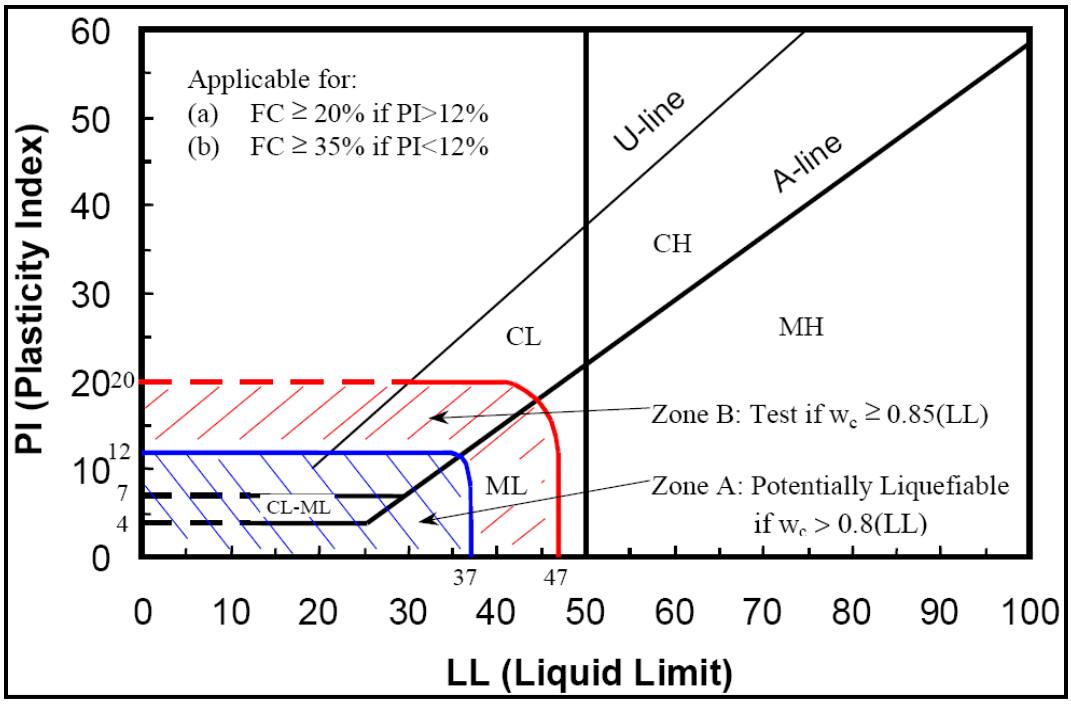


**Figure 13-6, Liquefaction Susceptibility Based on Soil Plasticity (Seed, et al. (2003))**

The liquefaction guidelines described by Seed, et al. (2003) are best considered as envelopes of fine-grained soils that have been observed to experience significant strains or strength loss during seismic events (Boulanger and Idriss (2004, 2006, and 2007)). Boulanger and Idriss (2004, 2006, and 2007) recommend that the fine-grained cyclic soil behavior would be best described as either Sand-Like or Clay-Like based on the Plasticity Index (PI). Boulanger and Idriss (2004, 2006, and 2007) suggested that there is a narrow soil SSL behavior transition zone between Sand-Like and Clay-Like that ranges from about a PI of 3 to 8 as indicated in Figure 13-7.

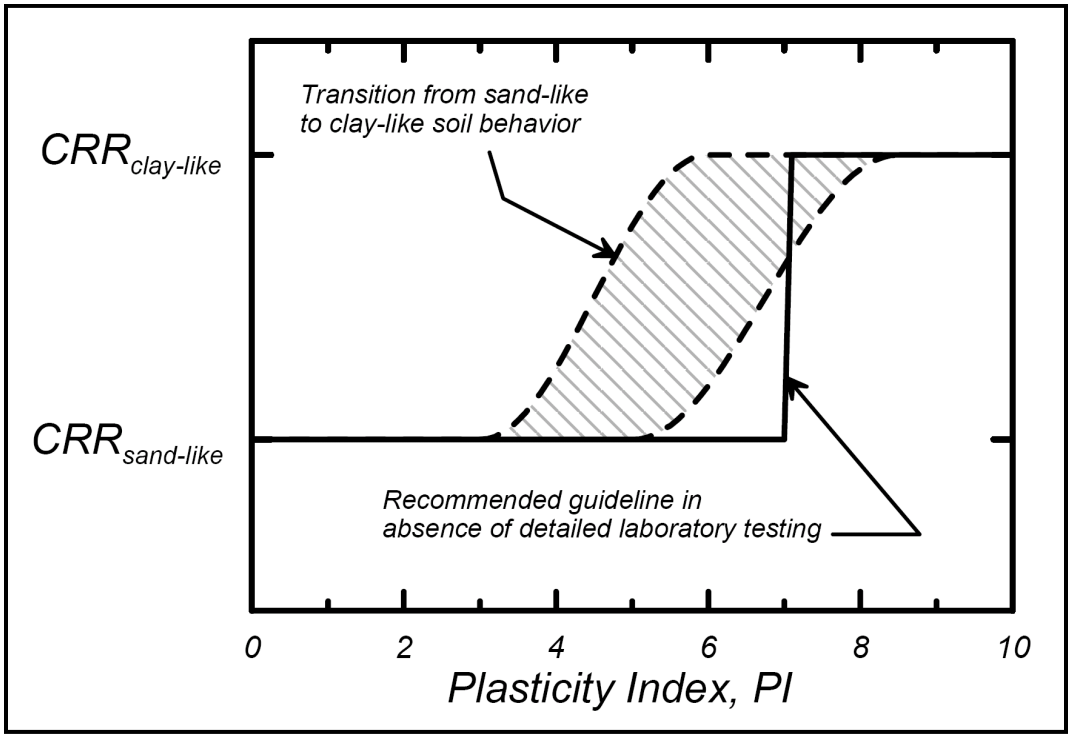


**Figure 13-7, Transition from Sand-Like to Clay-Like behavior (Boulanger and Idriss (2004, 2006, and 2007); Idriss and Boulanger (2008)) (With Permission from ASCE)**

The soil SSL behavior screening adopted by SCDOT in the following Sections is consistent with not only Idriss and Boulanger (2008) but also the soil behavior discussed in Chapter 7 and has been expanded to distinguish between NS and HS Clay-like soils as indicated below (see Figure J-2, Appendix J). The soil SSL susceptibility criteria shall be based on the following 3 categories:

1 Sand-Like soils
2 NS Clay-Like soils
3 HS Clay-Like soils

Laboratory cyclic load testing of Sand-Like or Clay-Like soils is typically not required for typical bridges or typical transportation structures but may be required by the OES/GDS on a project specific basis depending on the risk associated with the geotechnical seismic hazards under evaluation or may be requested by the GEOR with concurrence from the OES/GDS.

### 13.6.1 Sand-Like Soil

SSL in Sand-Like soils is caused by cyclic liquefaction as described in Section 13.5.1. Sand-Like soils will be screened to a minimum depth of 80 feet below the existing ground surface or 20 feet beyond the lowest deep foundation element; whichever extent of screening is deeper.

The following steps shall be used to determine if a soil is Sand-Like and whether a full soil SSL analysis is required:

1. Sand-Like soils susceptible to cyclic liquefaction must not only be below the water table, but must also be fully saturated. Based on Kokusho (2000) and Hossain, Andrus and Camp (2013) compression wave velocity ($V_p$) may be used to determine if a Sand-Like soil is fully saturated. If the $V_p$ is greater than or equal to 3,000 feet per second, Sand-Like soils shall be considered to be fully saturated and therefore, susceptible to SSL. Sand-Like soils with a $V_p$ less than 3,000 feet per second shall be considered unsaturated to the point that SSL is unlikely to happen. The water table selection for this evaluation must take into account the seasonal fluctuation of the ground water and the historic and/or possible future rise of the ground water level with respect to the soils being analyzed for liquefaction susceptibility. To determine the depth that soils are adequately saturated for liquefaction to occur, seasonally averaged groundwater elevations shall be used. The Natural Resources Conservation Service (NRCS) website (http://websoilsurvey.nrcs.usda.gov/app/) may be consulted for determining the seasonal fluctuation of groundwater. Groundwater fluctuations caused by tidal action or seasonal variations will cause a portion of the soil to be saturated only during a limited period of time, significantly reducing the risk that liquefaction could occur within the zone.

2. Sand-Like soils have less than or equal to 20 percent passing the No. 200 sieve (i.e., %200 $\leq$ 20%) regardless of the plasticity or an $I_c$ of less than or equal to 2.05 ($I_c \leq 2.05$). If these soils are below the water table (see Step 1 for determining the depth to the water table) go to Step 4. If these Sand-Like soils are above the water table (see Step 1), then soil SSL cannot occur. For soils with fines contents greater than 20 percent (i.e., %200 $>$ 20%), go to Step 3 and check PI.

3. For soils with fines contents greater than 20 percent (i.e., %200 $>$ 20%), check the PI to determine if these soils are Sand-Like. Soils with PI less than or equal to 10 ($PI \leq 10$) will be treated as Sand-Like (see Figure 13-8). Proceed to Step 4 to complete the screening process.

4. Soils characterized as Sand-Like that have normalized corrected SPT blow counts, $N^*_{1,60,CS}$ less than 30 blows/foot ($N^*_{1,60,CS} < 30$ bpf) or normalized corrected CPTu tip resistances, $q_{C,1,N,CS}$ less than 170 unitless ($q_{C,1,N,CS} < 170$) are susceptible to cyclic liquefaction; therefore a full soil SSL analysis shall be conducted.

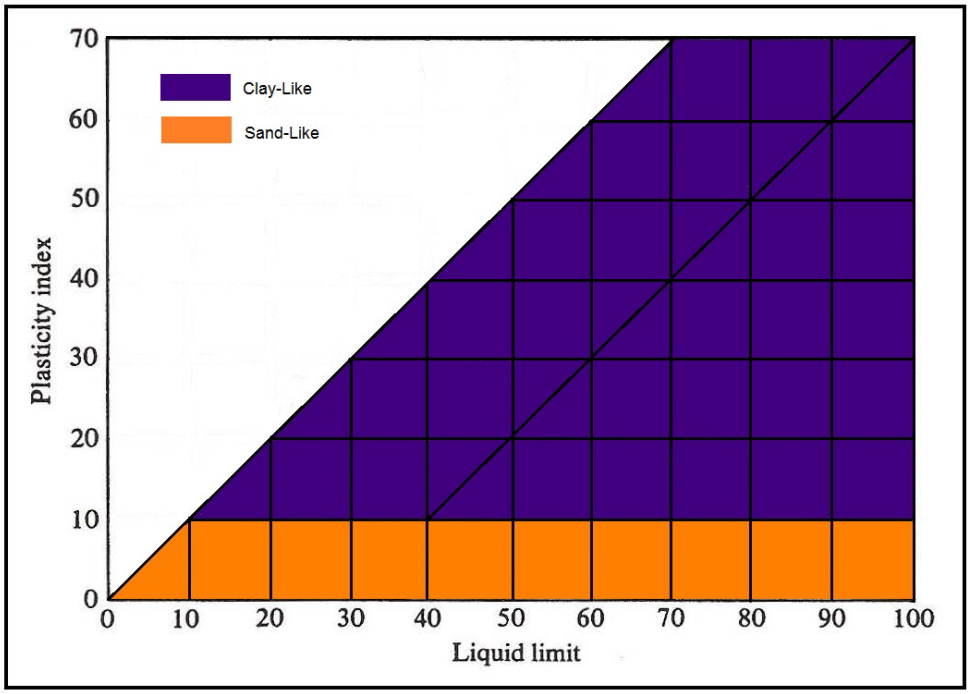


**Figure 13-8, Plasticity Chart – Sand-Like/Clay-Like Soils**

### 13.6.2 Normally Sensitive (NS) Clay-Like Soil

SSL in NS Clay-Like soils is caused by cyclic softening as described in Section 13.5.2. Clay-Like soils will be screened to a minimum depth of 80 feet below the existing ground surface or 20 feet beyond the lowest deep foundation element; whichever extent of screening is deeper.

The following steps shall be used to determine if a soil is NS Clay-Like and whether the soil is susceptible to cyclic softening:

1. Soils with fines contents greater than 20 percent (i.e., %200 > 20%), check PI to determine if these soils are Clay-Like. Soils with PI more than 10 (PI > 10 (see Figure 13-8)) or an $I_c$ of greater than or equal to 2.6 ($I_c \geq 2.6$) will be treated as Clay-Like.

2. Soils with $I_c$ greater than 2.05, but less than 2.6 ($2.05 < I_c < 2.6$) may require pore pressure dissipation testing during CPTu testing to determine whether the soil will behave Sand-Like or Clay-Like. The GEOR shall document how the soil behavior determination was made.

3. Soils with a sensitivity less than 5, $S_t < 5$ (Chapter 7), are NS Clay-Like.

4. Soils that meet these criteria shall have a full soil SSL analysis conducted.

### 13.6.3 Highly Sensitive (HS) Clay-Like Soil

SSL in HS Clay-Like soils is caused by cyclic softening as described in Section 13.5.2. Clay-Like soils will be screened to a minimum depth of 80 feet below the existing ground surface or 20 feet beyond the lowest deep foundation element; whichever extent of screening is deeper.

The following steps shall be used to determine if a soil is HS Clay-Like and whether the soil is susceptible to cyclic softening:

1. Soils with fines contents greater than 20 percent (i.e., %200 > 20%), check PI to determine if these soils are Clay-Like. Soils with PI more than 10 (PI > 10 (see Figure 13-8)) or an $I_c$ of greater than or equal to 2.6 ($I_c \geq 2.6$) will be treated as Clay-Like.

2. Soils with $I_c$ greater than 2.05, but less than 2.6 ($2.05 < I_c < 2.6$) may require pore pressure dissipation testing during CPTu testing to determine whether the soil will behave Sand-Like or Clay-Like. The GEOR shall document how the soil behavior determination was made.

3. Soils with a sensitivity equal to or greater than 5, $S_t \geq 5$ (Chapter 7), are HS Clay-Like.

4. Soils that meet these criteria shall have a full soil SSL analysis conducted.

## 13.7 SOIL SHEAR STRENGTH LOSS TRIGGERING

The soil SSL triggering analyses will include an evaluation of Sand-Like and Clay-Like soils that were identified to be susceptible to cyclic liquefaction or cyclic softening during the screening process described in Section 13.6. The ground conditions and any surcharges or surface loads that will induce static shear stresses in the underlying soils must be accounted for when evaluating soil SSL triggering for both Sand-Like and Clay-Like soils.

The *Simplified Procedure* for determining liquefaction triggering of Sand-Like soils shall be based on SPT in-situ testing or on CPT in-situ testing using the methods described in the Earthquake Engineering Research Institute (EERI) Monograph MNO-12, Soil Liquefaction During Earthquakes (Idriss and Boulanger (2008)).

The *Simplified Procedure* for determination of cyclic liquefaction triggering is an empirical method based on field investigations of sites with Sand-Like soils. The *Simplified Procedure* for Sand-Like soils cannot differentiate between the types of liquefaction (flow liquefaction or cyclic softening). The *Simplified Procedure* for determining the onset/triggering of cyclic softening of Clay-Like soils during seismic events is based on laboratory investigations. The OES/GDS may require on a project specific basis, more rigorous analytical methods such as non-linear effective stress site response methods and advanced laboratory testing, which are not included in this Manual.

The *Simplified Procedure* compares the ratio of the seismic-induced stresses plus the static shear stresses (D) to the soils resistance to soil SSL (C), thus defining the strength loss ratio $(D/C)_{SL}$. The Demand, D, is expressed in terms of the equivalent uniform cyclic stress ratio that has been magnitude-weighted ($CSR^{*}_{eq} = CSR_{eq,M=7.5}$), while the Capacity, C, is the soil's resistance to soil SSL expressed in terms of corrected cyclic resistance ratio that also has been magnitude-weighted and normalized to an effective overburden stress of 1 tsf ($CRR^{*}_{eq} = CRR_{M=7.5,1\ tsf}$). The LRFD equation that is to be used to evaluate the onset of strength loss (SL) is provided below:

$$\left(\frac{D}{C}\right)_{SL} = \frac{CSR^{*}_{eq}}{CRR^{*}_{eq}} \leq \varphi_{SL} \qquad \textbf{Equation 13-2}$$

The onset of cyclic liquefaction (Sand-Like soils) or cyclic softening (Clay-Like soils) occurs when the SL ratio $(D/C)_{SL}$ is greater than the SL resistance factor ($\varphi_{SL}$) provided in Chapter 9.

Alternate methods of evaluating liquefaction triggering of Sand-Like soils such as those described in the 1996 NCEER and 1998 NCEER/NSF workshop (Youd, et al. (2001)) may be required on a project specific basis.

Since the *Simplified Procedure* is a deterministic procedure, a load factor, $\gamma$, of unity (1.0) is used and the resistance factor, $\varphi$, accounts for the site variability and the level of acceptable risk to triggering soil SSL. As research advances and soil SSL analytical models are calibrated for LRFD design methodology, adjustments will be made in the implementation of the LRFD design methodology.

The overall process for conducting a soil SSL triggering analysis using the *Simplified Procedure* for level project site conditions is presented in a flow chart in Figure J-2 in Appendix J. The analytical procedures for computing cyclic stress ratio (CSR) and cyclic resistance ratio (CRR) of Sand-Like soils and Clay-like soils are provided in Section 13.8 and Section 13.9, respectively.

Soils that are susceptible to cyclic liquefaction or cyclic softening will require additional analyses to evaluate the effects of the soil shear strength degradation as discussed in Section 13.10. Project sites that have subsurface soils with the potential for soil SSL will require the evaluation for soil SSL-induced geotechnical seismic hazards such as flow slide failure, global instability, and soil settlements. The analytical procedures to determine the magnitude and extent of these SSL-induced hazards are provided in Sections13.11 – 13.15 of this Chapter.

The effects of initial static shear stress must be included in the evaluation of soil SSL triggering by the methods indicated below:

1. **<u>Static Shear Stress Ratio Correction Factor, $K_\alpha$, Method:</u>** The static shear stress ratio (SSSR) correction factor ($K_\alpha$) method (Section 13.9.6) is presented by Idriss and Boulanger (2008) to account for static shear stresses in the *Simplified Procedure* method of evaluating soil SSL triggering. The SSSR correction factor, $K_\alpha$, method is further explained in Section 13.9.6, and shall be used.

2. **Shear Strength Ratio Method:** The shear strength ratio (SSR) triggering method computes the ratio of shear stress demand on the soil layer susceptible to soil SSL with the soil's yield strength. This method, developed by Olson and Stark (2003), uses the yield shear strength ratio and soil SSL ratio to evaluate the triggering of soil SSL. The SSR method is further explained in Appendix I.

The $K_\alpha$ method presented above should be used to evaluate soil SSL triggering evaluation when the initial static stress ratio ($\alpha$) is less than or equal to 0.35 ($\alpha \leq 0.35$). When the maximum initial static stress ratio ($\alpha$) is greater than 0.35 ($\alpha > 0.35$), or when complex geometries and loadings need to be evaluated, the shear strength ratio (SSR) method presented in Appendix I shall be used. Soils that are susceptible to cyclic liquefaction or cyclic softening will require additional analyses to evaluate the soil shear strength degradation (Section 13.10).

## 13.8 CYCLIC STRESS RATIO (CSR)

The seismic-induced cyclic stresses in the soil are quantified by CSR. The equivalent uniform cyclic stress ratio, $CSR^*_{eq}$, is the equivalent uniform seismic-induced stress that has been magnitude-weighted ($M_w = 7.5$) as shown in the following equation:

$$CSR^*_{eq} = CSR_{eq,7.5} = \frac{CSR_{eq}}{MSF} \qquad \textbf{Equation 13-3}$$

Where,

$CSR_{eq}$ = Equivalent seismic-induced stress (Section 13.8.1)
MSF = Magnitude Scaling Factor (Section 13.8.2)

### 13.8.1 Equivalent Seismic-Induced Stress ($CSR_{eq}$)

The equivalent seismic-induced stress, $CSR_{eq}$, sometimes referred to as the average seismic-induced stress, is defined as shown in the following equation:

$$CSR_{eq} = 0.65 * CSR_{Peak} \qquad \textbf{Equation 13-4}$$

Where,

$CSR_{Peak}$ = Maximum seismic-induced CSR (Section 13.8.1.1)

Note that a factor of 0.65 is included in Equation 13-4 to obtain an "average" or equivalent $CSR_{eq}$ value. The method of computing the maximum seismic-induced stress ratio, $CSR_{Peak}$, depends on the method of performing the site response analysis discussed in Chapter 12.

#### 13.8.1.1 Simplified Procedure Determination of $CSR_{Peak}$

The *Simplified Procedure* for determination of the $CSR_{Peak}$ should typically be used for evaluation of soil SSL. The *Simplified Procedure* for computing $CSR_{Peak}$ is shown in the following equation:

$$CSR_{Peak} = \frac{\tau_{max}}{\sigma'_{vo}} = \left(\frac{a_{max}}{g}\right) * \left(\frac{\sigma_v}{\sigma'_{vo}}\right) * r_d \qquad \textbf{Equation 13-5}$$

Where,

$a_{max}$ = PGA, gravity (g). The PGA is determined from the 3-Point ADRS curve developed according to Chapter 12.

$\sigma_v$ = Total overburden stress

$\sigma'_{vo}$ = Effective overburden stress

$r_d$ = Shear stress reduction coefficient (dimensionless)

$\tau_{max}$ = Maximum seismic induced stress with depth. In the *Simplified Procedure* the maximum seismic induced stress ($\tau_{max}$) is approximated by the following equation.

$$\boldsymbol{\tau_{max} = \left(\frac{a_{max}}{g}\right) * \sigma_v * r_d} \qquad \textbf{Equation 13-6}$$

The shear stress reduction coefficient, $r_d$, is a parameter that describes the ratio of cyclic stresses for a flexible column to the cyclic stresses of a rigid column ($r_d = \tau_{flexible}/\tau_{rigid}$). For an $r_d = 1$, the flexibility of the soil column would correspond to rigid body behavior. One-dimensional dynamic site response studies (Seed and Idriss (1971), Golesorkhi (1989). Idriss (1999), and Cetin, et al. (2004)) have shown that the shear stress reduction factor is dependent on the ground motion characteristics (i.e., intensity and frequency content), shear wave velocity profile of the site (i.e., site stiffness), and nonlinear dynamic soil properties. Idriss (1999) performed several hundred parametric site response analyses and developed a shear stress reduction coefficient, $r_d$ that was expressed as a function of depth and seismic moment magnitude ($M_W$) as indicated in Figure 13-9.

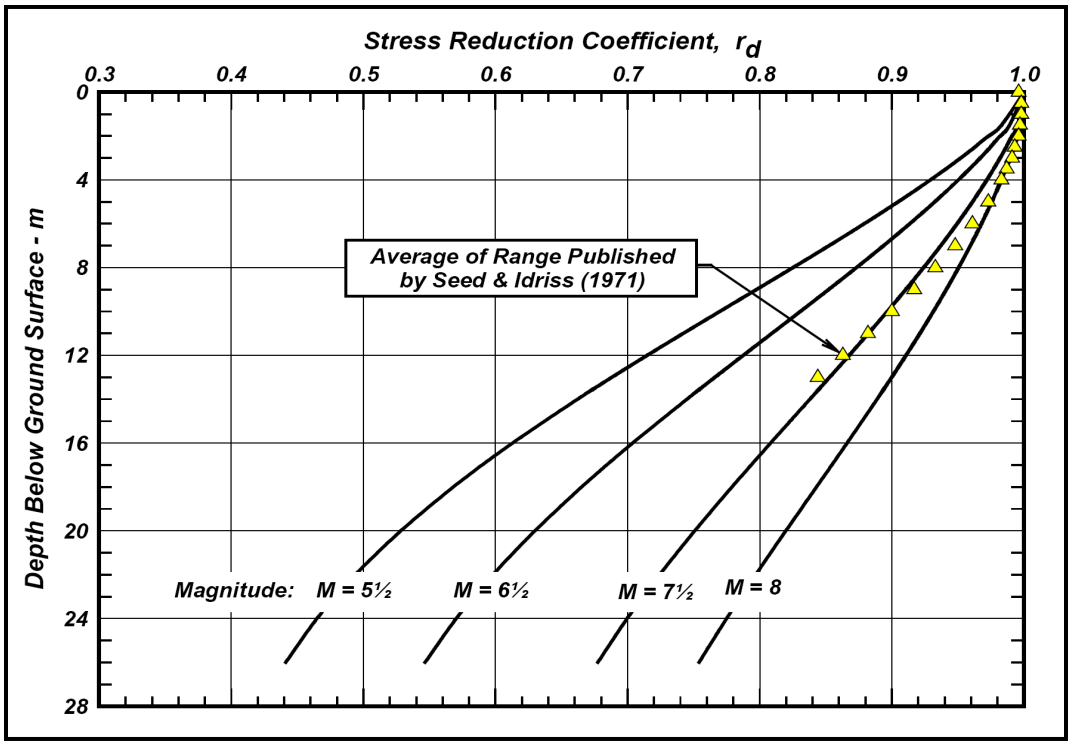


**Figure 13-9, Variations of Shear Stress Reduction Coefficient, $r_d$ (Idriss (1999))**

Shear stress reduction coefficient ($r_d$) equations for US customary units were modified from SI equations proposed by Idriss (1999) as indicated below.

$$r_d = exp\{\alpha + [\beta * (M_w)]\}$$ **Equation 13-7**

$$\alpha = -1.012 - 1.126\, sin\left[\left(\frac{\left(\frac{z}{3.28}\right)}{11.73}\right) + 5.133\right]$$ **Equation 13-8**

$$\beta = 0.106 + 0.118\, sin\left[\left(\frac{\left(\frac{z}{3.28}\right)}{11.28}\right) + 5.142\right]$$ **Equation 13-9**

Where,

z = Depth below ground surface, feet
$M_w$ = Seismic moment magnitude

Note that the arguments inside the "**sin**" terms above are in radians. For the purposes of evaluating soil SSL, the $CSR_{Peak}$ should not be evaluated using this method for depths greater than 80 feet (24 m). The uncertainty increases for shear stress reduction coefficients ($r_d$) at depths greater than $z$ > 65 feet (20 m). When the maximum seismic-induced stress ratio, $CSR_{Peak}$, is required for depths greater than 80 feet, a site-specific response analysis (Section 13.8.1.2) may be warranted with approval of the OES/GDS.

### 13.8.1.2 Site Specific Response Determination of $CSR_{Peak}$

When approved by the OES/GDS, the maximum seismic-induced stress ratio, $CSR_{Peak}$, can be computed for depths greater than 80 feet (24 m) by using the results of a site-specific seismic response analysis (Chapter 12) as indicated by the following equation.

$$CSR_{Peak} = \frac{\tau_{max}}{\sigma'_{vo}}$$ **Equation 13-10**

Where,

$\tau_{max}$ = Maximum seismic-induced cyclic shear stress obtained from the site-specific response analysis of the ground motions
$\sigma'_{vo}$ = Effective overburden stress at the depth being evaluated

Site-specific seismic response analyses referenced in Chapter 12 are typically 1-dimensional equivalent linear analyses. Because the 1-dimensional equivalent linear analyses have a reduced reliability as ground shaking levels (PGA) increase above 0.40g in softer soils or where the maximum shearing strain amplitudes exceed 1 to 2 percent, a comparison with the *Simplified Procedure* should be performed for depths greater than 80 feet (24 m) and the more conservative values should be used. In lieu of using the more conservative analytical results, the OES/GDS should be consulted to determine if a nonlinear effective stress site response method should be used to determine the maximum seismic-induced shear stress, $\tau_{max}$.

### 13.8.2 Magnitude Scaling Factor

The Magnitude Scaling Factor (MSF) is used to scale the equivalent uniform seismic-induced stresses, $CSR_{eq}$, to the number of uniform cycles that is typical of an average seismic event of magnitude $M_w$ = 7.5. A large amount of scatter in the MSF is observed from various studies presented in Youd, et al. (2001), particularly at the lower range of seismic moment magnitudes ($5.5 < M_w < 6.5$). Boulanger and Idriss (2007) have recommended MSF for Sand-Like soils ($MSF_{Sand}$) and for Clay-Like soils ($MSF_{Clay}$) as indicated in Figure 13-10. Because the predominant seismic event in South Carolina had an approximate seismic magnitude of 7.3 and the target scaling seismic is a 7.5, the variability observed in the magnitude scaling factor studies should have minimal impact on the liquefaction analyses.

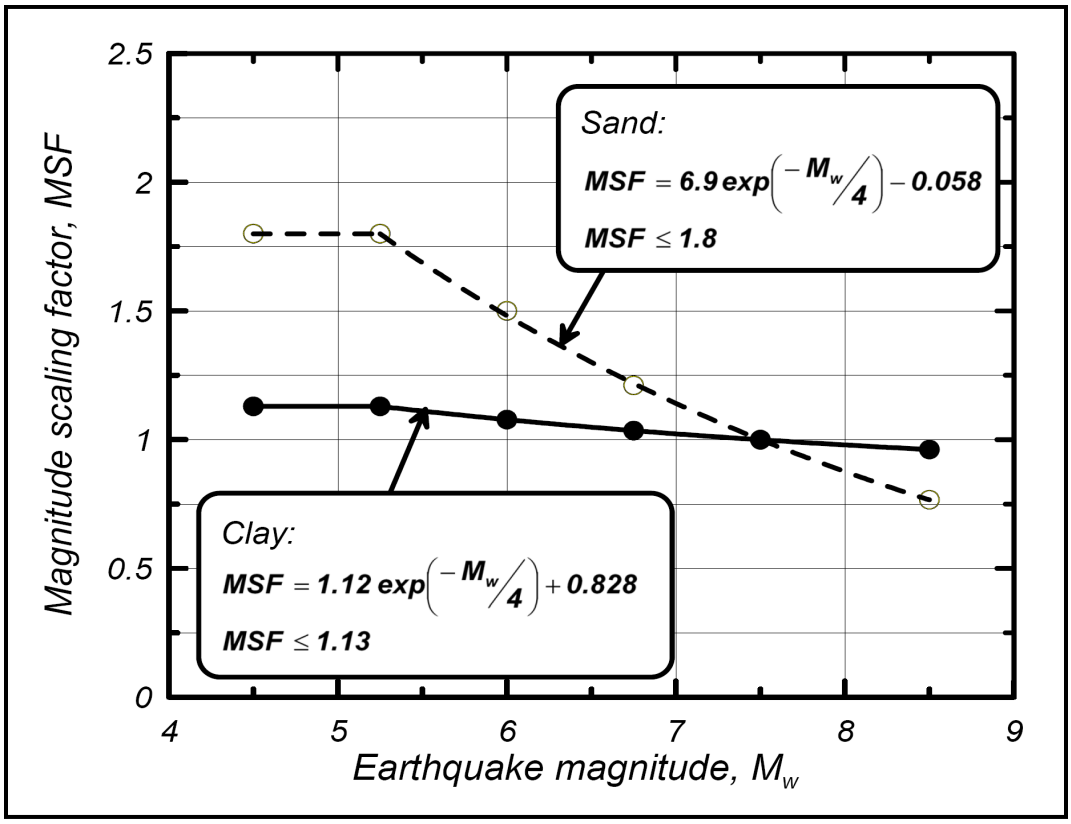


**Figure 13-10, Magnitude Scaling Factor (MSF)**
**(Boulanger and Idriss (2007) with permission from ASCE)**

In lieu of using Figure 13-10, the following equations may be used to compute the $MSF_{Sand}$ and $MSF_{Clay}$.

$$MSF_{Sand} = 6.9 * exp(-0.25 * M_w) - 0.058 \le 1.80 \quad \textbf{Equation 13-11}$$

$$MSF_{Clay} = 1.12 * exp(-0.25 * M_w) + 0.828 \le 1.13 \quad \textbf{Equation 13-12}$$

Where,

$M_w$ = Moment magnitude of the design seismic event being evaluated for soil SSL triggering.

## 13.9 CYCLIC RESISTANCE RATIO (CRR)

The soil's resistance to SSL is quantified by the CRR. The CRR for Sand-Like soils is typically characterized as a curvilinear boundary that indicates the relationship between CSR and in-situ testing results from SPT or CPTu. The CRR for Clay-Like soils is typically characterized as a linear reduction of the undrained shear strength that indicates the relationship between CSR and in-situ testing results from SPT or CPTu. A typical CRR curve for Sand-Like soils is shown in Figure 13-11(A) and for Clay-Like soils is shown in Figure 13-11(B).

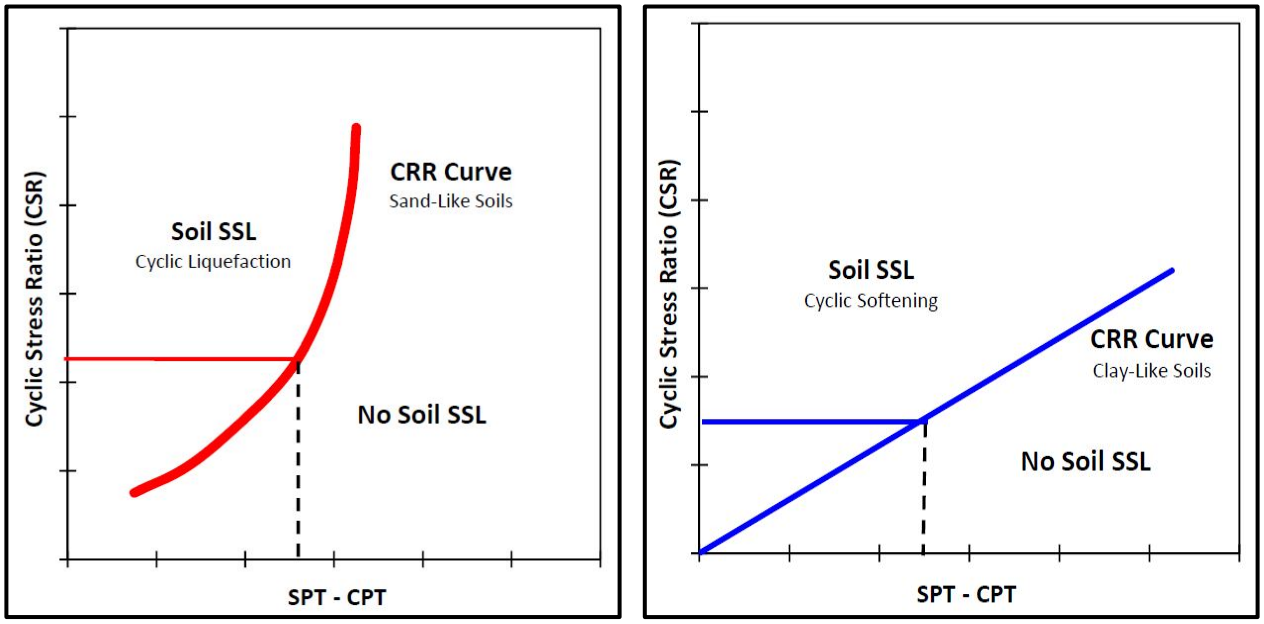


**(A) CRR Curve Sand-Like Soils** **(B) CRR Curve Clay-Like Soils**

**Figure 13-11, Typical CRR Curve**

For a specific seismic-induced CSR value, the value located on the CRR boundary establishes a threshold in-situ testing value whereas in-situ testing results greater than the threshold value will not be susceptible to soil SSL and values less than the threshold value are subject to soil SSL.

Several empirical procedures have been developed to determine the CRR of Holocene (< 10,000 years) Sand-Like soils based on in-situ testing. In-situ tests acceptable to be used on SCDOT projects are SPT and CPTu. A comparison of advantages and disadvantages of these in-situ tests for determination of CRR are presented in Table 13-2. SPT and CPTu measured results must be adjusted in accordance with subsequent Sections of this Chapter.

**Table 13-2, CRR Determination Based on Types of In-situ Testing (Modified after Youd and Idriss (1997))**

| Feature | Type of In-situ Testing | |
|---|---|---|
| | SPT | CPT |
| Number of test measurements at liquefaction sites | Substantial | Several |
| Type of stress-strain behavior influencing test | Partially Drained, Large strain | Drained, Large Strain |
| Quality control and repeatability | Poor to Good | Very Good |
| Detection of variability of soil deposits | Good | Very Good |
| Soil types in which test is recommended | Non-Gravel | Non-Gravel |
| Test provides sample of soil | Yes | No |
| Test measures index or engineering property | Index | Index |

The normalized CRR curves ($CRR^{*} = CRR_{M=7.5,1\ tsf}$) for Sand-Like soils presented in Sections 13.9.1 and 13.9.2 are magnitude weighted ($M_w$=7.5) and normalized to a reference effective overburden stress of $\sigma'_V$ = 1 tsf. These correlations were derived based on the relative state parameter index ($\xi_R$) by Idriss and Boulanger (2006). The $\xi_R$ is the difference between the $D_R$ and the $D_{R,CS}$ (the critical state $D_R$) at the same mean effective normal stress. The corresponding CRR-$\xi_R$ relationships derived from these 2 liquefaction correlations are shown in Figure 13-12 to illustrate the consistency between the SPT and CPTu methods to predict field cyclic resistance ratio. It is noted that the agreement in Figure 13-12 is for soils meeting the condition depicted in the Figure and that direct relationship between the correlated SPT and correlated CPT $\xi_R$ should not be anticipated for other soil conditions.

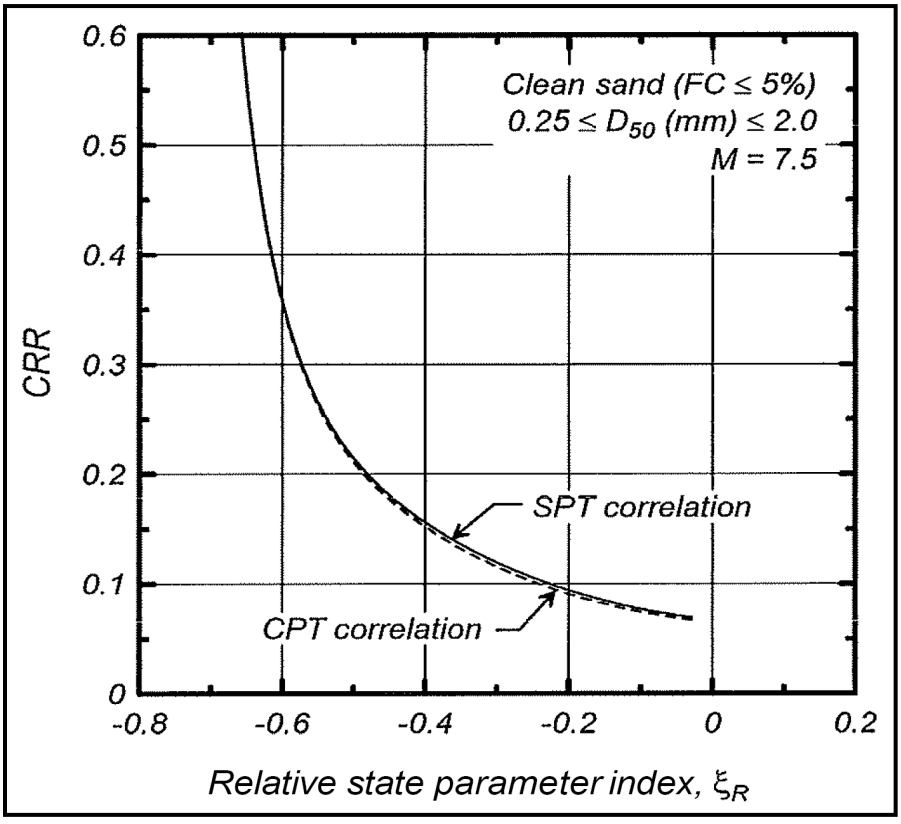


**Figure 13-12, Field CRR-$\xi_R$ Correlations Based on SPT and CPTu (Idriss and Boulanger (2006))**

The normalized $CRR^*$ = $CRR_{M=7.5,1\ tsf}$ for Clay-Like soil presented in Section 13.9.3 is magnitude weighted ($M_w$ = 7.5).

Shear wave velocities ($V_s$) and the Becker Penetration Tests (BPT) methods for determination of the soil's resistance for liquefaction shall not be used for routine SCDOT soil SSL evaluations unless approved in writing by the OES/GDS.

The $CRR^*$ correlations must be further corrected to account for the effects of high overburden stress on Sand-Like soils ($K_\sigma$); effects of soil aging in Sand-Like soils ($K_{DR}$); effects of initial static shear stress on Sand-Like Soils and Clay-Like Soils ($K_\alpha$). The $CRR^*_{eq}$ curves are computed as indicated in the following general equation:

$$\boldsymbol{CRR^*_{eq} = CRR^* * (K_\sigma) * (K_{DR}) * (K_\alpha)} \qquad \textbf{Equation 13-13}$$

Where,

CRR* = $CRR_{M=7.5,1\ tsf}$ = Magnitude weighted ($M_w$ = 7.5) and normalized ($\sigma'_v$ = 1 tsf) cyclic resistance ratio. (Sand-Like Soil: Sections 13.9.1 and 13.9.2; Clay-Like Soil: Section 13.9.3)

$K_\sigma$ = High overburden stress correction factor for Sand-Like Soils (Section 13.9.4)

$K_{DR}$ = Age and cementation correction factor for Sand-Like Soils (Section 13.9.5)

$K_\alpha$ = Static shear stress ratio correction factor for Sand-Like and Clay-Like soils (Section 13.9.6)

$CRR^*$ values determined using the procedures of Sections 13.9.1 and 13.9.2 will have a 16 percent probability of SSL occurring in these soils. In other words, soils with $CRR^*$ values that do not indicate SSL will have a 16 percent chance of actually undergoing SSL.

### 13.9.1 Sand-Like Soil - SPT Based $CRR^*$ Curves

The CRR correlations for SPT in-situ testing presented by Idriss and Boulanger (2008) shall be used to evaluate Sand-Like soils. Deterministic $CRR^*$ curves are $M_w$ weighted, adjusted to a reference effective overburden stress of $\sigma'_V$ = 1 tsf, and adjusted for fines content. Similar to the CSR, a reference seismic event of $M_w$ equal to 7.5 is used. The corrected SPT blow count ($N^*_{1,60}$) is adjusted to an equivalent clean sand (CS) blow count based on the FC as indicated by the following equation.

$$\boldsymbol{N^*_{1,60,CS} = N^*_{1,60} + \Delta N^*_{1,60}} \qquad \textbf{Equation 13-14}$$

Where,

$N^*_{1,60}$ = SPT blow count normalized to a reference effective overburden stress of $\sigma'_V$ = 1 tsf, corrected for energy (60%) (see Chapter 7). Units of blows/foot

$\Delta N^*_{1,60}$ = Fines content correction for 5% < FC < 35%. The variation in $\Delta N^*_{1,60}$ with fines content is shown in Figure 13-13

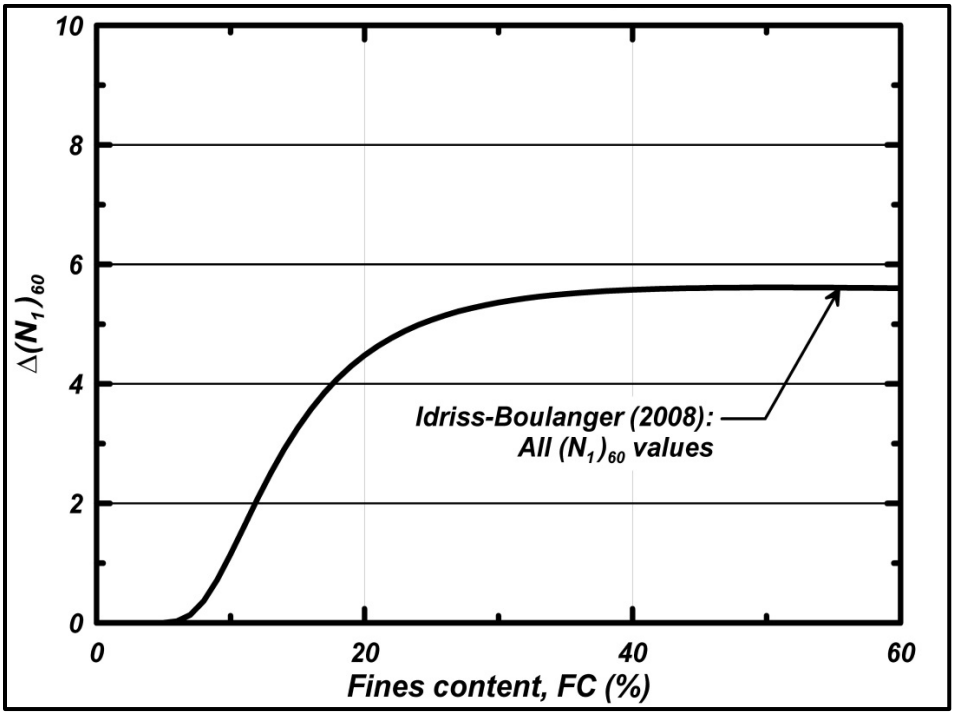


**Figure 13-13, Variation in $\Delta N^{*}_{1,60}$ With Fines Content (Idriss and Boulanger (2014))**

In lieu of using Figure 13-13 the following equation may be used.

$$\Delta N^{*}_{1,60} = exp\left[1.63 + \left(\frac{9.7}{FC+0.01}\right) - \left(\frac{15.7}{FC+0.01}\right)^{2}\right] \leq 5.5 \qquad \textbf{Equation 13-15}$$

Where,

FC = Fines content of the soil fraction passing the No. 200 sieve, percent

The Idriss and Boulanger (2006) recommended deterministic $CRR^{*}$ curve (Curve 5 in Figure 13-14) for SPT in-situ testing based on a seismic moment magnitude, $M_w$ = 7.5, effective overburden reference stress, $\sigma'_v$ = 1.0 tsf, and fines content FC < 5%.

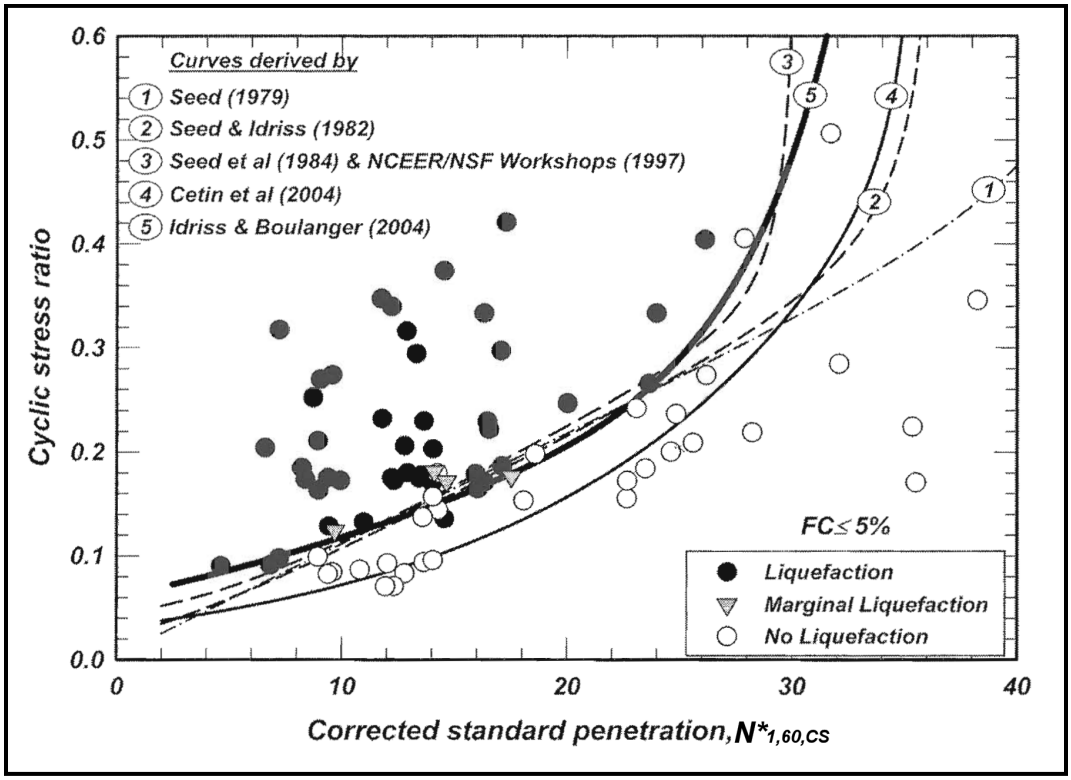


**Figure 13-14, SPT Liquefaction Triggering Correlation (CRR*)**
**$M_w$ = 7.5; $\sigma'_{vo}$ = 1.0 tsf; FC ≤ 5%**
**(Idriss and Boulanger (2006))**

In lieu of using Curve 5 in Figure 13-14, the following equation may be used.

$$CRR^* = exp\left[\left(\frac{N^*_{1,60,CS}}{14.1}\right) + \left(\frac{N^*_{1,60,CS}}{126}\right)^2 - \left(\frac{N^*_{1,60,CS}}{23.6}\right)^3 + \left(\frac{N^*_{1,60,CS}}{25.4}\right)^4 - 2.8\right] \quad \textbf{Equation 13-16}$$

Where,

$CRR^*$ = CRR for a $M_w$ of 7.5 and normalized to 1 tsf overburden pressure

$N^*_{1,60,CS}$ = Normalized corrected SPT blow count (see Chapter 7) including FC correction (see Equation 13-14), blows/foot

### 13.9.2 Sand-Like Soil - CPTu Based CRR* Curves

The CRR correlations for CPTu in-situ testing presented by Idriss and Boulanger (2008) shall be used to evaluate Sand-Like soils. Deterministic $CRR^*$ curves are $M_w$ weighted, adjusted to a reference effective overburden stress of $\sigma'_V$ = 1 tsf, and adjusted for fines content. Similarly to the CSR, a reference seismic event of $M_w$ equal to 7.5 is used. The normalized corrected CPTu tip resistance ($q_{t,1,N}$) is adjusted to an equivalent CS tip resistance based on the FC as indicated by the following equation.

$$q_{t,1,N,CS} = q_{t,1,N} + \Delta q_{t,1,N} \quad \textbf{Equation 13-17}$$

Where,

$q_{t,1,N}$ = Normalized corrected CPT tip resistance (see Chapter 7) (unitless)

$\Delta q_{t,1,N}$ = Fines content correction for FC > 5%

The variation in $\Delta q_{t,1,N}$ with fines content (FC) based on Boulanger and Idriss (2014) can be obtained from Figure 13-15 for FC > 5%.

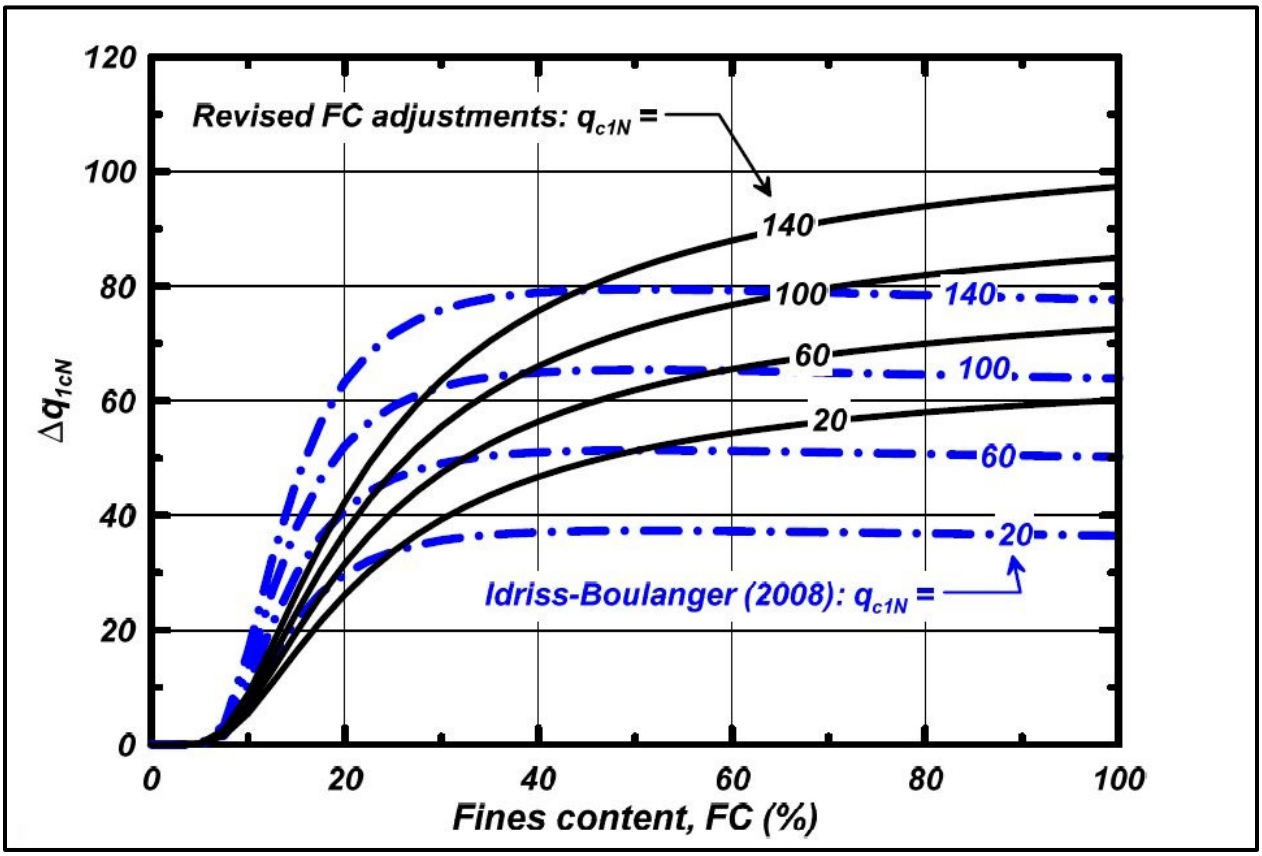


Note: $\Delta q_{c,1,N} = \Delta q_{t,1,N}$ in this Figure

**Figure 13-15, Variation in $\Delta q_{c,1,N}$ With Fines Content (Boulanger and Idriss (2014))**

In lieu of using Figure 13-15 the following equation may be used.

$$\Delta q_{t,1,N} = \left[11.9 + \left(\frac{q_{t,1,N}}{14.6}\right)\right] * exp\left[1.63 + \left(\frac{9.7}{FC+2}\right) - \left(\frac{15.7}{FC+2}\right)^2\right] \quad \textbf{Equation 13-18}$$

Where,

FC = Fines content of the soil fraction passing the No. 200 sieve, percent

Figure 13-16 shows the Boulanger and Idriss (2014) recommended deterministic CRR* curve for CPTu in-situ testing based on a seismic moment magnitude, $M_w$ = 7.5, effective overburden reference stress, $\sigma'_v$=1.0 tsf, and fines content FC < 5%.

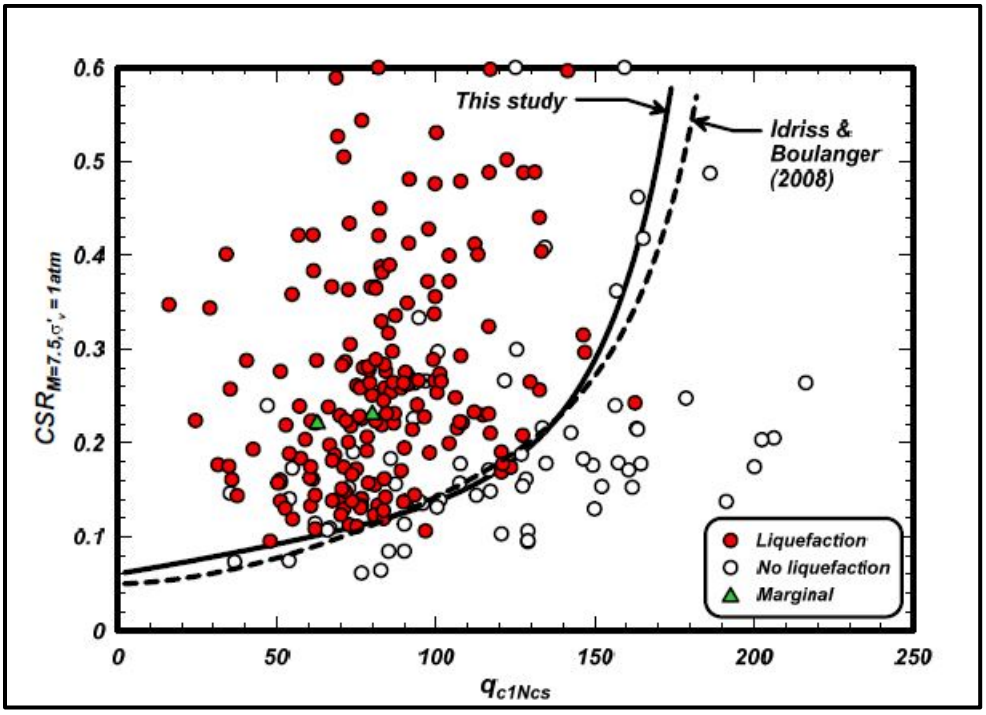


Note: $q_{c,1,N,CS} = q_{t,1,N,CS}$ in this Figure

**Figure 13-16, CPTu Liquefaction Triggering Correlation (CRR*)**
**$M_w$ = 7.5; $\sigma'_{vo}$ = 1.0 tsf; *FC* ≤ 5%**
**(Boulanger and Idriss (2014))**

In lieu of using Figure 13-16 the following equation may be used.

$$CRR^* = exp\left[\left(\frac{q_{t,1,N,CS}}{14.1}\right) + \left(\frac{q_{t,1,N,CS}}{126}\right)^2 - \left(\frac{q_{t,1,N,CS}}{23.6}\right)^3 + \left(\frac{q_{t,1,N,CS}}{25.4}\right)^4 - 2.8\right]$$ **Equation 13-19**

Where,

$CRR^*$ = CRR for a $M_w$ of 7.5 and normalized to 1 tsf overburden pressure

$q_{t,1,N,CS}$ = Normalized corrected CPT tip resistance (see Chapter 7) including FC correction (see Equation 13-17). (unitless)

### 13.9.3 Clay-Like Soil CRR* Curves

The CRR correlations presented by Idriss and Boulanger (2008) shall be used to evaluate Clay-Like soils. Deterministic CRR* curves are $M_w$ weighted. Similar to the CSR, a reference seismic event $M_w$ equal to 7.5 is used. The CRR of Clay-Like soils will typically be determined by using empirical correlations. CRR of Clay-Like soils can also be determined by cyclic laboratory testing with approval from the OES/GDS. Boulanger and Idriss (2007) developed empirical correlations based on the undrained shear strength profile and the consolidation stress history profile.

The preferred empirical correlation for determining the CRR* curves for Clay-Like soils is based on the undrained shear strength profile using the relationship shown in Figure 13-17, where undrained shear strengths have been obtained from laboratory testing. If in-situ testing methods

(SPT or CPTu) are used to estimate undrained shear strengths then CRR* correlations using the consolidation stress history profile presented in Figure 13-17 should be used as a check on the in-situ testing shear strength correlations.

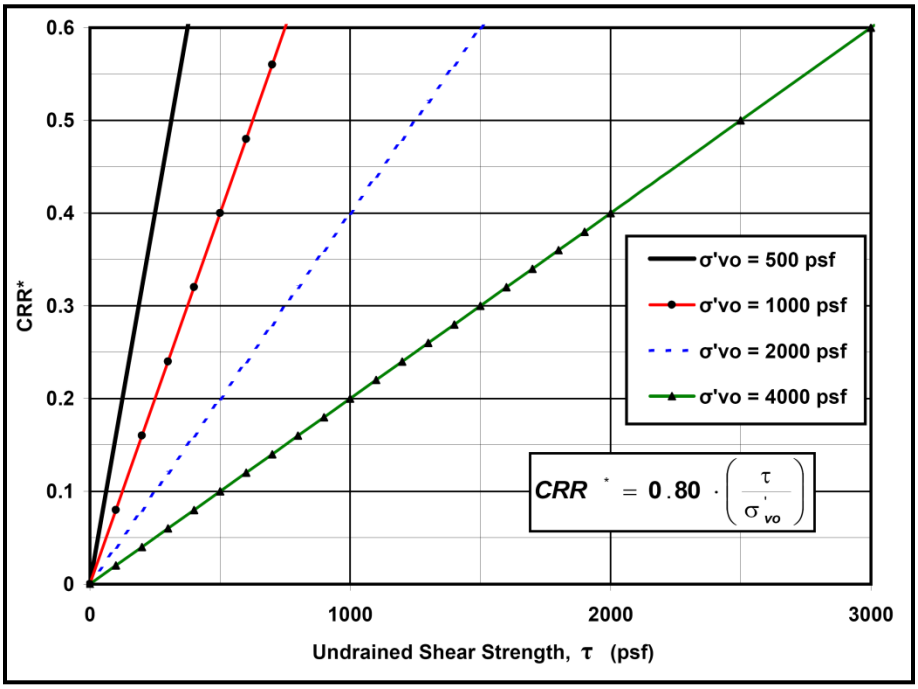


**Figure 13-17, CRR* Clay-Like – Shear Strength Correlation**
**(Modified from Boulanger and Idriss (2007) with permission from ASCE)**

In lieu of using Figure 13-17, the following equation may be used to determine the CRR* curves for Clay-Like soils.

$$CRR^* = CRR_{Mw=7.5} = 0.80 * \left(\frac{\tau}{\sigma'_{vo}}\right) \qquad \textbf{Equation 13-20}$$

Where,

$\tau$ = Undrained shear strength ($S_u$)

$\sigma'_{vo}$ = Effective overburden stress

Boulanger and Idriss (2007) have suggested using the empirical correlations developed from SHANSHEP laboratory testing (Ladd, et al. (1977)) shown in Figure 13-18. These correlations are based on a relationship between the undrained shear strength ratio and the consolidation stress history. The overconsolidation ratio (OCR) provides a measure of the consolidation stress history. These correlations require a consolidation stress history profile that is sometimes difficult to accurately evaluate without performing consolidation tests on undisturbed samples from representative depths. It has also been observed that the undrained shear strength ratio can vary based on the type of clay formation used as shown in Chapter 7 and in Figure 13-18. Estimating CRR solely from OCR should only be used for preliminary analyses or to compare with the CRR* determined by the undrained shear strength ratio, particularly if in-situ testing is used to estimate the undrained shear strength of Clay-Like soils.

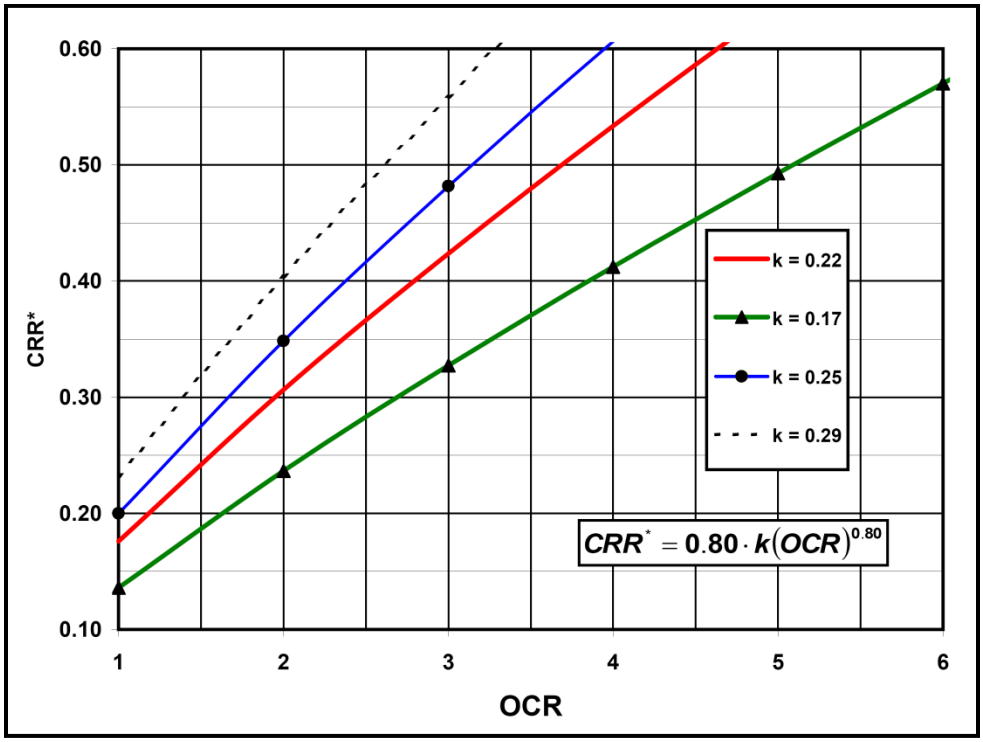


**Figure 13-18, CRR* Clay-Like Soils – OCR Correlation**

In lieu of using Figure 13-18, the following equation may be used to compute the CRR* curves for Clay-Like soils based on OCR.

$$CRR^* = 0.80 * k * (OCR)^n \qquad \textbf{Equation 13-21}$$

Where,

k = Shear strength ratio for normally consolidated soils (OCR = 1) typically ranges between 0.17 and 0.29. Use k = 0.22 (DSS testing) as recommended by Boulanger and Idriss (2007) unless laboratory testing and local correlations indicate otherwise.

OCR = Overconsolidation ratio ($\sigma'_p / \sigma'_{vo}$) (See Chapter 7)

n = Soil constant typically taken as 0.80 for unstructured and uncemented soils.

### 13.9.4 High Overburden Correction ($K_\sigma$)

The high overburden correction, $K_\sigma$, accounts for the increased susceptibility of Sand-Like soils to cyclic liquefaction, at the same CSR, under large effective overburden stresses. For Clay-Like soils there is no increased susceptibility, therefore, $K_\sigma$ = 1.0 shall be used.

The high overburden correction factors for Sand-Like soils presented by Idriss and Boulanger (2008) shall be used. These high overburden correction factors are based on the relative state parameter index ($\xi_R$), and were correlated with corrected SPT blow counts ($N^*_{1,60}$ – Section 13.9.1) and normalized corrected CPTu tip resistance ($q_{t,1,N}$ – Section 13.9.2). The high overburden corrections, $K_\sigma$, for effective overburden $\sigma'_{vo}$ > 1 tsf, are plotted for selected values of $N^*_{1,60}$ and $q_{t,1,N}$ in Figure 13-19.

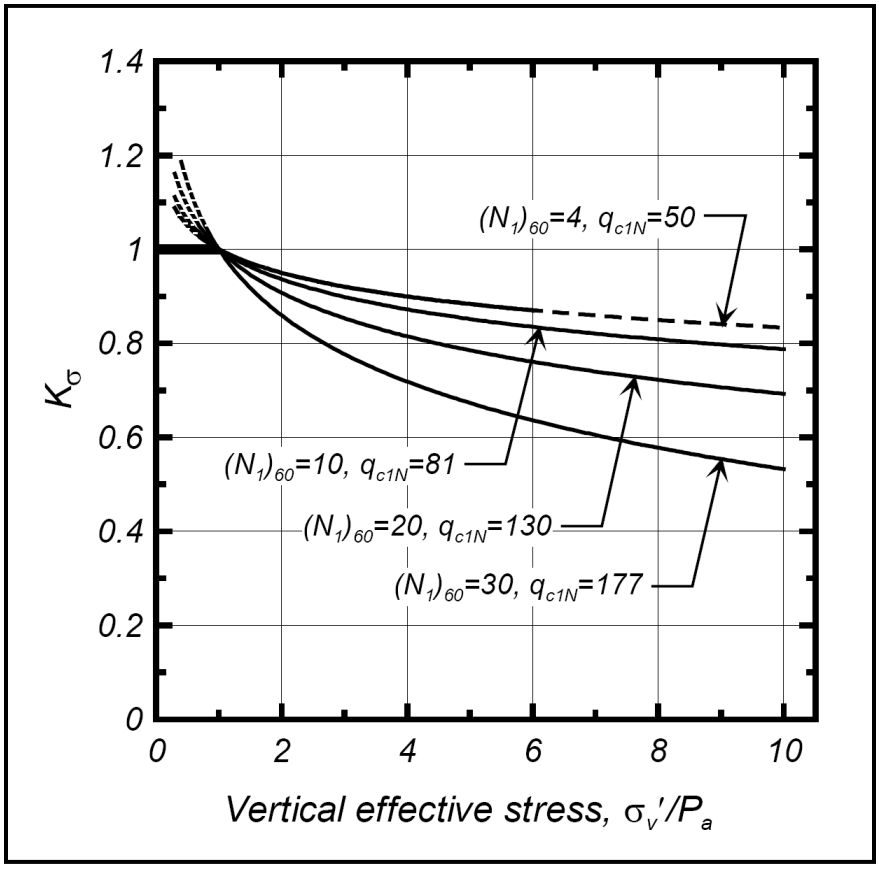


Note: $q_{c,1,N} = q_{t,1,N}$ in this Figure

**Figure 13-19, High Overburden Correction ($K_\sigma$) ($\sigma'_{vo}$ > 1 tsf) (Boulanger (2003a) with permission from ASCE)**

In lieu of using Figure 13-19, the following equation may be used to compute the $K_\sigma$ of Sand-Like soils. These correlations are based on Q ≈ 10, $K_o$ ≈ 0.45, $D_R \leq 0.9$, and $(\sigma'_{vo}/P_a) \leq 10$.

$$K_\sigma = 1 - C_\sigma * ln\left(\frac{\sigma'_{vo}}{P_a}\right) \leq 1.1 \qquad \textbf{Equation 13-22}$$

Where,

$\sigma'_{vo}$ = Effective overburden stress (or $\sigma'_v$), tsf.
$P_a$ = Atmospheric pressure, taken as 1 tsf
$C_\sigma$ = Coefficient used to correlate $D_R$, $N^*_{1,60}$, and $q_{c,1,N}$ to $K_\sigma$
$D_R$ = Relative density, where $D_R \leq 0.90$ (90%)
$N^*_{1,60}$ = Corrected SPT blow count, where $N^*_{1,60} \leq 37$ blows/foot
$q_{c,1,N}$ = Corrected and normalized CPTu tip resistance, where $q_{c,1,N} \leq 211$ unitless

The coefficient $C_\sigma$ can be expressed in terms of relative density ($D_R$), corrected SPT blow count ($N^*_{1,60}$), and corrected and normalized CPTu tip resistance ($q_{c,1,N}$) based on Boulanger and Idriss (2004) as indicated by the following equations.

$$C_\sigma = \frac{1}{18.9 - 17.3 * D_R} \leq 0.3 \qquad \textbf{Equation 13-23}$$

$$C_\sigma = \frac{1}{18.9-2.55\left(N^*_{1,60}\right)^{0.5}} \leq 0.3 \qquad \textbf{Equation 13-24}$$

$$C_\sigma = \frac{1}{37.3-8.27*\left(q_{t,1,N}\right)^{0.264}} \leq 0.3 \qquad \textbf{Equation 13-25}$$

### 13.9.5 Age Correction Factor ($K_{DR}$)

The susceptibility of Sand-Like soils to cyclic liquefaction has been found to be a function of geologic age and origin; therefore an age correction factor ($K_{DR}$) shall be applied to Sand-Like soils. Currently there is no research indicating the influence of age on the susceptibility or non-susceptibility of Clay-Like soils to undergo soil SSL, therefore, a $K_{DR}$ = 1.0 shall be used. Soils that were formed during the Quaternary period (past 1.6 million years ago - MYA), including the Holocene and Pleistocene Epochs, shall be considered to have a moderate to very high potential for liquefaction. Pre-Pleistocene age (more than 1.6 MYA) deposits shall be considered to have a lower susceptibility to liquefaction. Youd and Perkins (1978) proposed a geologic susceptibility chart for cyclic liquefaction of sedimentary cohesionless soil deposits that was based on soil deposition and geologic age as indicated in Table 13-3. The soil resistance to cyclic liquefaction tends to increase with increase in age as observed in Table 13-3. Table 13-3 shall only be used as a guide and shall not be used to determine the susceptibility of a Sand-Like soil for liquefaction.

Soil formations that are Pre-Pleistocene (>1.6 MYA) typically will have a lower susceptibility to experience cyclic liquefaction. Therefore, Pre-Pleistocene (>1.6 MYA) soils should be considered not susceptible to cyclic liquefaction. In addition, Sand-Like residual soils (see Chapter 11) should be considered to be Pre-Pleistocene and therefore, not susceptible to cyclic liquefaction. However, Pre-Pleistocene soils that have been subjected to cyclic liquefaction during previous seismic events should be treated similar to soils formed during the Holocene period. Evidence to justify the Pre-Pleistocene (>1.6 MYA) soils susceptibility to cyclic liquefaction shall be submitted to the OES/GDS for review and acceptance. Figure 13-4 provides the location of paleoliquefaction sites that have been previously studied. In addition, Figure 13-5 maps the areas in South Carolina that potentially have experienced Quaternary liquefaction (USGS website). Clay-Like residual soils that have are firm ($N^*_{1,60} \geq 5$ bpf) or have low to medium plasticity (PI $\leq$ 20) should not be considered to be susceptible to SSL. Similarly to Sand-Like residual soils, if these Clay-Like residual soils have undergone a reduction in shear strength during previous seismic events, then these soils should be checked for SSL. Clay-Like residual soils that have high plasticity to very plastic (PI $>$ 20) should be checked for SSL regardless of the N-value.

Simplified liquefaction-triggering methods used to compute the CRR for Sand-Like soils such as those proposed by Youd and Idriss (1997) and Idriss and Boulanger (2008) were developed from case histories of relatively young Holocene (< 10,000 years ago) soils. A study by Leon, et al. (2006) has demonstrated that Pleistocene Sand-Like soils in the upper 20 feet of several locations within the South Carolina Coastal Plain may have increased resistance to liquefaction due to aging. The location of paleoliquefaction sites in the Coastal Plain that were used by Leon, et al. (2006) are shown in Figure 13-4.

**Table 13-3, Liquefaction Susceptibility of Sedimentary Deposits (Modified after Youd and Perkins (1978) with permission from ASCE)**

| Type of Deposit [1] | General Distribution of Cohesionless Sediments in Deposits | Likelihood that Cohesionless Sediments, When Saturated, Will be Susceptible to Liquefaction (By Age of Deposit) | | | |
|---|---|---|---|---|---|
| | | Modern < 500 yr | Holocene 500 yr to 10 ka | Pleistocene 10ka – 1.6 MYA | Pre-Pleistocene > 1.6 MYA |
| **(a) Continental Deposits** | | | | | |
| River Channel | Locally Variable | Very High | High | Low | Very Low |
| Floodplain | Locally Variable | High | Moderate | Low | Very Low |
| Alluvial Fan & Plain | Widespread | Moderate | Low | Low | Very Low |
| Marine Terraces & Plains | Widespread | --- | Low | Very Low | Very Low |
| Delta and Fan-delta | Widespread | High | Moderate | Low | Very Low |
| Lacustrine and Playa | Variable | High | Moderate | Low | Very Low |
| Colluvium | Variable | High | Moderate | Low | Very Low |
| Talus | Widespread | Low | Low | Very Low | Very Low |
| Dunes | Widespread | High | Moderate | Low | Very Low |
| Loess | Variable | High | High | High | Unknown |
| Glacial Till | Variable | Low | Low | Very Low | Very Low |
| Tuff | Rare | Low | Low | Very Low | Very Low |
| Tephra | Widespread | High | High | Unknown | Unknown |
| Residual Soils | Rare | Low | Low | Very Low | Very Low |
| Sebka | Locally Variable | High | Moderate | Low | Very Low |
| **(b) Coastal Zone** | | | | | |
| Delta | Widespread | Very High | High | Low | Very Low |
| Estuarine | Locally Variable | High | Moderate | Low | Very Low |
| Beach - High Wave-energy | Widespread | Moderate | Low | Very Low | Very Low |
| Beach - Low Wave-energy | Widespread | High | Moderate | Low | Very Low |
| Lagoonal | Locally Variable | High | Moderate | Low | Very Low |
| Fore Shore | Locally Variable | High | Moderate | Low | Very Low |
| **(c) Artificial** | | | | | |
| Uncompacted Fill | Variable | Very High | --- | --- | --- |
| Compacted Fill | Variable | Low | --- | --- | --- |

Definitions:
ka = thousands of years ago
Mya = millions of years ago

[1] Notes:
The above types of soil deposits may or may not exist in South Carolina. All of the soil deposits included by the original authors have been kept for completeness.

A study was recently conducted at the Savannah River Site (SRS) by Lewis, et al. (2007) to re-evaluate the soil aging effects on the liquefaction resistance of Sand-Like soils that were encountered within shallow subsurface Tertiary soils from the Eocene (53 MYA) and Miocene (23 MYA) Epochs. The results of these and other studies indicate that there is a significant increase in the CRR of sand with time as indicated by Figure 13-20.

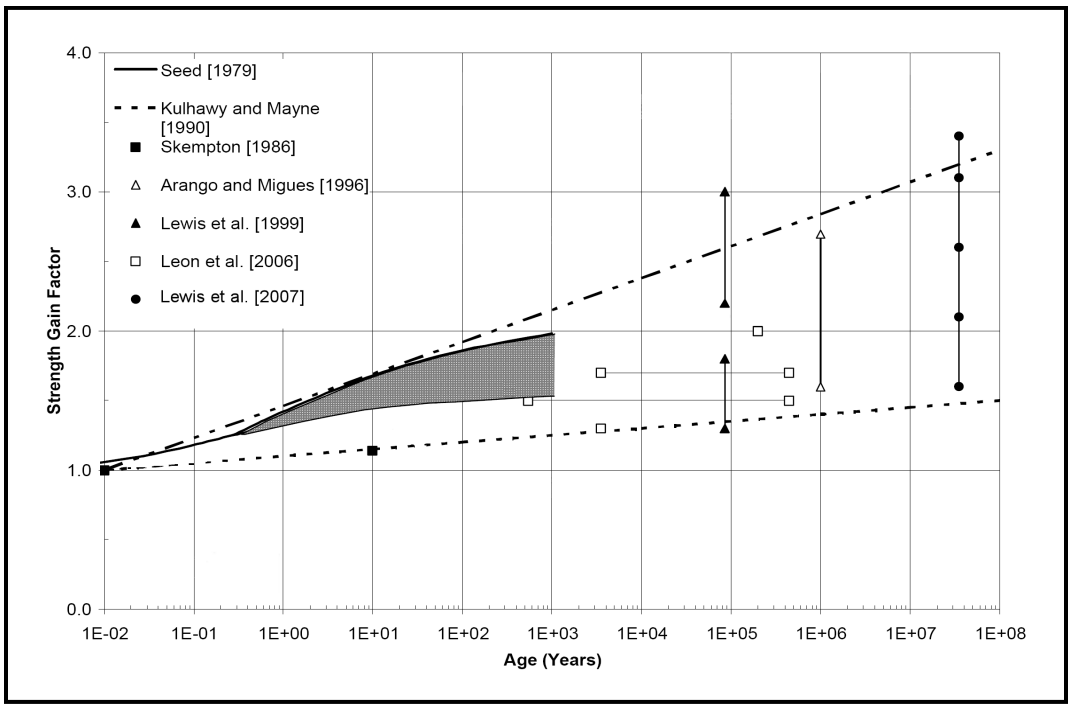


**Figure 13-20, Sand-Like Soil Strength Gain With Age (Adapted from Lewis, et al. (2007))**

Hayati and Andrus (2008 and 2009) reviewed the results of 16 published studies on the effects of aging on liquefaction resistance of soils and developed a regression line (Solid Line) shown in Figure 13-21 that represents the average variation in liquefaction $K_{DR}$ with time (t). The $K_{DR}$ is the ratio of resistance-corrected cyclic resistance ratio of the aged soil ($CRR_{DR}$) to the cyclic resistance ratio of recently deposited soil ($CRR_{Holocene}$) as indicated by the following equation.

$$K_{DR} = \frac{CRR_{DR}}{CRR_{Holocene}} \qquad \textbf{Equation 13-26}$$

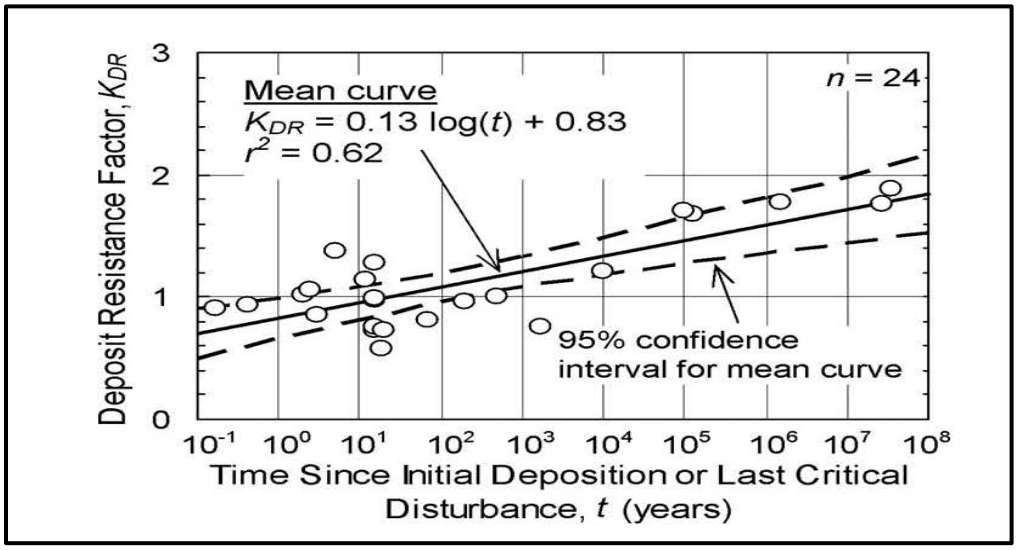


**Figure 13-21, Relationship Between Strength Gain Factor and Time (Hayati and Andrus, 2009 with permission from ASCE)**

There are 2 methods that may be used to develop $K_{DR}$. The first is the measured to estimated $V_s$ ratio (MEVR). The second uses the actual age of the formation. It should be noted that the use of age is limited to non-cemented soils and those soils that have a good prediction of age. Both methods are discussed in the following Sections.

### 13.9.5.1 $K_{DR}$ using MEVR

The use of MEVR is the preferred method for determining $K_{DR}$. MEVR is an index that quantifies the aging processes during the time since deposition or last critical disturbance (e.g., liquefaction or excavation and placement). In addition, $K_{DR}$ also accounts for cementation and stress history. The measured $V_s$ shall conform to the requirements contained in other Chapters of the GDM.

MEVR may be determined using either SPT or CPTu data Hayati and Andrus (2008 and 2009) as indicated in the following equations.

$$\boldsymbol{MEVR = \frac{(V_{s,1,CS})_{meas}}{(V_{s,1,CS})_{SPT}}} \qquad \textbf{Equation 13-27}$$

$$\boldsymbol{MEVR = \frac{(V_{s,1,CS})_{meas}}{(V_{s,1,CS})_{CPT}}} \qquad \textbf{Equation 13-28}$$

Where,

$(V_{s,1,CS})_{meas}$ = Measured shear wave velocity corrected for overburden and fines content, ft/sec

$(V_{s,1,CS})_{SPT}$ = Estimated shear wave velocity based on SPT N-values corrected for overburden and fines content (see Chapter 7), ft/sec

$(V_{s,1,CS})_{CPT}$ = Estimated shear wave velocity based CPTu data corrected for overburden and fines content (see Chapter 7), ft/sec

Hayati and Andrus (2009) recommend the following $K_{DR}$ and MEVR relationship be used.

$$\boldsymbol{K_{DR} = (1.08 * MEVR) - 0.08} \qquad \textbf{Equation 13-29}$$

### 13.9.5.2 $K_{DR}$ Based on Deposit Age

As an alternate to determining $K_{DR}$ using MEVR the actual age of the soil may be used. The age determination shall be from either first deposition or from the last critical disturbance (e.g., liquefaction or excavation and placement), whichever is most recent. In addition, these soils cannot be cemented for this procedure to be used. Therefore, because of the critical nature of the age determination, the age and time since liquefaction event for a specific soil formation shall be determined either by a Professional Geologist (PG) or Professional Engineer (PE). The PG or PE shall be registered in South Carolina and shall be required to provide a minimum of 3 years of experience in determining the age of a soil formation. A separate letter signed and sealed by the professional making the age and time since last liquefaction event determination shall be required and shall be included in the geotechnical engineering reports.

A liquefaction age correction factor of $K_{DR}$ = 1.0 corresponds to a soil deposit with an age of approximately 23 years. The t is the time since initial deposition ($K_{DR}$ = 1.0) or critical disturbance in years, whichever is most recent. Critical disturbance occurs when the effects of soil aging are removed as a result of grain-to-grain contacts being broken and reformed such as has been observed when Sand-Like soils experience cyclic liquefaction.

The $K_{DR}$ shown in Figure 13-21 can be computed using the following equation.

$$K_{DR} = (0.13 * log_{10} t) + 0.83 \leq 2.09 \qquad \textbf{Equation 13-30}$$

Where,

t = Time since initial soil deposition or last critical disturbance (e.g., liquefaction), whichever is most recent, years

### 13.9.6 Static Shear Stress Ratio Correction Factor ($K_\alpha$)

The static shear stress ratio correction factor, $K_\alpha$, accounts for the effects of initial static shear stresses on cyclic resistance of the soils beneath sloping ground. Sloping ground for SCDOT projects is any site that contains an embankment or free-face.

The static shear stresses are typically expressed as the static shear stress ratio ($\alpha$) that is defined as the initial static shear stress ($\tau_{static}$) divided by the effective vertical (normal) consolidation stress ($\sigma'_{vc}$) as indicated by the following equation.

$$\alpha = \frac{\tau_{static}}{\sigma'_{vc}} = \frac{\tau_{static}}{\sigma'_{vo}} \qquad \textbf{Equation 13-31}$$

The initial static shear stress ($\tau_{static}$) is the static soil shear stress that exists prior to the seismic shaking onset and can be computed as indicated in Section 13.9.6.1. The effective normal consolidation stress is typically assumed to be equal to the effective overburden stress ($\sigma'_{vc}$ = $\sigma'_{vo}$) because most design situations assume enough time has elapsed that the soils have been fully consolidated under sustained loading. For under consolidated soils, the existing effective consolidation stress ($\sigma'_{vc}$) shall be used. $K_\alpha$ is defined by the following equation.

$$K_\alpha = \frac{(CRR)_\alpha}{(CRR)_{\alpha=0}} \qquad \textbf{Equation 13-32}$$

Where,

$CRR_\alpha$ = CRR at some value of $\alpha$

$CRR_{\alpha=0}$ = CRR at a value of $\alpha$ = 0

$K_\alpha$ for Sand-Like soils and Clay-Like soils can be computed in accordance with Sections 13.9.6.2 and 13.9.6.3, respectively.

The static shear stress ratio (SSSR) $K_\alpha$ can be used with the *Simplified Procedure* to evaluate the effects of initial static shear stresses for sites containing embankments or ERSs. This is

accomplished by multiplying the SSSR $K_\alpha$ by the soil's CRR* as indicated in this Section. The SSSR $K_\alpha$ proposed by Idriss and Boulanger (2008) is computed as indicated in Section 13.9.6. The SSSR $K_\alpha$ method is limited to a maximum initial static stress ratio $\alpha$ less than or equal to 0.35 ($\alpha \leq 0.35$). When $\alpha$ is greater than 0.35 ($\alpha > 0.35$) then the procedure provided in Appendix I shall be used. Because of the difficulty in determining $K_\alpha$, $K_\alpha$ can be assumed to be 1.0 for either Sand-Like soils or Clay-Like soils. However, $K_\alpha$ may be determined as indicated in the following Sections.

### 13.9.6.1 Initial Static Shear Stress ($\tau_{static}$) of Soils

The $\tau_{static}$ for each soil layer (Sand-Like soils and Clay-Like soils) can be computed by performing a slope stability analysis of the pre-failure geometry with reduced soil shear strengths that achieves a condition of the slope just being stable (i.e., FS = 1 or $\varphi$ = 1). The slope stability analysis shall be performed in accordance with Chapter 17 with Spencer's method (Spencer (1967)). The slope stability analysis should be evaluated using both circular and sliding wedge potential failure surfaces. Determine the slope stability ratio, $(D/C)_{SSSR}$ using the following equation.

$$\left(\frac{D}{C}\right)_{SSSR} = \frac{1}{FS_{SSSR}} = \varphi_{SSSR} = 1 \qquad \textbf{Equation 13-33}$$

The $\tau_{static}$ is defined as the soil shear stress along the failure surface that corresponds to slope stability ratio of $(D/C)_{Stability} = 1$. The $\tau_{static}$ along the critical failure surface can be computed by reducing soil shear strengths based on the computed slope stability ratio, $(D/C)_{Stability}$ for the pre-failure geometry. The reduced undrained shear strengths for cohesive soil layers, $c_{static}$, can be computed using the following equation.

$$c_{static} = c * \left(\frac{D}{C}\right)_{SSSR} = \frac{c}{FS_{SSSR}} = c * \varphi_{SSSR} \qquad \textbf{Equation 13-34}$$

Where,

$c_{static}$ = Reduced undrained shear strength required to just maintain stability (i.e., $\varphi_{SSSR}$ = 1)

c = Undrained shear strength, $S_u$ = c

$\left(\frac{D}{C}\right)_{SSSR}$ = Demand to capacity ratio for the pre-failure geometry where the Demand equals the Capacity

$FS_{SSSR}$ = Factor of Safety for the pre-failure geometry where the Factor of Safety equals 1

$\varphi_{SSSR}$ = Resistance Factor for the pre-failure geometry where the soil resistance is equal to the soil loading

The $\tau_{static}$ along the critical failure surface for cohesive soils is computed by the following equation.

$$\tau_{static} = c_{static} \qquad \textbf{Equation 13-35}$$

The reduced drained shear strength for a cohesionless soil layer is computed by reducing the internal friction angle, $\phi_{static}$, and can be computed using the following equation.

**Equation 13-36**

$$\boldsymbol{\phi_{static} = tan^{-1}\left[tan\,\phi * \left(\frac{D}{C}\right)_{SSSR}\right] = tan^{-1}[tan\,\phi * (\varphi_{SSSR})]}$$

Where,

$\phi_{static}$ = Reduced internal friction angle required to just maintain stability (i.e., $\phi_{SSSR} = 1$)

$\phi$ = Internal friction angle

$\left(\frac{D}{C}\right)_{SSSR}$ = Demand to capacity ratio for the pre-failure geometry where the Demand equals the Capacity

$\varphi_{SSSR}$ = Resistance Factor for the pre-failure geometry where the soil resistance is equal to the soil loading

The $\tau_{static}$ along the critical failure surface for cohesionless soils is computed by the following equation.

$$\boldsymbol{\tau_{static} = \sigma'_{vo} * tan\,\phi_{static}} \quad \textbf{Equation 13-37}$$

Alternatively, some slope stability software allows the input of the shear strength ratio directly ($\tau/\sigma'_{vo}$). The $\alpha$ for Clay-Like soils can be computed using the following equation:

$$\boldsymbol{\alpha = \left(\frac{\tau_{static}}{\sigma'_{vo}}\right) = \left(\frac{\tau}{\sigma'_{vo}}\right) * \left(\frac{D}{C}\right)_{SSSR} = \frac{\tau}{\sigma'_{vo} * FS_{SSSR}} = \varphi_{SSSR} * \left(\frac{\tau}{\sigma'_{vo}}\right)} \quad \textbf{Equation 13-38}$$

The $\alpha$ for Sand-Like soils can be computed using the following equation:

$$\boldsymbol{\alpha = \left(\frac{\tau_{static}}{\sigma'_{vo}}\right) = (tan\,\phi) * \left(\frac{D}{C}\right)_{SSSR} = \frac{tan\,\phi}{FS_{SSSR}} = \varphi_{SSSR} * tan\,\phi} \quad \textbf{Equation 13-39}$$

The computed $\tau_{static}$ should be checked by using the reduced soil shear strengths ($\tau_{static}$ or $\alpha$) to perform a slope stability analysis and to determine if the slope stability ratio, $(D/C)_{SSSR}$, for the critical failure surface corresponds to a slope stability ratio of $(D/C)_{SSSR} = \varphi_{SSSR} = 1$.

If the slope stability ratio of $(D/C)_{SSSR} \neq 1$, the soil shear strength should be further adjusted until a slope stability ratio of $(D/C)_{SSSR} = 1$ is achieved.

The $\tau_{static}$ ($(D/C)_{SSSR} = 1$) for each soil layer (Sand-Like soils and Clay-Like soils) can be computed by performing a slope stability back analysis of the pre-failure geometry using reduced soil shear strengths. The slope stability search should evaluate both circular and sliding wedge potential failure surfaces in accordance with Chapter 17 with Spencer's method being required. Slope stability back analysis of the static shear stress ($\tau_{static}$) for a single soil layer is relatively straight forward when compared to slope failure surfaces that have multiple soil layers.

The soil layers that intersect the failure surface are initially assigned reduced "trial" soil shear strengths ($\tau$). The soil shear strength ($\tau$) for the layer is varied iteratively until the slope stability ratio, $(D/C)_{SSSR} = 1$ that is equivalent to the static driving stress ($\tau_{static}$) induced by the slope on the subgrade soils. Alternatively, some slope stability software programs allow the input of the static shear strength ratio directly ($\alpha = \tau_{static}/\sigma'_{vo}$). For this software option, the static shear strength ratio ($\alpha$) is varied iteratively until the slope stability ratio, $(D/C)_{SSSR} = 1$ is obtained.

### 13.9.6.2 $K_\alpha$ For Sand-Like Soils

Harder and Boulanger (1997) observed variations in cyclic shear stresses as a function of $D_R$ and $\sigma'_{vo}$ when they summarized available cyclic laboratory test data. It was observed that cyclic resistance of dense sands can increase significantly as $\alpha$ increases and that cyclic resistance of loose sands decreases as $\alpha$ increases.

Boulanger (2003b) developed $K_\alpha$ for Sand-Like soils based on $\xi_R$. These correction factors were then correlated for use with normalized SPT N-values ($N^*_{1,60}$ – Section 13.9.1) normalized and effective overburden corrected CPT tip resistance ($q_{c,1,N}$ – Section 13.9.2). The $K_\alpha$ for selected effective overburden stresses of $\sigma'_{vo}$ = 1 tsf and $\sigma'_{vo}$ = 4 tsf, $K_o$ = 0.45 and Q = 10 (Sand), are provided for SPT values of $N^*_{1,60}$ in Figure 13-22 and CPT values of $q_{c,1,N}$ in Figure 13-23.

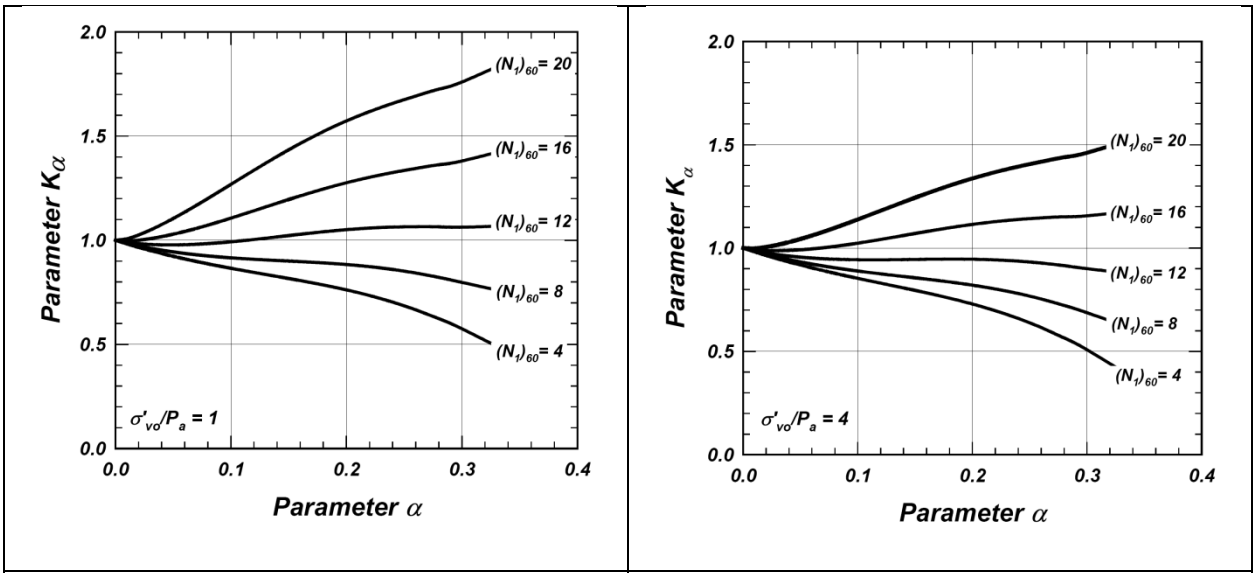


**(a) Effective Vertical Stress, $\sigma'_{vo}$ = 1 tsf** | **(b) Effective Vertical Stress, $\sigma'_{vo}$ = 4 tsf**

**Figure 13-22, Variations of $K_\alpha$ with SPT Blow Count ($N^*_{1,60}$) (Idriss and Boulanger (2003))**

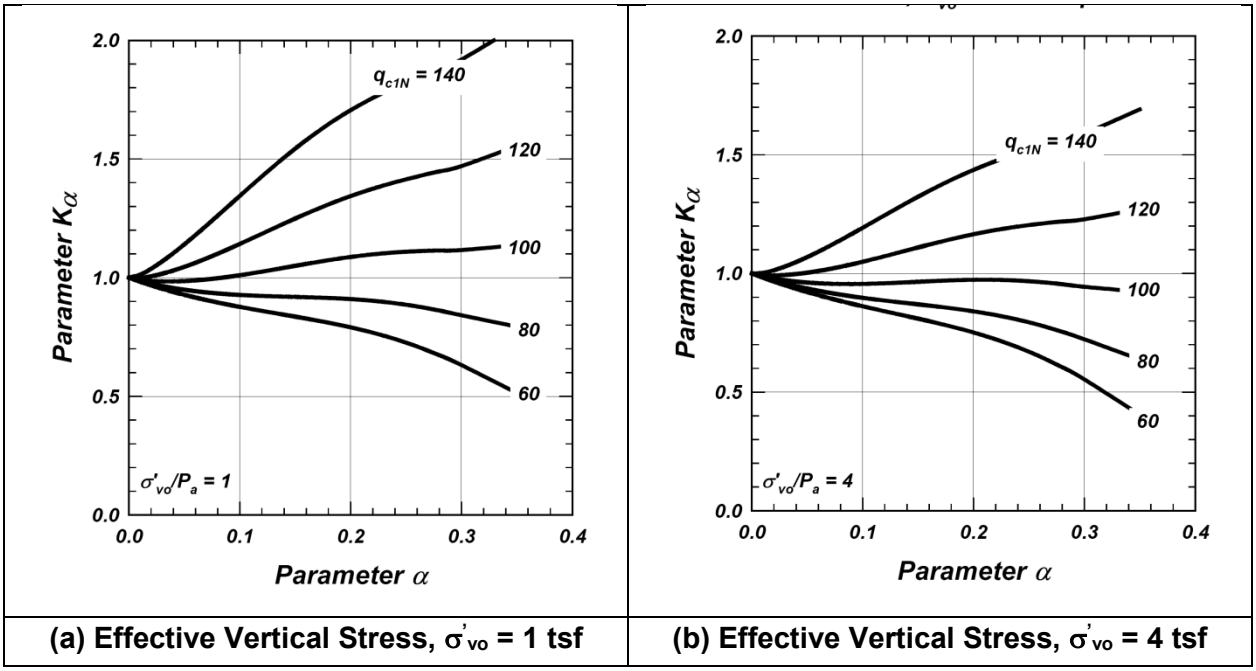


**(a) Effective Vertical Stress, $\sigma'_{vo}$ = 1 tsf** | **(b) Effective Vertical Stress, $\sigma'_{vo}$ = 4 tsf**

**Figure 13-23, Variations of $K_\alpha$ with CPT Tip Resistance ($q_{c,1,N}$) (Idriss and Boulanger (2003))**

In lieu of using Figures 13-22 and 13-23, the following equation may be used to compute $K_\alpha$. The following equations were developed from data that limit the static shear stress ratio to $\alpha \leq 0.35$ and relative state parameter index to $-0.6 \leq \xi_R \leq 0.1$.

$$K_\alpha = a + b * \left[exp\left(\frac{-\xi_R}{c}\right)\right] \quad \textbf{Equation 13-40}$$

Where,

$a = 1267 + 636\alpha^2 - (634 \cdot \exp(\alpha)) - (632 \cdot \exp(-\alpha))$

$b = \exp(-1.11 + 12.3\alpha^2 + (1.31 \cdot \ln(\alpha + 0.0001)))$

$c = 0.138 + 0.126\alpha + 2.52\alpha^3$

$\alpha$ = Static shear stress ratio as per Equation 13-39 and Section 13.9.6.1 (limited to $\alpha \leq 0.35$)

$\xi_R$ = Relative state parameter index used to correlate $D_r$, $N^*_{1,60}$, and $q_{c,1,N}$ to $K_\alpha$ (Limited to: $-0.6 \leq \xi_R \leq 0.1$)

$$\xi_R = \frac{1}{Q - \Psi} - D_r \quad \textbf{Equation 13-41}$$

$$\xi_R = \frac{1}{Q - \Psi} - \left(\frac{N^*_{1,60}}{46}\right)^{0.5} \quad \textbf{Equation 13-42}$$

$$\xi_R = \frac{1}{Q - \Psi} - \left[0.478 * \left(q_{c,1,N}\right)^{0.264} - 1.063\right] \quad \textbf{Equation 13-43}$$

$$\Psi = ln\left[\frac{100*(1+2*K_o)*\sigma'_{vo}}{3*P_a}\right] \quad \textbf{Equation 13-44}$$

Where,

$D_r$ = Relative density, where $D_r \leq 0.90$ (90%)

$N^*_{1,60}$ = Standardized and normalized SPT blow count, where $N^*_{1,60} \leq 37$ blows/foot

$q_{c,1,N}$ = Normalized CPT tip resistance, where $q_{c,1,N} \leq 211$ (unitless)

Q = Empirical Constant: Q=10 for Quartz and feldspar (Sand), Q=8 for limestone, Q=7 for anthracite, and Q=5.5 for chalk.

$K_o$ = At-rest lateral earth pressure coefficient

$\sigma'_{vo}$ = Effective vertical overburden stress, tsf

$P_a$ = Atmospheric Pressure, tsf

The procedure provided in the preceding paragraphs is complex. Therefore, the $K_\alpha$ provided in Table 13-4 may be used. Note that values provided are based on an $\alpha$ less than or equal to 0.35 ($\alpha \leq 0.35$) and an overburden stress of less than 4 tsf (approximately 50 feet of fill). These values are anticipated to be conservative. The GEOR may elect to use the proceeding equations to determine $K_\alpha$. The GEOR shall provide the necessary computations used to determine $K_\alpha$. For $N^*_{1,60}$ and $q_{c,1,N}$ that between the values indicated linear interpolation may be used.

**Table 13-4, Simplified $K_\alpha$ Values for Sand-Like Soils**

| $N^*_{1,60}$ | $K_\alpha$ | $q_{c,1,N}$ | $K_\alpha$ |
|---|---|---|---|
| $\leq 4$ | 0.50 | $\leq 60$ | 0.50 |
| 8 | 0.75 | 80 | 0.75 |
| $\geq 12$ | 1.00 | $\geq 100$ | 1.00 |

### 13.9.6.3 $K_\alpha$ For Clay-Like Soils

Boulanger and Idriss (2004 and 2007) developed $K_\alpha$ for Clay-Like soils based on laboratory testing of Drammen clay (Goulois, et al. (1985)) that was consolidated under a sustained static shear stress. The relationship developed from these laboratory tests for $K_\alpha$ versus $(\tau_{static}/S_U)_{\alpha=0}$ for Clay-Like soils are shown in Figure 13-24.

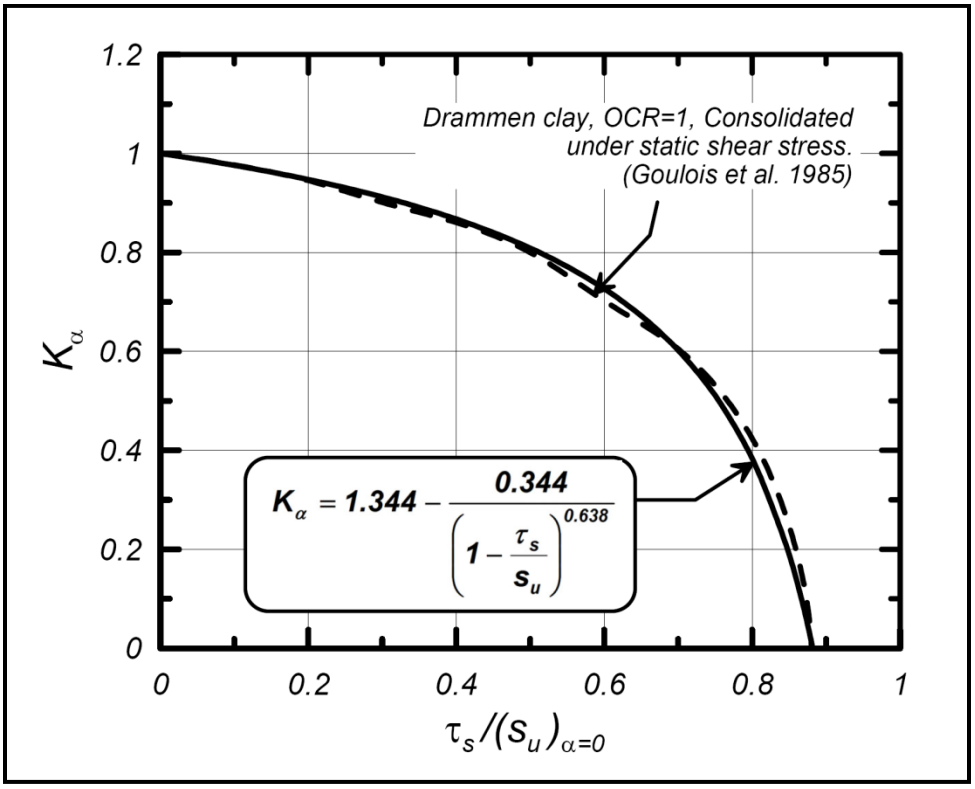


$\tau_s = \tau_{static}$

**Figure 13-24, $K_\alpha$ versus $(\tau_s/S_U)_{\alpha=0}$ For Clay-Like Soil (NC Drammen Clay) (Boulanger and Idriss (2004))**

The $K_\alpha$ relationship shown in Figures 13-24 is presented in the following equation as a function of $(\tau_{static}/S_u)$ and $(\alpha = \tau_{static}/\sigma'_{vc})$.

$$K_\alpha = 1.344 - \frac{0.344}{\left(1-\frac{\tau_{static}}{S_u}\right)^{0.638}} = 1.344 - \frac{0.344}{\left[1-\left(\frac{\alpha}{S_u/\sigma'_{vo}}\right)\right]^{0.638}} \qquad \textbf{Equation 13-45}$$

Where,

$\tau_{static}$ = Initial static shear stress

$S_u$ = Undrained shear strength

$\sigma'_{vc}$ = Effective vertical consolidating stress

$S_u/\sigma'_{vc}$ = Undrained shear strength ratio (See Chapter 7)

$\alpha$ = Static shear stress ratio as per Equation 13-38 and Section 13.9.6.1 (limited to $\alpha \leq 0.35$)

Boulanger and Idriss (2007) recommended using an empirical shear strength ratio relationship $(S_u/\sigma'_{vc})$ such as those developed by Ladd and Foot (1974) that take the form of the following equation:

$$\left(\frac{S_u}{\sigma'_{vo}}\right) = k * (OCR)^n \qquad \textbf{Equation 13-46}$$

Where,

k = Shear strength ratio for normally consolidated soils (OCR=1). Typically range between 0.17 and 0.29. Use k=0.22 (DSS testing) as recommended by Boulanger and Idriss (2007) unless laboratory testing available.

OCR = Overconsolidation ratio ($\sigma'_p / \sigma'_{vo}$) (See Chapter 7)

n = Soil constant typically taken as 0.80 for unstructured and uncemented soils.

The $K_\alpha$ presented in Equation 13-45 can be combined with the empirical shear strength ratio shown in Equation 13-46 to develop $K_\alpha$ as a function of the consolidation stress history as shown in Figure 13-25 and Equation 13-47.

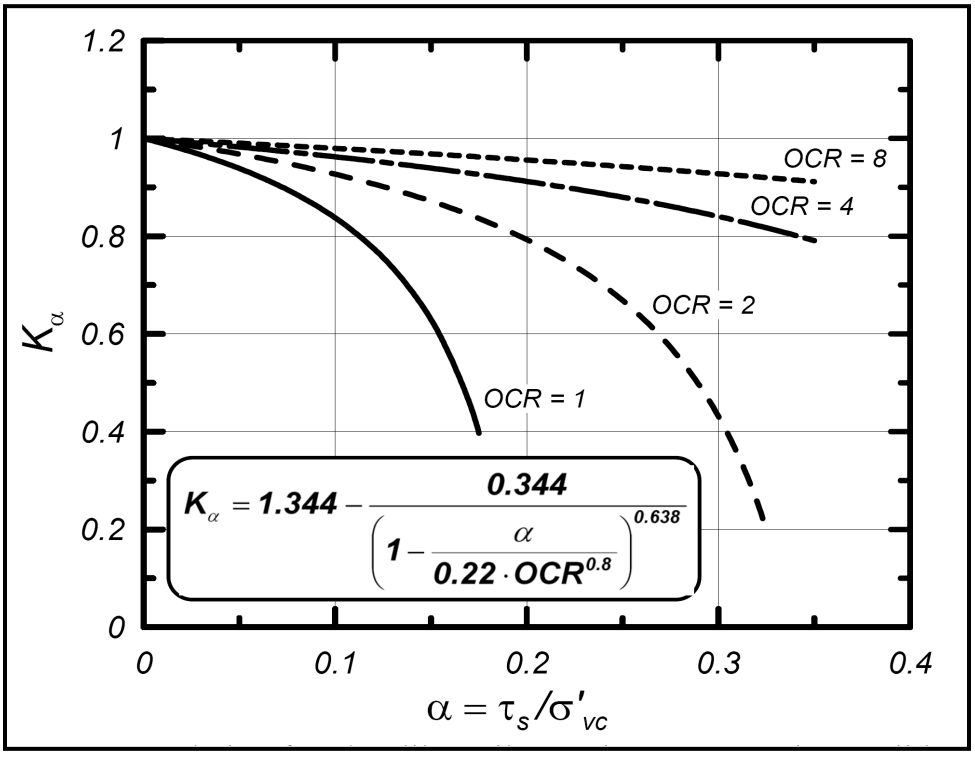


**Figure 13-25, $K_\alpha$ versus $(\tau_s/S_u)_{\alpha=0}$ For Clay-Like Soil ($1 \le OCR \le 8$) (Boulanger and Idriss (2004 and 2007))**

$$K_\alpha = 1.344 - \frac{0.344}{\left\{1 - \left[\frac{\alpha}{k*(OCR)^n}\right]\right\}^{0.638}} = 1.344 - \frac{0.344}{\left\{1 - \left[\frac{\alpha}{0.22*(OCR)^{0.8}}\right]\right\}^{0.638}} \qquad \textbf{Equation 13-47}$$

The procedure provided in the preceding paragraphs is complex. Therefore, similarly to Sand-Like soils, the $K_\alpha$ provided in Table 13-5 may be used. Note that values provided are based on the OCR value to the soil. For OCR values ranging from 4 to 8, the $\alpha$-value is less than or equal to 0.35 ($\alpha \le 0.35$). These values are anticipated to be conservative. The GEOR may elect to use the proceeding equations to determine $K_\alpha$. The GEOR shall provide the necessary computations

used to determine $K_\alpha$. For $N^*_{1,60}$ and $q_{c,1,N}$ that between the values indicated linear interpolation may be used.

**Table 13-5, Simplified $K_\alpha$ Values for Clay-Like Soils**

| OCR | $K_\alpha$ |
|---|---|
| $\leq 1$ | 0.10 |
| 2 | 0.20 |
| 4 | 0.80 |
| $\geq 8$ | 1.00 |

## 13.10 SOIL SHEAR STRENGTH FOR SEISMIC ANALYSES

When performing seismic analyses, for soils that are not subject to losses in shear strength, the appropriate undrained shear ($\tau$) or drained shear ($\tau'$) strengths should be used, in accordance with Chapter 7. Soils that are subject to cyclic strain-softening should use residual soil shear strengths. Undrained/drained soil shear strengths can be evaluated in accordance with the field and laboratory testing procedures specified in Chapter 5.

During strong seismic shaking, cyclic liquefaction of Sand-Like soils or cyclic softening of Clay-Like soils may result in a sudden loss of strength and stiffness. Laboratory testing to determine residual shear strength of soils that have been subject to cyclic liquefaction or cyclic softening is difficult and not typically performed. The standard-of-practice is to use correlated residual undrained shear strengths of cohesionless soils as indicated in Sections 13.10.1 and 13.10.2 and to use correlated cyclic shear strength of cohesive soils as indicated in Sections 13.10.3 and 13.10.4. Guidance in selection of soil shear strengths for seismic analyses is presented in Section 13.10.5.

### 13.10.1 Sand-Like Soil Cyclic Shear Strength Triggering

The shear strength of Sand-Like soils that should be used in seismic analyses is dependent on the results of the liquefaction triggering and on pore pressure generation. The liquefaction triggering resistance ratio $(D/C)_{SL}$ is presented in Section 13.7. Figure 13-26 shows a relationship between liquefaction triggering resistance ratio $(D/C)_{SL}$ and the excess pore pressure ratio, $R_u$, that was proposed by Marcuson, et al. (1990).

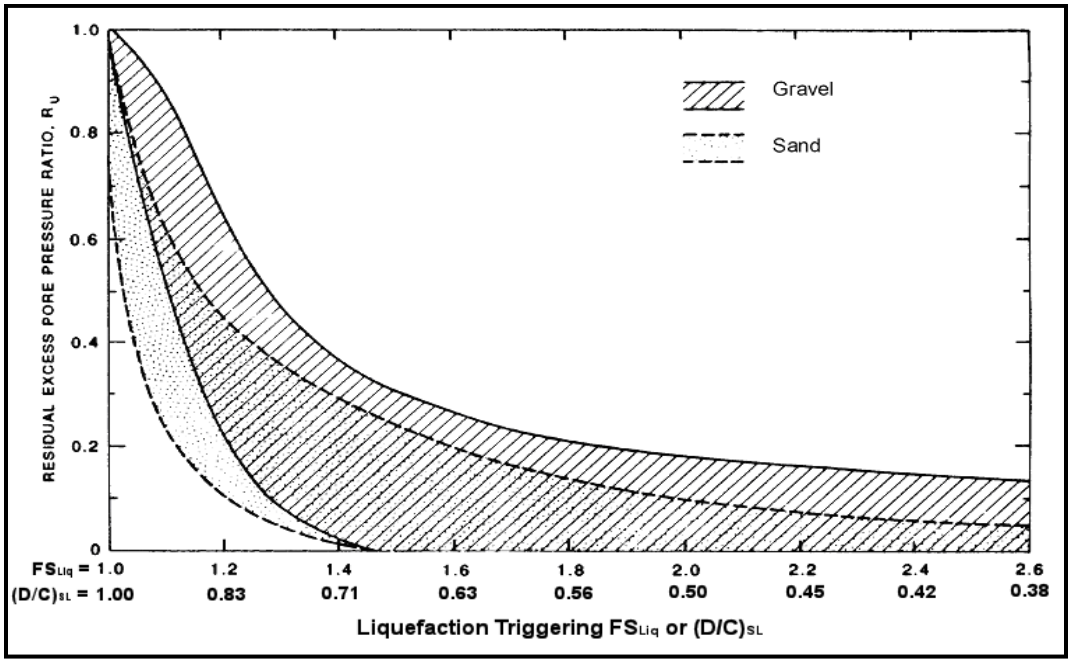


**Figure 13-26, Excess Pore Pressure Ratio - Liquefaction Triggering (Modified Marcuson, et al. (1990))**

The excess pore pressure ratio, $R_u = \Delta u/\sigma'_{vo}$ is the ratio of excess pore water pressure ($\Delta u$) to effective overburden stress ($\sigma'_{vo}$). The liquefaction triggering resistance ratio $(D/C)_{SL}$ of Sand-Like soils can be defined based on the excess pore pressure ratio generated as either Cyclic Liquefaction or No Liquefaction. Resistance factors used for design shall be those presented in Chapter 9.

Guidelines for determining the shear strength of Sand-Like soils are provided in Table 13-6.

**Table 13-6, Sand-Like Shear Strengths**

| Liquefaction Potential | Liquefaction Triggering Criteria | Soil Shear Strength |
|---|---|---|
| *Cyclic Liquefaction* | $(D/C)_{SL\text{-}Sand} > \varphi_{SL\text{-}Sand}$ ($0.7 \le R_u \approx 1.0$) | Use Idriss and Boulanger (2008) or Olson and Johnson (2008) residual shear strength of liquefied soils ($\tau_{rl}$) correlations. Sections 13.10.2.1 and 13.10.2.2<br>**Equation 13-48**<br>$\boldsymbol{\phi_{rl} = tan^{-1}\left(\frac{\tau_{rl}}{\sigma'_{vo}}\right) \le \phi_{Peak}}$<br>or<br>**Equation 13-49**<br>$\boldsymbol{\tau_{rl} = \sigma'_{vo} * tan\,\phi_{rl} \le \sigma'_{vo} * tan\,\phi_{peak}}$ |
| *No Liquefaction* | $(D/C)_{SL\text{-}Sand} \le \varphi_{SL\text{-}Sand}$ ($R_u < 0.70$) | Peak undrained shear strength ($\tau_{peak}$). See Chapter 7. |

### 13.10.2 Sand-Like Soil Cyclic Liquefaction Shear Strength

The following methods are currently used to estimate the residual shear strength of liquefied Sand-Like soils.

1. SPT and CPT – Idriss and Boulanger (2008)
2. SPT and CPT - Olson and Johnson (2008)
3. SPT – Kramer and Wang (2015)

The Idriss and Boulanger (2008) method is the preferred method because it incorporates case histories from Olson and Johnson (2008). The Idriss and Boulanger (2008) method is also more advanced in that it uses residual shear strength ratios, permits adjustment for fines content, and allows residual shear strengths to be evaluated for void redistribution effects. Both methods are presented below to provide the designer with the appropriate background to evaluate the appropriate residual shear strength for liquefied Sand-Like soils. Kramer and Wang (2015) discuss some discrepancies that occur in both Idriss and Boulanger (2008) and Olson and Johnson (2008) with relating normalization of $\tau_{rl}$ using $\sigma'_{vo}$, which can indicate very low $\tau_{rl}$ at low $\sigma'_{vo}$. These discrepancies and the recommended procedure to eliminate these discrepancies are provided in the following Sections.

#### 13.10.2.1 Idriss and Boulanger (2008) – Liquefied Residual Shear Strength

The Idriss and Boulanger (2008) method allows for the computation of the liquefaction residual shear strength ratio ($\tau_{rl}/\sigma'_{vo}$), which is the ratio of liquefied residual shear strength ($\tau_{rl} = S_{rl}$) to effective overburden stress ($\sigma'_{vo}$). Both SPT-based and CPTu-based relationships with $\tau_{rl}/\sigma'_{vo}$ were proposed by Idriss and Boulanger (2008). Furthermore, the Idriss and Boulanger 2008) relationships distinguish between 2 types of cases:

**Case 1:** Condition in which the effects of void redistribution can be confidently judged to be negligible. This condition occurs at sites where the site stratigraphy would not impede dissipation of excess pore water pressure and the dissipation of excess pore water pressure would be accompanied by densification of the soils.

**Case 2:** Condition in which the effects of void redistribution can be significant. This condition occurs at sites where the site stratigraphy would impede dissipation of excess pore water pressure. Sites that meet this condition include sites with relatively thick layers of liquefiable soils that are overlain by lower permeability soils that would impede the dissipation of excess pore water pressure by trapping the upwardly seeping pore water beneath the lower permeability soil. This condition would lead to localized loosening, strength loss, and possibly even the formation of water film beneath the lower permeability soil.

The SPT correlation uses a corrected fines content SPT blow count, $N^*_{1,60,cs}$, computed as shown in Equation 13-50. Corrected and normalized SPT blow counts, $N^*_{1,60}$, should be computed in accordance with Chapter 7. Values for $\Delta N_{1,60\text{-}rl}$ can be found in Table 13-7.

$$N^*_{1,60,CS} = N^*_{1,60} + \Delta N_{1,60-rl}$$ **Equation 13-48**

**Table 13-7, Values of $\Delta N_{1,60\text{-}rl}$ (Seed, 1987)**

| Fines Content, FC (% passing No. 200 sieve) | $\Delta N_{1,60\text{-}rl}$ |
|---|---|
| 10 | 1 |
| 25 | 2 |
| 50 | 4 |
| 75 | 5 |

The $\tau_{rl}/\sigma'_{vo}$ for SPT can be determined for Case 1 and Case 2 using Figure 13-27.

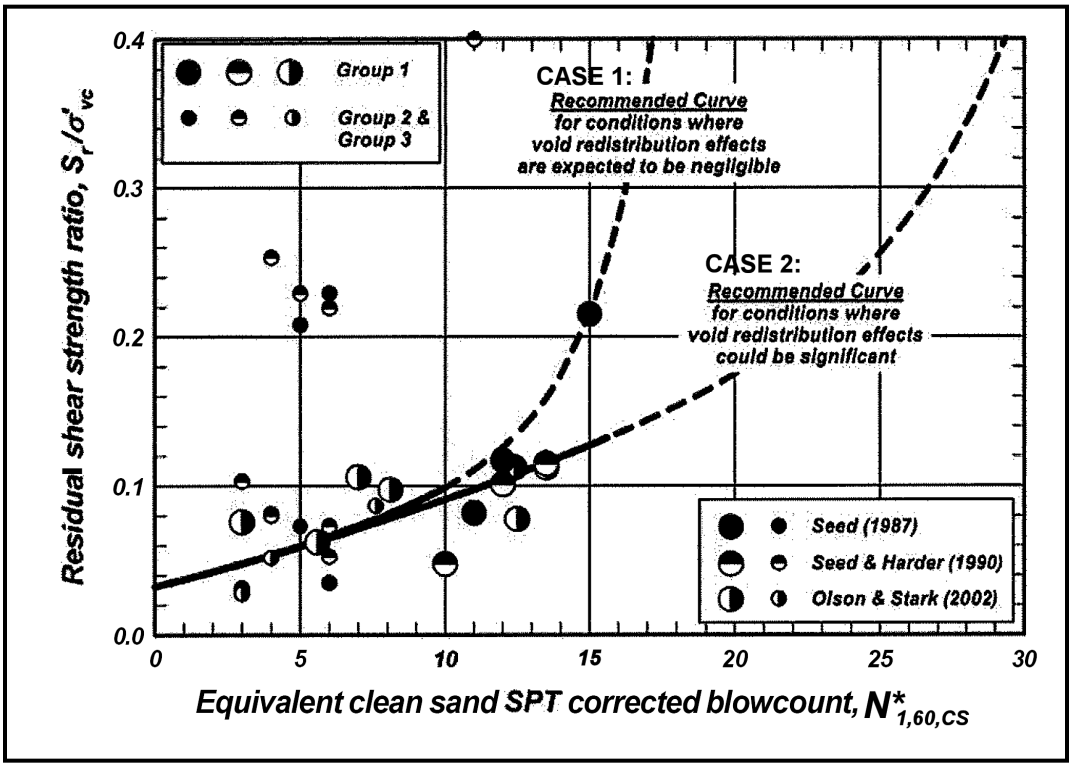


Note: $\tau_{rl} = S_r$

**Figure 13-27, Liquefied Shear Strength Ratio - SPT (Idriss and Boulanger (2008))**

In lieu of using Figure 13-27, $\tau_{rl}/\sigma'_{vo}$ for SPT can be determined for Case 1 and Case 2 by using the following equations.

**Case 1:**

$$\left(\frac{\tau_{rl}}{\sigma'_{vo}}\right) = (\psi) * \left[1 + exp\left(\frac{N^*_{1,60,CS}}{2.4} - 6.6\right)\right] \leq tan\,\phi'_{rl}$$ **Equation 13-49**

for, $N^*_{1,60,CS} \leq 17$ blows per foot

**Case 2:**

$$\left(\frac{\tau_{rl}}{\sigma'_{vo}}\right) = (\psi) \leq \tan \phi'_{rl} \qquad \textbf{Equation 13-50}$$

Where,

$$\psi = exp\left[\frac{N^*_{1,60,CS}}{16} + \left(\frac{N^*_{1,60,CS}-16}{21.2}\right)^3 - 3.0\right] \qquad \textbf{Equation 13-51}$$

for, $N^*_{1,60,CS} \leq 30$ blows per foot

The CPTu correlation uses a corrected, normalized CPTu tip resistance adjusted for fines content, $q_{t,1,N,CS}$, computed as shown in Equation 13-54. Corrected and normalized tip resistances, $q_{t,1,N}$, should be computed in accordance with Chapter 5. Values for $\Delta q_{t,1,N\text{-}rl}$ can be found in Table 13-8.

$$q_{t,1,N,CS} = q_{t,1,N} + \Delta q_{t,1,N-rl} \qquad \textbf{Equation 13-52}$$

**Table 13-8, Values of $\Delta q_{t,1,N,\text{-rl}}$**
**(Idriss and Boulanger (2008))**

| Fines Content, FC (% passing No. 200 sieve) | $\Delta q_{t,1,N\text{-rl}}$ |
|---|---|
| 10 | 10 |
| 25 | 25 |
| 50 | 45 |
| 75 | 55 |

The $\tau_{rl}/\sigma'_{vo}$ for CPTu can be determined for Case 1 and Case 2 using Figure 13-28.

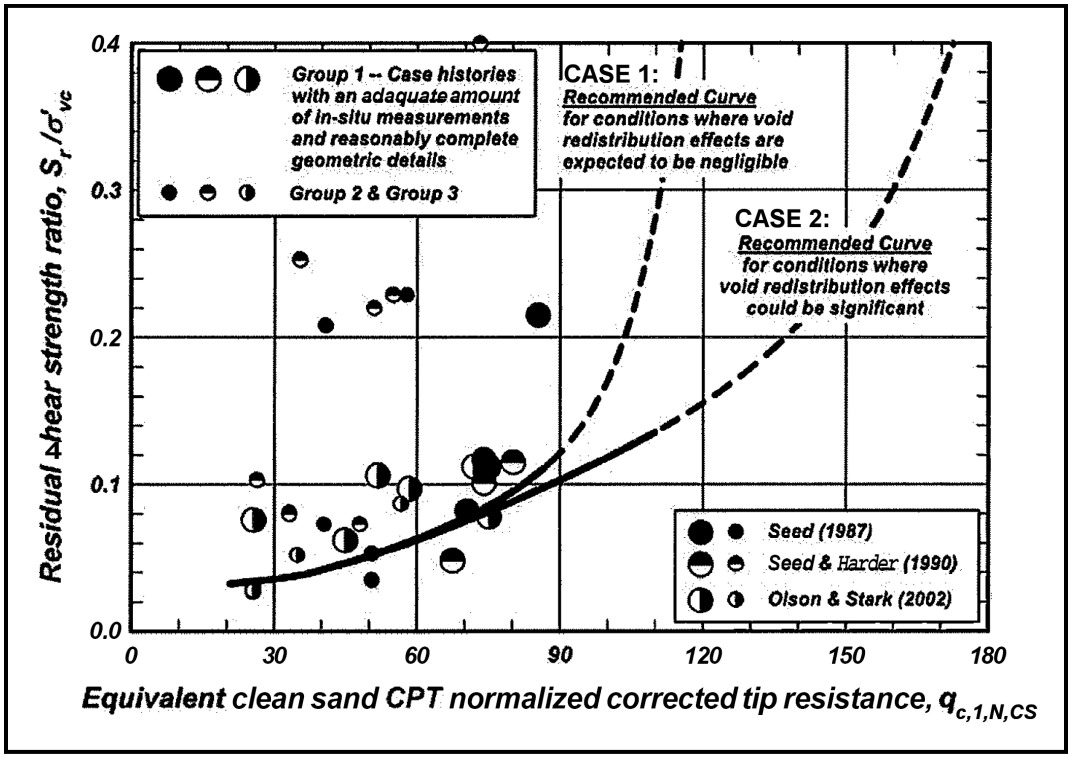


Note: $\tau_{rl} = S_r$; $q_{c,1,N,CS} = q_{t,1,N,CS}$

**Figure 13-28, Liquefied Shear Strength Ratio - CPTu Tip Resistance (Idriss and Boulanger (2008))**

In lieu of using Figure 13-28, $\tau_{rl}/\sigma'_{vo}$ for CPTu can be determined for Case 1 and Case 2 by using the following equations.

**Case 1:**

$$\left(\frac{\tau_{rl}}{\sigma'_{vo}}\right) = (\psi) \leq \tan \phi'_{rl} \qquad \textbf{Equation 13-53}$$

for, $q_{t,1,N,CS} \leq$ ~115

**Case 2:**

$$\left(\frac{\tau_{rl}}{\sigma'_{vo}}\right) = (\psi) * \left\{1 + exp\left[\left(\frac{q_{c,1,N,CS}}{11.1}\right) - 9.82\right]\right\} \leq \tan \phi'_{rl} \qquad \textbf{Equation 13-54}$$

for, $q_{t,1,N,CS} \leq$ ~170

Where,

$$\psi = exp\left[\left(\frac{q_{c,1N,CS}}{24.5}\right) - \left(\frac{q_{c,1,N,CS}}{61.7}\right)^2 + \left(\frac{q_{c,1,N,CS}}{106}\right)^3 - 4.42\right] \qquad \textbf{Equation 13-55}$$

### 13.10.2.2 Olson and Johnson (2008) – Liquefied Residual Shear Strength

The Olson and Johnson (2008) methods also allow for the computation of the $\tau_{rl}/\sigma'_{vo}$. The relationship between liquefaction shear strength ratio and the normalized SPT blow count ($N^*_{1,60}$)

is provided in Figure 13-29. The average trend line for Figure 13-29 can be computed using the following equation.

$$\left(\frac{\tau_{rl}}{\sigma'_{vo}}\right) = 0.03 + 0.0075 * \left(N^*_{1,60}\right) \pm 0.03 \qquad \textbf{Equation 13-56}$$

Where,

$N^*_{1,60}$ = Normalized SPT blow count and values of $N^*_{1,60} \leq 16$ blows per foot.

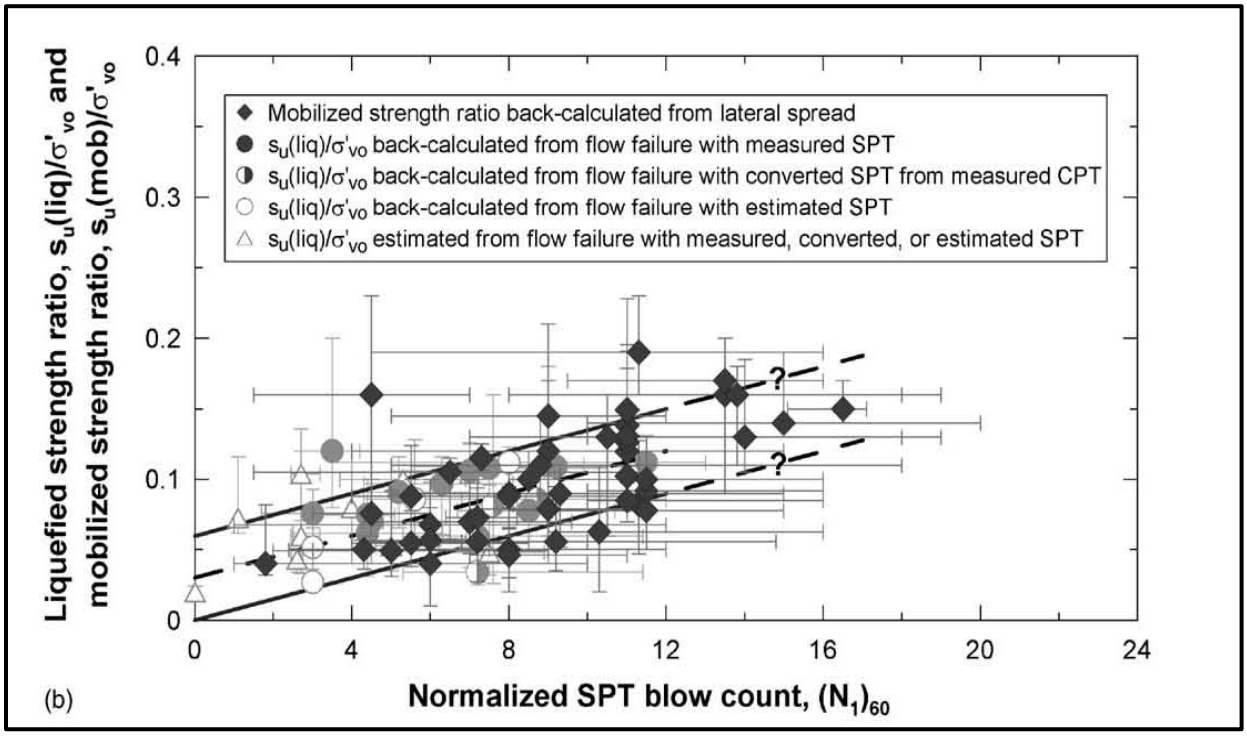


**Figure 13-29, Liquefied Shear Strength Ratio - SPT Blow Count (Olson and Johnson (2008) with permission from ASCE)**

The relationship between liquefaction shear strength ratio and the normalized CPTu tip resistance ($q_{t,1}$) is provided in Figure 13-30. The average trend line for Figure 13-30 can be computed using the following equation.

$$\left(\frac{\tau_{rl}}{\sigma'_{vo}}\right) = 0.03 + 0.0143 * \left(q_{t,1}\right) \pm 0.03 \qquad \textbf{Equation 13-57}$$

Where,

$q_{t,1}$ = Normalized CPT tip resistance (MPa) for values $q_{t,1} \leq 10$ MPa (approximately 104 tsf)

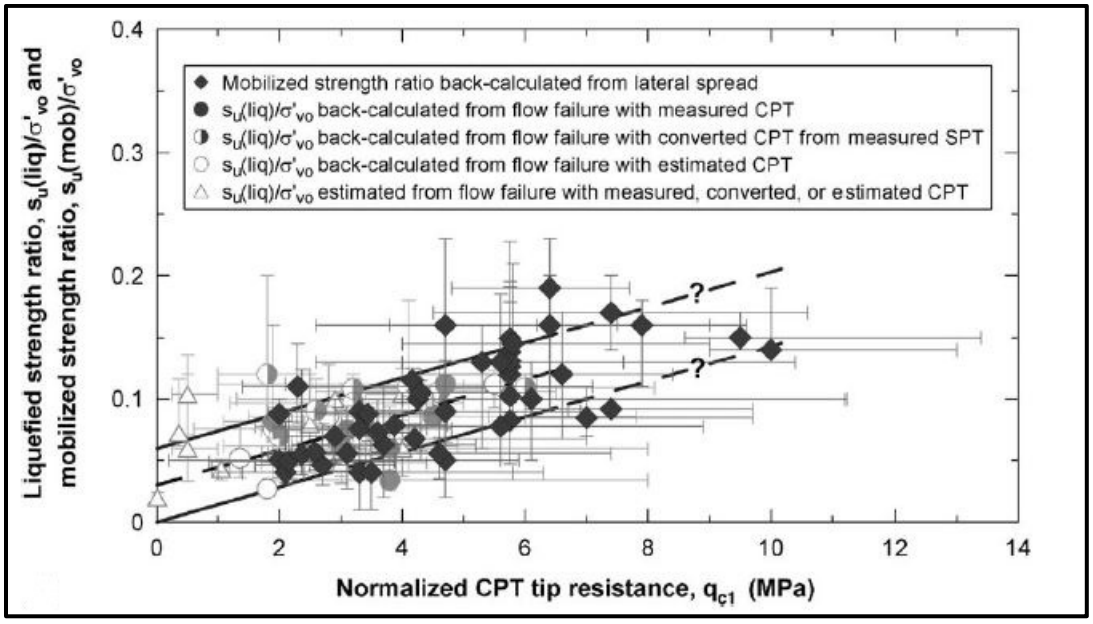


Note: $q_{c,1} = q_{t,1}$

**Figure 13-30, Liquefied Shear Strength Ratio - CPT Tip Resistance (Olson and Johnson (2008) with permission from ASCE)**

### 13.10.2.3 Kramer and Wang (2015) – Liquefied Residual Shear Strength

The previously discussed Idriss and Boulanger (2008) and Olson and Johnson (2008) procedures both rely on normalized shear strength (i.e., $\tau_{rl}/\sigma'_{vo}$) to determine the liquefied shear strength ($\tau_{rl}$); however, according to Kramer and Wang (2015) this can lead to extremely low residual strength values at low initial vertical stresses. The normalized shear strength approach assumes the liquefied shear strength is affected by both the corrected N-values as well as being proportional to the effective overburden pressure. Kramer and Wang (2015) also point that the direct method (Seed (1987) and Seed and Harder (1990)) assumes the liquefied shear strength only varies with corrected N-values. The direct method tends to predict high liquefied shear strengths at shallow depths and low liquefied shear strengths at deeper depths. Kramer and Wang (2015) have developed a procedure to determine the liquefied shear strength that accounts for both the direct and normalized shear strength approaches. The equation is provided below:

$$\tau_{rl} = e^{Z} \qquad \textbf{Equation 13-58}$$

$$Z = -8.444 + 0.109\left(N^{*}_{1,60}\right) + 5.379\left(\sigma'_{vo}\right)^{0.1} \qquad \textbf{Equation 13-59}$$

Where,

$N^{*}_{1,60}$ = Standardized and normalized SPT blow count

$\sigma'_{vo}$ = Effective vertical overburden stress, atmospheres (atm) (1 atm = 2,116.22 psf)

It is noted that $\tau_{rl}$ provided in Equation 13-60 is in atm.

### 13.10.3 Clay-Like Soil Cyclic Shear Strength Triggering

Clay-Like soils with soil SSL triggering resistance ratio $(D/C)_{SL}$ greater than the Clay-Like soil SSL triggering resistance factor ($\varphi_{SL\text{-}Clay}$) will be subject to soil SSL approximately equal to the cyclic softening residual shear strength, $\tau_{rs}$. Resistance factors used for design shall be those presented in Chapter 9.

### 13.10.4 Clay-Like Soil Cyclic Softening Shear Strength

Saturated NS Clay-Like soils having low sensitivity ($S_t < 5$) and subjected to modest cyclic shear stresses can produce significant permanent strains that can lead to stresses near the soil's yield stress. The degree of saturation of the NS Clay-Like sols should be determined using appropriate laboratory testing. It is noted that the groundwater table may be used as a general indicator of saturation with soils below the groundwater table being considered saturated. Alternatively, all Clay-Like soils may be considered saturated regardless of the depth of the groundwater table. The residual cyclic softening shear strength, $\tau_{rs}$, of cohesive soils can be estimated by reducing the soil's undrained shear strength ($\tau_{Peak} = S_u$) using the following equation.

$$\boldsymbol{\tau_{rs} = 0.8 * \tau_{Peak}} \qquad \textbf{Equation 13-60}$$

HS Clay-Like soils having sensitivity ratio, $S_t \geq 5$ that are subject to modest cyclic shear stresses can experience moderate to significant loss in soil shear strengths. The reduced shear strength can be estimated with the remolded soil shear strength ($\tau_{remolded}$) as indicated in Chapter 7.

### 13.10.5 Seismic Soil Shear Strength Selection

The use of drained/undrained soil shear strengths is dependent on the type of soil and the shear strain level the soil is experiencing. Large variations in shear strain levels can occur during a seismic event from small strains during cyclic loadings to large strains during soil failures. The EE I limit state is used to perform geotechnical analyses for seismic loadings (Design Seismic Events FEE and SEE). Because performance limits for the EE I limit state allow for deformations, the selected shear strength will depend on the strain level that the soil will experience and it's potential for soil SSL.

Soil shear strength selection for seismic analyses should be made based on laboratory testing and soil strain level anticipated from analyses. Table 13-7 provides a summary of "general" soil behavior (shear stress vs. strain) observed from published soil stress-strain curves from Holtz and Kovacs (1981), Terzaghi, Peck, and Mesri (1996), and Duncan and Wright (2005). Table 13-9 should be used for "general" guidance on the selection of seismic shear strengths based on soil type and soil strain level anticipated from analyses.

**Table 13-9, Seismic Soil Shear Strength Selection**

| **Sand-Like Soils (Undrained)** | **Strain Level at Failure (1)** | | | |
|---|---|---|---|---|
| | **Cyclic Strains** | **±5% Strains** | **15–20% Strains** | **Large Strains >20%** |
| Med. To Dense Sand | $\tau_{Peak}$ | $\tau_{Peak}$ | $\tau_r$ | $\tau_r$ |
| Non-Liquefying Loose Sands | $\tau_{Peak}$ | $\tau_{Peak}$ | $\tau_{Peak}$ | $\tau_{Peak}$ |
| Liquefied Soils | $\tau_{rl}$ | $\tau_{rl}$ | $\tau_{rl}$ | $\tau_{rl}$ |
| **NS Clay-Like Soils (Undrained)** | **Strain Level at Failure (1)** | | | |
| | **Cyclic Strains** | **±2% Strains** | **10–15% Strains** | **Large Strains >15%** |
| OCR =1, $S_t < 5$ | $\tau_{rs}$ | $\tau_{Peak}$ | $\tau_{Peak}$ | $\tau_{Peak}$ |
| OCR >1, $S_t < 5$ | $\tau_{rs}$ | $\tau_{Peak}$ | $\tau_r$ | $\tau_r$ |
| **HS Clay-Like Soils (Undrained)** Highly Sensitive ($S_t \geq 5$) | **Strain Level at Failure (1)** | | | |
| | Typically Failure < 3% | | | |
| | $\tau_{remolded}$ | | | |

**Shear Strength Nomenclature:**

$\tau_{Peak}$ = Peak Soil Shear Strength

$\tau_{rl}$ = Cyclic Liquefaction Residual Shear Strength

$\tau_r$ = Residual Soil Shear Strength

$\tau_{rs}$ = Cyclic Softening Residual Shear Strength

$\tau_{remolded}$ = Remolded Soil Shear Strength

(1) Strain levels indicated are generalizations and are dependent on the stress-strain characteristics of the soil and should be verified by laboratory testing.

## 13.11 FLOW SLIDE FAILURE

Flow failure occurs when the soils exhibit strain softening and have static gravitational shear stresses larger than the soil shear strengths after soil SSL has occurred. The strain softening can be a result of monotonic or cyclic undrained loading. Flow liquefaction failures typically occur rapidly and are usually catastrophic. Seismic-induced flow failure tends to occur after the cyclic loading ceases due to the progressive nature of the load redistribution; however, if the soils are sufficiently loose and the static shear stresses are sufficiently large, the seismic loading may trigger essentially “spontaneous liquefaction” within the first few cycles of loading leading to flow failure during seismic shaking.

Flow failure is characterized by substantial masses of surficial soils undergoing large translational or rotational deformations that typically occur after the seismic shaking has ceased. The surficial soils undergo deformations when static gravitational driving forces exceed the average soil shear strength after soil SSL has occurred, where the critical failure surface passes through the soil layers that have undergone soil SSL. Because flow liquefaction is driven by the imbalance of $\tau_{static}$ versus $\tau_{rl}$; $\tau_{rs}$; or $\tau_{remolded}$, the effects of seismic ground motions (inertial forces due to the seismic shaking) are not included in the analyses.

The evaluation of flow failure proceeds as follows:

**1.** Perform a soil SSL Triggering analysis to determine which soils are susceptible to soil SSL.

**2.** Assign appropriate soil shear strengths to Sand-Like, NS Clay-Like, and HS Clay-Like soils susceptible to soil SSL and undrained/drained shear strengths to soils not susceptible to soil SSL.

**3.** Perform a conventional static slope stability analysis using Spencer's method (no seismic acceleration coefficient). Determine the static resistance to flow failure $(D/C)_{Flow}$ and the required resistance factor against flow failure, $\varphi_{Flow}$. If the static resistance to flow failure $(D/C)_{Flow} > \varphi_{Flow}$, flow failure potential exists at the site. The LRFD equation for use in determining the onset of flow failure is shown below.

$$\left(\frac{D}{C}\right)_{Flow} \leq \boldsymbol{\varphi_{Flow}} \qquad \textbf{Equation 13-61}$$

The magnitude of flow failure deformations is typically in excess of 25 feet, depending on the geometry of the flowing ground, the extent of strain softening of the subsurface soils, and the soil stratification. Estimation of lateral flow deformation is very complex and there are currently no accepted methods for evaluating this type of deformation. Since flow failure deformations cannot be reliably estimated, it is assumed that the soils will undergo unlimited deformation and as a result will exert soil pressure loadings on any structures that are affected by the flow failure movements.

## 13.12 LATERAL SPREAD

As defined in Chapter 2, lateral spreading is the horizontal displacement that occurs on mostly level ground or gentle slopes (≤ 6 degrees) as a result of cyclic liquefaction of shallow Sand-Like soil deposits. The gentle slope referred to here is the slope of the existing ground surface prior to any construction (see Figure 13-31). The slope of the bridge embankment (i.e., a "structure" for this case) is not included in the determination of gently sloping ground. The soil can slide as intact blocks down the slope towards a free face such as an incised river channel. Case studies have reported displacements as great as 30 feet with smaller associated settlements. Youd (2018) indicates that if the depth to the liquefied layer below the deepest point of the crossing is more than H (i.e., the height of the river embankment) then lateral spread should not affect the bridge (see Figure 13-32).

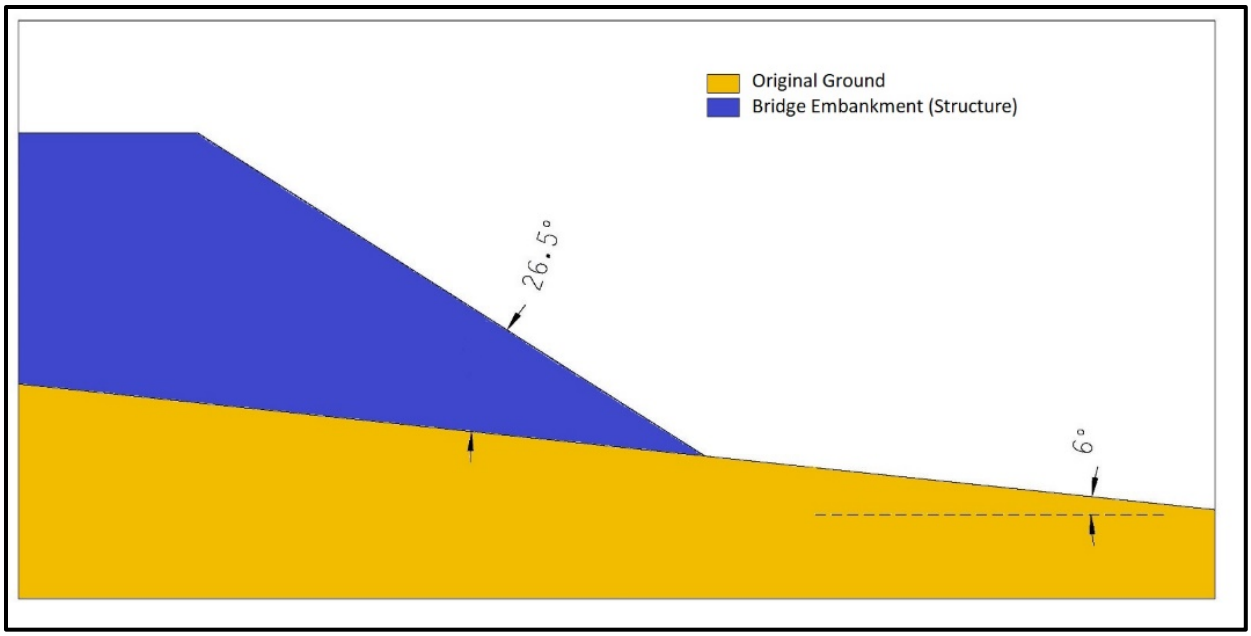


**Figure 13-31, Gently Sloping Ground with Embankment**

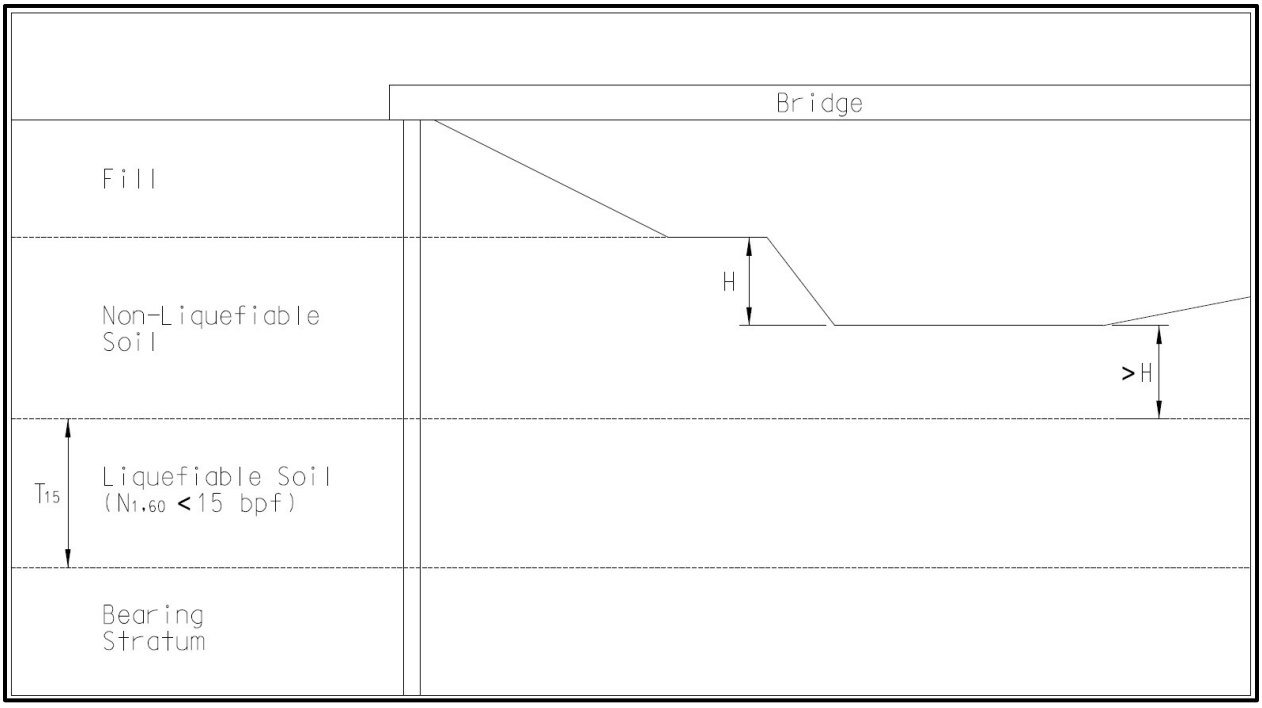


**Figure 13-32, Depth of Lateral Spread not Affecting Bridge**

Lateral spread occurs as a result of the dynamic (earthquake shaking) driving forces applied to surficial soils (typically located within the upper 10 feet) that have experienced or undergone significant reduction in soil shear strength. As a result of the slope instability, a failure surface resembling a sliding block typically develops along the liquefied soils and is subject to lateral displacements until equilibrium is restored. In addition to lateral spread deformations, the ground is also susceptible to seismic settlement. A liquefaction potential assessment in accordance with Sections 13.6 and 13.7 should first be made to determine if screening and triggering of SSL is

possible at a site and therefore, the potential for lateral spread exists. Since cyclic soil strength degradation or liquefaction may occur during the earthquake shaking, the effects of earthquake ground motions (inertial forces) and residual shear strengths (liquefied soils and non-liquefied soils) shall be used during the evaluation of the potential for lateral spread.

The lateral spread displacement evaluation process is as follows:

**Step 1.** Perform an SSL Triggering analysis for level ground sites to determine which soils are susceptible to SSL.

**Step 2.** Assign appropriate soil shear strengths to Sand-Like, NS Clay-Like, and HS Clay-Like soils susceptible to SSL and undrained/drained shear strengths to soils not susceptible to SSL.

**Step 3.** Perform a conventional pseudo-static slope stability analysis with average horizontal acceleration coefficient with adjustments for wave scattering ($k_h$). Determine the static resistance ratio to lateral spread $(D/C)_{Spread}$ and the required resistance factor against lateral spread, $\varphi_{Spread}$. If the static resistance ratio to lateral spread $(D/C)_{Spread} > \varphi_{Spread}$, lateral spread potentially exists at the site. The LRFD equation used in determining the onset of lateral spread is shown below.

$$\left(\frac{D}{C}\right)_{Spread} \leq \varphi_{Spread} \qquad \text{Equation 13-62}$$

**Step 4.** Perform empirical or semi-empirical deformation analyses as described in this Section.

**Step 5.** If the displacements computed in Step 4 exceed the performance limits established for the project, additional displacement calculations should be performed using all of the empirical and semi-empirical methods for computing lateral spread deformations that are presented in this section. The Newmark displacement methods may be used with caution provided that the requirements stated below are adhered to.

**Step 6.** From the displacement computations performed in Steps 4 and 5, the designer will need to evaluate if there are any trends in the displacements computed.

Empirical/semi-empirical methods have been developed based on case history databases for specific types of failure modes, earthquake characteristics, site geometry, and subsurface soils. Methods indicated as semi-empirical are based on some numerical basis to estimate residual shear strains in the soils after liquefaction. Empirical and semi-empirical methods are only used for screening purposes because of the low reliability of the predictions. The Youd, Hansen and Bartlett (2002), “Revised Multilinear Regression Equations for Prediction of Lateral Spread Displacements” shall be used for lateral spread analysis using the SPT.

Newmark methods of displacement analysis are typically not appropriate for evaluation of lateral spreads when soil SSL are greater than 50% when compared to the shear strengths prior to the SSL. If it can be shown that the shear failure surface as a whole has not lost more than 50% of the shear failure resistance prior to the soils SSL, the Newmark method may be used. The Newmark method may also be used without adjusting soil shear strengths to obtain a lower bound

displacement. If the lower bound displacement exceeds the performance limits mitigation of the hazard will be required. Newmark methods described in Section 13.15 should be used with caution.

### 13.12.1 Multilinear Regression of Lateral Spread Displacements

Youd et al. (2002) revised the multilinear regression (MLR) empirical equations previously developed by Bartlett and Youd (1992, 1995) for prediction of lateral spread displacement. This method used a large database of lateral spread case histories from past earthquakes. A review of the Bartlett and Youd, 1992, case history database reveals measured displacements that range from less than one inch to as much as 30 feet. The predicted displacements vary from one-half of the measured value to twice the measured value. Because of the high uncertainty associated with lateral displacement values computed with this method it is only used for screening of potential for lateral spread displacements. It should be noted that the following equations are valid when liquefaction occurs over a widespread area, and not just isolated pockets. If this method predicts displacements in excess of 20 feet (i.e., 6 meters), then the predicted displacements should be taken as indication of large displacements and not an actual displacement prediction. In addition, the parameters used in this method must meet the boundary conditions indicated in Table 13-10. Liquefiable soils layers must be identified as indicated in Sections 13.6 and 13.7. Guidance for specific input of each of the parameters in the following equations is provided by Youd, et al. (2002).

**Table 13-10, Boundary Conditions of MLR Approach**

| Parameter | Minimum | Maximum |
|---|---|---|
| $M_w$ | 6 | 8 |
| W | 1% | 20% |
| S | 0.1% (~0.06°) | 6% (~3.43°) |
| $T_{15}$ | 3.25 feet | 49 feet |
| $Z_T$ | 3.25 feet | 33 feet |
| $D_{50(15)}$ | 0.06 mm | 10 mm |
| $F_{15}$ | 0 | 70% |

Where $Z_T$ is the depth to the top of the first layer of $T_{15}$. If the boundary condition indicated in Table 13-10 are not met, extreme caution should be used in applying this method to a specific site.

For ground slope condition (Figure 13-27: Case 1):

**Equation 13-63**

$$\begin{aligned} log\ D_H = &-16.213 + 1.532\,M_w - 1.406\,log(R^*) - 0.012R \\ &+ 0.338\log(S) + 0.540\,log(T_{15}) \\ &+ 3.413\,log\,(100 - F_{15}) - 0.795\,log\,(D_{50(15)} + 0.1\,mm) \end{aligned}$$

For free-face condition (Figure 13-27 Case 2):

**Equation 13-64**

$$\log D_H = -16.713 + 1.532 M_w - 1.406 \log(R^*) - 0.012R + 0.592 \log(W) + 0.540 \log(T_{15}) + 3.413 \log(100 - F_{15}) - 0.795 \log(D_{50(15)} + 0.1\,mm)$$

Where:

$D_H$ = Estimated lateral ground displacement in meters

$T_{15}$ = Cumulative thickness of saturated granular layers with corrected blow counts, $(N_1)_{60}$, less than or equal to 15, in meters.

$D_{50(15)}$ = Average mean grain size in granular layer included in $T_{15}$ in mm.

$F_{15}$ = Average fines content (passing #200 sieve) for granular layers included in $T_{15}$ in percent.

$M_w$ = Design earthquake magnitude (moment magnitude).

R = Site-to-source distance, in kilometers. For sites with R < 0.5 km, use R = 0.5 km.

$R_o$ = Distance factor that is a function of earthquake magnitude, $M_w$ and is computed using the following equation.

$$R_o = 10^{(0.89M_w - 5.64)}$$ **Equation 13-65**

$R^*$ = Modified source distance and is computed using the following equation.

$$R^* = R + R_o$$ **Equation 13-66**

S = Ground slope, in percent.

W = Ratio of the height (H) of the free face to the distance (L) from the base of the free face to the point in question, in percent (i.e.,100H/L).

These equations may be applied to materials that have a $D_{50(15)}$ up to 10 mm, provided the site has impeded drainage, (i.e., SSL occurs at the site). The thickness of the Sand-Like SSL layers should be greater than 3.25 feet (~1.0 meter) (i.e., $T_{15} \geq$ 3.25 feet (~1.0 meter). If T15 is less than 1 meter, then these equations will over predict the lateral displacements. Further Equations 13-64 and 13-65 may be applied to sites that have up to 70 percent silty fines ($F_{15} \leq 70\%$) as long as the fines are non-plastic. The design earthquake moment magnitude, $M_w$, and the site-to-source distance, R, shall be those determined for the design earthquake under evaluation as required in Chapter 12.

## 13.13 SEISMIC ACCELERATION COEFFICIENTS

The magnitude of seismic inertial forces and seismic loading (active / passive pressures) that are used in pseudo-static stability analyses or limit-equilibrium analyses of ERSs are based on computing average horizontal acceleration coefficients adjusted for wave scattering ($k_h$). The $k_h$ is computed using the PGA at the ground surface with adjustments that typically reduce the acceleration by taking into account wave scattering of the horizontal ground accelerations and

displacements of a yielding structure. The wave scattering scaling factor ($\alpha_w$) is dependent on the design pseudo-spectral acceleration at 1 second ($S_{D1}$) from the ADRS curve and the height of the embankment, slope, or ERS.

Seismic inertial loadings are typically estimated by pseudo-static analytical methods that consist of multiplying the average $k_h$ and average vertical seismic coefficient ($k_v$) by the mass of the soil or structure that is being accelerated due to the seismic shaking. The $k_v$ is typically neglected ($k_v = 0$) by the fact that the vertical accelerations will be out of phase with the horizontal accelerations. According to AASHTO LRFD Specifications, $k_v$ is usually very small when $k_h$ approaches its maximum value. The $k_h$ is used to compute a constant horizontal force in global seismic stability of slopes and ERSs. The $k_h$ has typically been assigned some fraction (0.3 to 0.7) of the PGA. Reductions in PGA are typically attributable to either wave scattering or stress relief associated with displacements. The displacement dependent stress relief reduction of the horizontal seismic coefficient is computed using the Newmark displacement method as shown in Section 13.14.

Wave scattering is a term used to account for the seismic wave incoherence or variations behind a wall or slope. Kavazanjian, et al. (2012) provides a relationship utilizing a scale factor, $\alpha_w$, (reduction factor) to account for wave scattering as indicated by the following equation.

$$\boldsymbol{k_h = k_{avg} = \alpha_w * PGA} \qquad \textbf{Equation 13-67}$$

Where,

$k_h$ = Average seismic horizontal coefficient due to wave scattering

$\alpha_w$ = Wave scattering scaling factor (reduction factor)

PGA = Peak ground acceleration coefficient for the design event ($k_{max}$)

The $\alpha_w$ was found to be dependent on the ground motion and the height of the wall or slope as shown in Figure 13-31. For wall or slope heights greater than 100 feet a $\alpha_w$ of 0.5 shall be used.

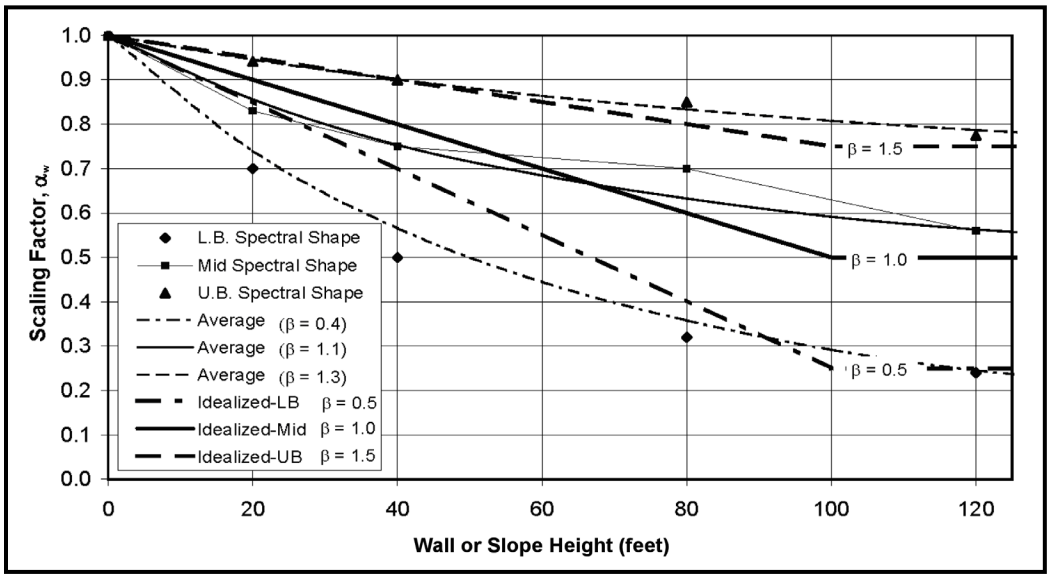


**Figure 13-33, Simplified Wave Scattering Scaling Factor (Kavazanjian, et al. (2012))**

For wall or slope heights less than or equal to 100 feet, $\alpha_w$ shall be determined by the following equation.

$$\boldsymbol{\alpha_w = 1.0 + 0.01 * H * [(0.5 * \beta) - 1] \leq 1.0} \qquad \textbf{Equation 13-68}$$

Where,

H = Height of slope or ERS above the natural ground surface, H ≤ 100 feet, feet

$\beta$ = Ground motion index that is used to characterized shape of the ADRS.

The ground motion index ($\beta$), is computed using the following equation and typically has a lower bound of 0.5 and an upper bound 1.5. The lower bound value is typically associated with seismic conditions in the eastern United States, ground conditions with average $V_s$ greater than or equal to 2,500 feet per second ( $\overline{V_s} \leq$ 2,500 ft/sec) and low acceleration levels. The upper bound is typically associated with seismic conditions in the Western United States, ground conditions with average Vs less than 2,500 feet per second ( $\overline{V_s} <$ 2,500 ft/sec) and high acceleration levels.

$$\boldsymbol{\beta = \frac{S_{D1}}{PGA}} \qquad \textbf{Equation 13-69}$$

Where,

$S_{D1}$ = Peak ADRS spectral acceleration at 1 second (Chapter 12)

PGA = Peak horizontal acceleration at ground surface (Chapter 12)

The $\alpha_w$ determined above is applicable to soil sites, for sites founded on rock, $\alpha_w$ should be increased by 20 percent.

## 13.14 SEISMIC GLOBAL STABILITY

The standard-of-practice for evaluating seismic global instabilities consists of performing pseudo-static limit equilibrium slope stability analyses. Global instability shall be checked when $(D/C)_{flow} \leq \varphi_{flow}$ (Section 13.11). The pseudo-static limit equilibrium slope stability analysis is a modified conventional slope stability analysis that allows the inclusion of inertial driving forces generated by the seismic event as an equivalent static horizontal force acting on the potential sliding mass (see Figure 13-32) or includes both the inertial driving forces as well as the reduced shear strength of any soil that has experienced soil SSL. The inclusion of both the inertial driving forces and the reduced shear strengths caused by soil SSL is called lateral spread. As required in Chapter 17 both circular and non-circular potential failure surfaces shall be checked. The pseudo-static slope stability method uses the average horizontal acceleration coefficients adjusted for wave scattering ($k_h$) as indicated in Section 13.12 to compute the inertial loadings in the seismic global stability analysis. If the seismic slope stability ratio $(D/C)_{EQ\text{-}Stability} \leq \varphi_{EQ\text{-}Stability}$, then the EE I limit state stability requirements and performance criteria have been satisfied. If the seismic slope stability ratio $(D/C)_{EQ\text{-}Stability} > \varphi_{EQ\text{-}Stability}$, then a Newmark sliding block analysis (Section 13.14) is performed to estimate the displacements and determine if they meet the performance critiera. If the failure surface is circular all displacements at the top of the slope

shall be considered to be vertical. All displacements at the top of the slope for a non-circular failure surface shall be considered horizontal.

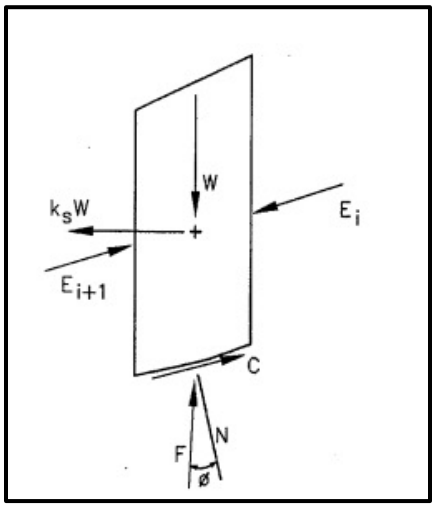


**Figure 13-34, Pseudo-Static Limit Equilibrium Analysis Slice (Kavazanjian, et al. (2012))**

No pseudo-static slope stability analysis is needed for bridge embankments meeting the requirements of Table 13-11 and the conditions established in this paragraph. No analysis is required when soil SSL is not predicted in the bridge embankment soil slope profile or the criteria for no soil SSL analysis is met (see Section 13.3.2); the water table is not located within the bridge embankment; and the soils that compose the bridge embankment are homogenous (i.e., there are no thin layers of soft soil within the slope model). In addition, it is assumed either less than 2 inches of horizontal movement occurs at the top of the slope (assumes non-circular failure surface) or less than 2 inches of vertical settlement occurs at the top of the slope (assumes circular failure surface).

**Table 13-11, No Slope Stability Analysis Required**

| Slope Angle | Total Embankment Height | PGA |
|---|---|---|
| 2H:1V | $\leq$ 10 ft | $\leq$ 0.2g |
| 3H:1V and flatter | $\leq$ 15 ft | $\leq$ 0.3g |

The overall seismic global slope stability evaluation process is shown as follows:

**1.** Determine seismic parameters (PGA, $S_{D1}$, and PGV) from Chapter 12.

**2.** Determine wave scattering scaling factor ($\alpha_w$) from Section 13.12.

**3.** Compute average horizontal seismic coefficient, $k_h$, in accordance with Section 13.12.

**4.** Perform a conventional pseudo-static slope stability analysis (using Spencer's method) conforming to the requirements of Chapter 17 with average horizontal

acceleration coefficient adjusted for wave scattering ($k_h$). The vertical acceleration coefficient ($k_v$) is assumed to equal zero. Assign appropriate soil shear strengths based on soil SSL triggering to Sand-Like soils, NS Clay-Like soils, and HS Clay-Like soils that are susceptible to soil SSL. Use peak undrained/drained shear strengths for soils not susceptible to soil SSL.

**5.** Determine the seismic stability resistance ratio $(D/C)_{EQ\text{-}Stability}$. Obtain the required seismic slope instability resistance factor ($\varphi_{EQ\text{-}Stability}$) from Chapter 9. The LRFD equation shown below is used to determine if the slope is seismically unstable.

$$\left(\frac{D}{C}\right)_{EQ-Stability} \leq \varphi_{EQ-Stability} \qquad \textbf{Equation 13-70}$$

If the seismic instability ratio $(D/C)_{EQ\text{-}Stability} \leq \varphi_{EQ\text{-}Stability}$, then there is no potential for seismic slope instability. If the seismic instability ratio $(D/C)_{EQ\text{-}Stability} > \varphi_{EQ\text{-}Stability}$, seismic instability potential exists at the site and the evaluation process should continue to Step 6 to evaluate the displacements.

**6.** Compute the horizontal yield acceleration ($k_y$) by varying the horizontal acceleration until the seismic instability ratio $(D/C)_{EQ\text{-}Stability} = 1.0$. If the ratio of $k_y$ to $k_h$ is more than 0.5 ($k_y/k_h \geq 0.5$), then a displacement ($\Delta L$) of 2 inches shall be assumed and reported. As indicated previously, if the failure surface is circular all displacements at the top of the slope shall be considered to be vertical, while all displacements at the top of the slope for a non-circular failure surface shall be considered horizontal.

**7.** If $k_y/k_h$ is less than 0.5 ($k_y/k_h < 0.5$), compute the deformations ($\Delta L$) induced by seismic slope instability using the Newmark sliding block method described in Section 13.14.

**8.** If the displacements are within the acceptable performance criteria established by the design team, then the seismic slope stability hazard is acceptable with respect to the EE I limit state. If the deformations computed exceed the performance criteria established by the design team then develop methods to mitigate this hazard as indicated in Chapter 14 and then evaluate the seismic global stability hazard again (Step 4).

## 13.15 NEWMARK SEISMIC DISPLACEMENT METHODS

The Newmark sliding block model is used to evaluate displacements that occur as a result of an imbalance between driving forces (static and seismic) and loss in resisting forces (strain softening of soils) acting on the displaced soil mass. The models that have been developed based on Newmark rigid sliding block assume that the deformation takes place on a well-defined failure surface, the yield acceleration remains constant during shaking, and the soil is perfectly plastic. The displacements are computed based on the cumulative displacements of the sliding mass generated when accelerations exceed the yield acceleration that defines the point of impending

displacement. Newmark type methods for computing deformations are typically associated with an improved reliability when compared to the empirical methods because it is a numerical method that permits modeling of the site response for the design seismic event being investigated.

The state-of-practice is that the assumptions used in the Newmark sliding block model provide reasonable results when the shear failure surface as a whole has not lost more than 50% of the shear resistance prior to the soil's SSL. These assumptions are applicable to seismic slope instability and to lateral seismic deformation of gravity ERSs that are not significantly affected by cyclic liquefaction. Bardet, et al. (1999) observed that when cyclic liquefaction occurs in a lateral spread, the assumptions of the Newmark sliding block model requirements are not met because (1) the shear strain in liquefied soil does not concentrate within a well-defined surface, (2) the shear strength and yield acceleration of saturated soils varies during cyclic loading as pore pressure varies, and (3) soils are generally not perfectly plastic materials, but commonly harden and/or soften.

Several analytical methods based on the Newmark sliding block model have been developed to estimate deformations induced by seismic cyclic loadings. The Newmark type methods typically fall into one of the following categories:

- Newmark Time History Analyses
- Simplified Newmark Charts

The Newmark Time History Analyses method can be performed using the design seismic time history acceleration record if a Site-specific Seismic Response Analysis is performed in accordance with Chapter 12. Alternatively, Simplified Newmark charts can be used when a site-specific seismic response is not performed. The Simplified Newmark charts are based on a large database of seismic records and the Newmark Time History Analysis method to develop charts that relate the ratio of acceleration to yield acceleration occurring at the base of the sliding mass to ground displacement.

If a Site-specific Seismic Response Analysis is performed in accordance with Chapter 12, then the Newmark Time History Analyses should be performed in combination with the Simplified Newmark evaluation to validate deformation analyses performed using the Newmark Time History Analyses. If a simplified site response method is used (i.e., 3-Point ADRS curves) to evaluate the local response site effects, then the Simplified Newmark charts should be used. The Newmark time history method and the Simplified Newmark charts are described in the following Sections.

### 13.15.1 Newmark Time History Analyses

The Newmark "sliding block" method for analyzing ground displacements along a shear plane was developed by Newmark (1965). Newmark's method has been applied to seismic slope stability performance of dams, embankments, natural slopes, and retaining walls (Newmark (1965), Makdisi and Seed (1978), Yegian, et al. (1991), Jibson (1994), and Richards and Elms (1979)). This method is typically incorporated into computer programs as described by Houston, Houston, and Padilla (1987).

Randall W. Jibson, Ellen M. Rathje, Matthew W. Jibson and Yong W. Lee have developed a computer program, SLAMMER, to model slope performance during seismic events. The Java

program uses a modification of Newmark's method where a decoupled analysis is performed that allows modeling landslides that are not assumed to be rigid blocks. The software and more information can be obtained at the USGS website https://pubs.usgs.gov/tm/12b1/.

Ebeling, et al. (2007) have developed a computer program for the US Army Corps of Engineers that estimates the translational response of retaining walls to seismic ground motions called $C_{orps}W_{all}$Slip (CWSlip) that could be used to estimate lateral displacements for gravity ERSs.

In the Newmark method, the deformations are assumed to occur along a well-defined plane and the sliding mass is assumed to be a rigid block as shown in Figure 13-33. When the seismic accelerations exceed a yield acceleration threshold, the sliding mass displaces as indicated in Figure 13-34. The displacement accumulates over a time span ($t_3 – t_1$) where the acceleration exceeds the $k_y$ at time $t_1$ to when the induced velocity drops to zero at time $t_3$. The displacements are computed by double integrating the accelerogram over the time span ($t_3 - t_1$). Displacement is cumulative over each cycle for the duration of the seismic event as indicated in Figure 13-34. The total displacement is computed as the cumulative displacement that occurs during the seismic shaking.

Note that the $k_y$, in Figure 13-34 varies with the level of acceleration as a result of the cyclic soil strength degradation or liquefaction. Soils that are subject to significant strain softening will develop lower $k_y$ thresholds as the seismic-induced cyclic soil strength degradation progresses. The $k_y$ generally remains constant because of the conservative approach used to determine its value.

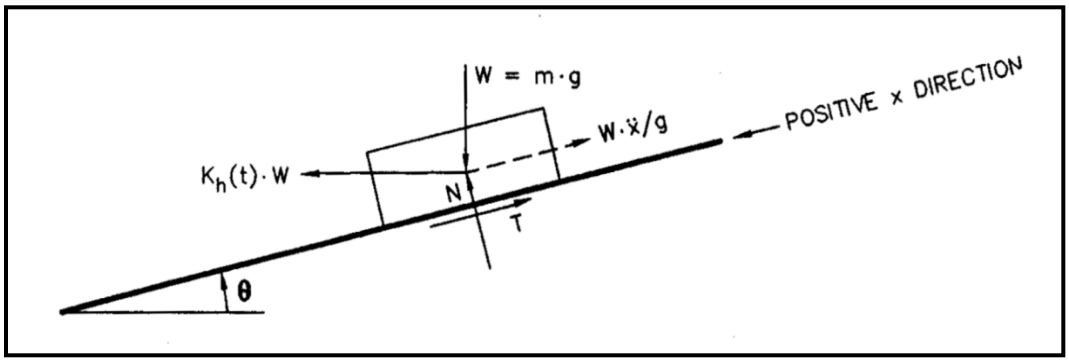


**Figure 13-35, Newmark Sliding Block Method (Matasovic, Kavazanjian, and Giroud (1998))**

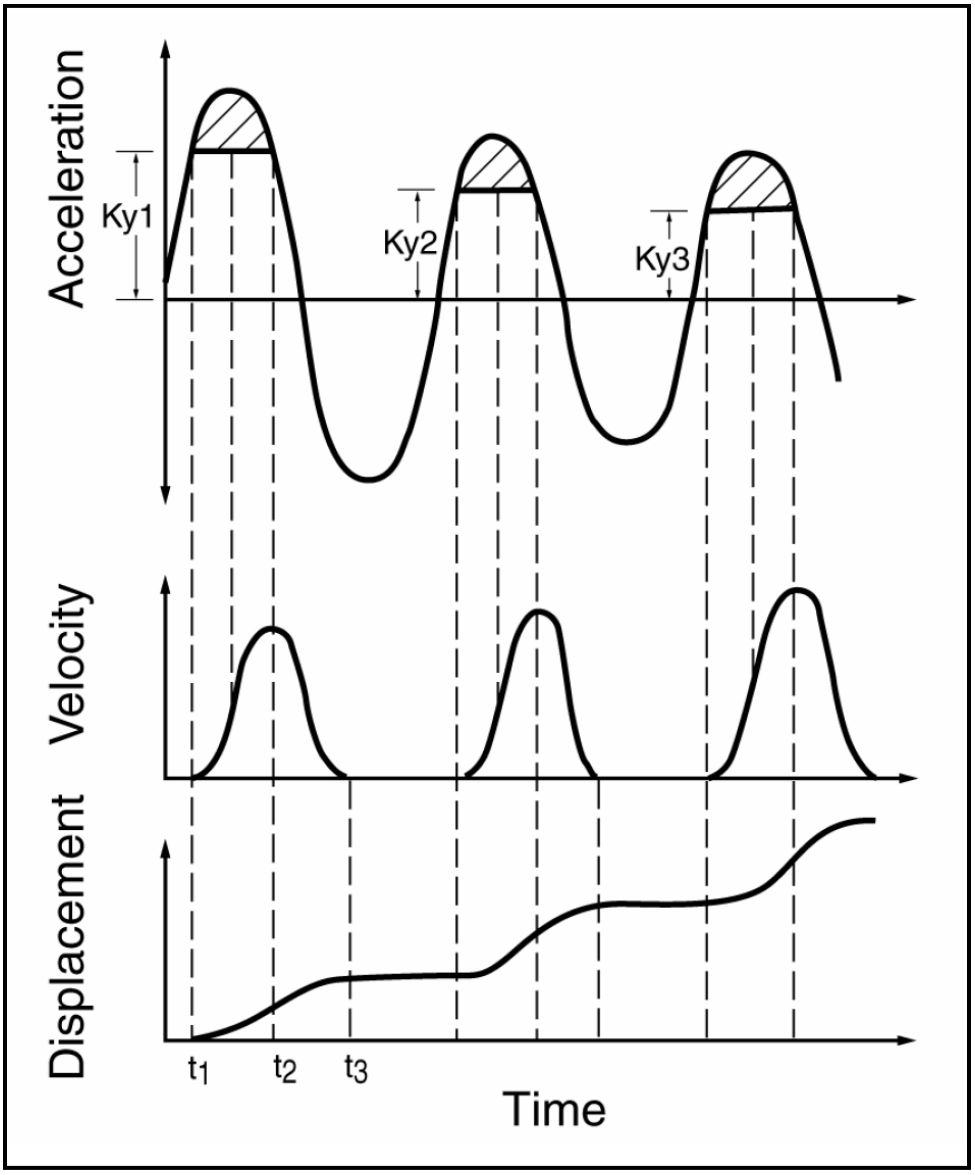


**Figure 13-36, Newmark Time History Analysis**
**(Goodman and Seed (1966) with permission from ASCE)**

The seismic shaking that triggers the displacement is characterized by an acceleration record at the base of the sliding mass for the design seismic event being evaluated. A minimum of 12 independent seismic records should be selected from a catalogue of seismic records that are representative of the source mechanism, $M_w$, and R. A sensitivity analysis of the input parameters used in the site-specific response analysis should be performed to evaluate its effect on the magnitude of the displacement computed.

A pseudo-static slope stability analysis is performed to determine the threshold $k_y$ where displacements begin to occur for a specific critical failure surface. The pseudo-static slope stability analysis should be performed with cyclic residual shear strength (Section 13.10) assigned to soils with the potential for soil SSL. The $k_y$ is the acceleration that corresponds to a pseudo-static slope stability analysis for a critical failure surface with a seismic stability resistance ratio of $(D/C)_{EQ\text{-}Stability} = 1.0$ (1/FS = 1.0).

The following are sources of uncertainty that are inherent when using the Newmark Time History Analysis method to compute displacements in the CEUS:

- Lack of strong motion time history records in the CEUS
- Seismic source mechanism is not well understood
- R is not well defined in the CEUS
- Infrequency of seismic events in the last 10,000 years (Holocene Period)
- Point in the time history when cyclic strength degradation or liquefaction is triggered
- Magnitude of the apparent post-liquefaction residual resistance
- Influence of the thickness of liquefied soil on displacement
- Changes in values of $k_y$ as deformation accumulates
- Influence of non-rigid sliding mass
- Influence of ground motion incoherence over the length of the sliding mass

Because of the uncertainties involved in the selection of the time history acceleration records in the CEUS, results of the Newmark Time History Analyses must be compared with the results obtained using Simplified Newmark Charts discussed in Section 13.14.2.

### 13.15.2 Simplified Newmark Charts

Simplified Newmark displacement charts were developed as a result of the Anderson, Martin, Lam, and Wang (2008) study based on Newmark's Time History Analyses discussed in Section 13.14.1. These Simplified Newmark displacement charts are based on the seismic database published by Hynes and Franklin (1984). The database of seismic records used for this study was limited to seismic events with moment magnitudes of $6.0 \leq M_w \leq 7.5$.

These charts have been developed as a function of a ratio ($k_y$ / $k_{max}$) or $k_y$ to $k_{max}$ ratio, PGV = $V_{Peak}$, PGA, and by region of the United States (WUS and CEUS) for either rock or soil site conditions. The charts shown in Figures 13-35 and 13-36 are based on a seismic moment magnitude of $6.0 \leq M_w \leq 7.5$ in the CEUS. Figure 13-35 is appropriate for a stiff site with a peak ground velocity of PGV = 30 $k_{max}$ in/sec (PGV= 760 $k_{max}$ mm/sec). Figure 13-36 is appropriate for a soft soil site with a peak ground velocity of PGV = 60 $k_{max}$ in/sec (PGV = 1520 $k_{max}$ mm/sec).

The computed displacements should be compared with the required Performance Limits as required in Chapter 10 that have been previously established by the design team.

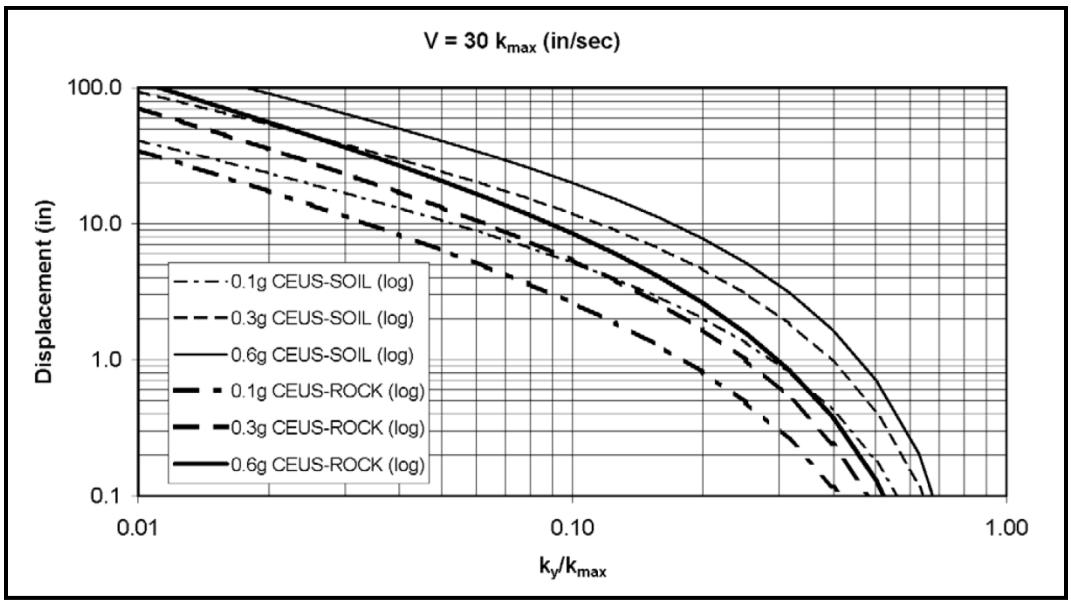


V=PGV; $k_{max}$ = PGA

**Figure 13-37, Simplified Newmark Chart (PGV = 30 $k_{max}$ in/sec) (Anderson, et al. (2008))**

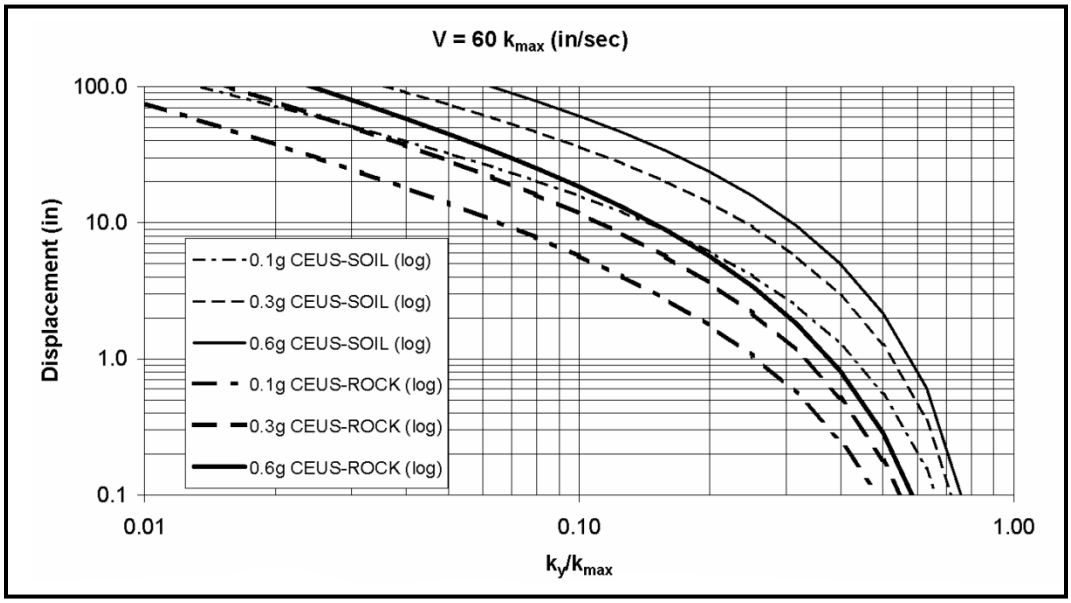


V=PGV; $k_{max}$ = PGA

**Figure 13-38, Simplified Newmark Chart (PGV = 60 $k_{max}$ in/sec) (Anderson, et al. (2008))**

In lieu of using charts in Figures 13-35 and 13-36 to compute the residual displacement, d, for predetermined site factors (PGA and PGV), the following may be used for design specific site factors.

**CEUS-Rock (Standard Error of 0.31 $\log_{10}$ units):**

**Equation 13-71**

$$\log d = -1.31 - 0.93 * \log\left(\frac{k_y}{PGA}\right) + 4.52 * \log\left[1 - \left(\frac{k_y}{PGA}\right)\right] - 0.46 * \log PGA + 1.12 \log PGV$$

**CEUS-Soil (Standard Error of 0.23 $\log_{10}$ units):**

**Equation 13-72**

$$\log d = -1.49 - 0.75 * \log\left(\frac{k_y}{PGA}\right) + 3.62 * \log\left[1 - \left(\frac{k_y}{PGA}\right)\right] - 0.85 * \log PGA + 1.61 * \log PGV$$

Where,

$k_y$ = Yield Acceleration, g (Sections 13.14 and 13.15.1)

PGV = Peak Ground Velocity, inches/sec. Correlations of peak ground velocity are found in Chapter 12.

## 13.16 SEISMIC SOIL SETTLEMENT

Seismically-induced ground settlements are one of the potential geotechnical seismic hazards that must be evaluated. Seismically induced ground settlements that are not due to flow failure or global instability are typically caused by densification of the underlying soils during shaking. Densification or seismic compression of soils has been observed in unsaturated sands, silts, and clayey sands above the water table. Densification of saturated loose sands subject to cyclic liquefaction has also been observed below the water table. Seismic settlements for depths greater than 80 feet, do not need to be computed unless the settlements are being computed to evaluate the effects of downdrag on deep foundations.

Soil settlements computed for unsaturated soils and saturated soils are additive as indicated by the following equation.

$$S_{TS} = S_{us} + S_{sat}$$ **Equation 13-73**

Where,

$S_{TS}$ = Total seismic settlement, inches.

$S_{us}$ = Total seismic settlement of unsaturated soils, inches (Section 13.15.3)

$S_{sat}$ = Total seismic settlement of saturated soils, inches (Section 13.15.4)

Given the relative shallow depth of groundwater throughout most of the South Carolina Coastal Plain, the unsaturated seismic settlement is anticipated to be small (less than 1 inch) and therefore, will not need to be determined. The procedures presented in the following Section for computing settlements are only applicable in the absence of flow failure and/or global instability. Soils susceptible to ground settlements that are located below sloping ground or adjacent to a free-face may be subject to static driving shear stresses oriented towards down-slope or free-face direction. The presence of static driving shear stresses for these site conditions will tend to

increase vertical settlements and lateral displacements. Since the simplified methods presented to analyze settlements do not account for static driving shear stresses, the GEOR should be aware that settlements may be on the order of 10 percent to 20 percent greater (Wu (2002)).

### 13.16.1 Soil Characterization

The corrected SPT driving resistance ($N^*_{1,60}$) will be computed in accordance with Chapter 7. For soils with FC greater than 5 percent, the SPT driving resistance must be adjusted for fines content to obtain an equivalent corrected clean sand SPT resistance ($N^*_{1,60,cs}$) in accordance with Section 13.9.1.

The normalized corrected CPTu tip resistance ($q_{c,1,N}$) will be computed in accordance with Chapter 7. For soils with FC greater than 5 percent, the normalized corrected CPTu tip resistance must be adjusted for fines content to obtain an equivalent normalized corrected clean sand tip resistance ($q_{c,1,N,CS}$) in accordance with Section 13.9.2.

When seismic settlement methods require an equivalent normalized corrected clean sand SPT resistance ($N^*_{1,60,cs}$) and only CPTu in-situ testing data are available to compute seismic settlements, the normalized cone tip resistance, $q_{c,1,N}$, (Chapter 7) will be correlated to corrected SPT $N^*_{1,60}$ values in accordance with Chapter 7. The correlated SPT blow count ($N^*_{1,60}$) should then be adjusted for FC greater than 5 percent, in accordance with Section 13.9.1.

### 13.16.2 Saturated Sand Settlement

Settlement of saturated sands can occur when Sand-Like soils have the potential to experience cyclic liquefaction due to dissipation of excess pore water pressure generated during the seismic shaking. These soils reconsolidate as the pore water pressure dissipates and the sand particles rearrange into a more compact state, causing settlement. Seismically induced settlements of Sand-Like soils that have the potential to experience cyclic liquefaction are typically larger than compaction settlements that result from unsaturated sands (these settlements are ignored). Several methods to evaluate the magnitude of seismic settlement of saturated sands have been proposed by Tokimatsu and Seed (1987), Ishihara and Yoshimine (1992), Shamoto, et al. (1998), and Wu (2002). These methods all use the reconsolidation volumetric strain due to cyclic liquefaction ($\varepsilon_v$). The total settlement, $S_{sat}$, of Sand-Like Soils with the potential to experience cyclic liquefaction is computed using the following equation.

$$\boldsymbol{S_{sat} = \sum_{n=1}^{i_{sat}} \delta_{sat} = \sum_{n=1}^{i_{sat}} \varepsilon_v * H_{sat}} \qquad \textbf{Equation 13-74}$$

Where,

$\delta_{sat}$ = Post-Liquefaction Settlement of Saturated Sand layer, inches
$\varepsilon_v$ = Reconsolidation Volumetric Strain due to Liquefaction, percent (%)
$H_{sat}$ = Layer Thickness of Saturated Sand layer, inches
$i_{sat}$ = Total number (n) of Potentially Liquefiable sand layers

The most referenced method used to compute the settlement potential of saturated liquefiable clean sands was proposed by Tokimatsu and Seed (1987). Several other methods (Ishihara and Yoshimine (1992), Shamoto, et al. (1998), and Wu (2002)) have been proposed that address

some of the deficiencies found with Tokimatsu and Seed (1987) with respect to soils that have higher fines content. Idriss and Boulanger (2008) compared these 3 alternate methods as shown in Figure 13-37.

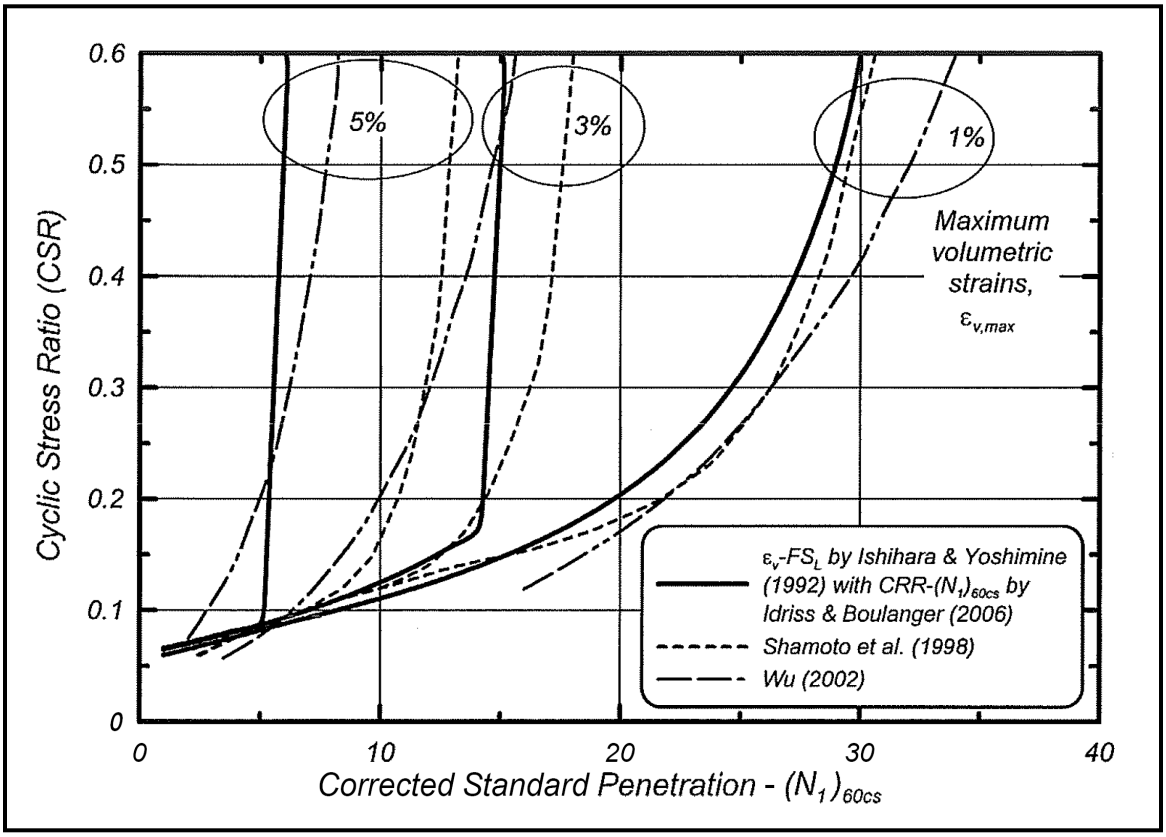


**Figure 13-39, Volumetric Strain Relationship Comparison - $M_w$=7.5; $\sigma'_{vc}$ = 1 atm (Idriss and Boulanger (2008))**

The settlement of saturated sands that are potentially liquefiable shall be computed based on Idriss and Boulanger (2008) recommended reconsolidation volumetric strain, $\varepsilon_v$, relationship based on Ishihara and Yoshimine (1992) shown in Figure 13-38. The $\varepsilon_v$ from Ishihara and Yoshimine (1992) has been approximated by Yoshimine, Nishizaki, Amano, and Hosono (2006) using the following equations for SPT N-values and CPT tip resistances.

$$\boldsymbol{\varepsilon_v = 1.5 * e^{\left(-0.3698\sqrt{N^*_{1,60,CS}}\right)} * min(0.08\ or\ \gamma_{max})} \qquad \textbf{Equation 13-75}$$

$$\boldsymbol{\varepsilon_v = 1.5 * e^{\left(2.551-1.147\left(q_{c,1,N,CS}\right)^{0.264}\right)} * min(0.08\ or\ \gamma_{max})} \qquad \textbf{Equation 13-76}$$

Where,

$N^*_{1,60,CS}$ = Normalized and corrected SPT N-values (Section 13.9.1)
$q_{c,1,N,CS}$ = Normalized and corrected CPT tip resistance (Section 13.9.2)
$\gamma_{max}$ = Maximum cyclic shear strain

Idriss and Boulanger (2008) recommend placing a limit on $\gamma_{max}$ ($\gamma_{lim}$) depending on the resistance factor for Sand-Like soil SSL $(D/C)_{SL}$. The limitations for $\gamma_{max}$ are listed as follows

$$If\ \left(\frac{D}{C}\right)_{SL} \leq 0.5\ then\ \gamma_{max} = 0 \quad \textbf{Equation 13-77}$$

$$If\ 0.5 < \left(\frac{D}{C}\right)_{SL} < \frac{1}{F_\alpha}\ then \cdots \quad \textbf{Equation 13-78}$$

$$\gamma_{max} = min\left\{0.08\ or\ \left[0.035 * (2 - \Phi_{SL}) * \left(\frac{1-F_\alpha}{\Phi_{SL}-F_\alpha}\right)\right]\right\} \quad \textbf{Equation 13-79}$$

$$If\ \left(\frac{D}{C}\right)_{SL} \geq \frac{1}{F_\alpha}\ then\ \gamma_{max} = \gamma_{lim} \quad \textbf{Equation 13-80}$$

Where,

$$\Phi_{SL} = \frac{1}{\left(\frac{D}{C}\right)_{SL}} \quad \textbf{Equation 13-81}$$

$$F_\alpha = 0.032 + 0.69 * \sqrt{N^*_{1,60,CS}} - 0.13 * N^*_{1,60,CS} \quad \textbf{Equation 13-82}$$

For $N^*_{1,60,CS} \geq 7$ blows per foot

$$F_\alpha = -11.74 + 8.34 * \left(q_{t,1,N,CS}\right)^{0.264} - 1.371 * \left(q_{t,1,N,CS}\right)^{0.528} \quad \textbf{Equation 13-83}$$

For $q_{t,1,N,CS} \geq 69$ unitless

$$\gamma_{lim} = 1.859 * \left(1.1 - \sqrt{\frac{N^*_{1,60,CS}}{46}}\right)^3 \geq 0 \quad \textbf{Equation 13-84}$$

$$\gamma_{lim} = 1.859 * \left(2.163 - 0.478 * \left(q_{t,1,N,CS}\right)^{0.264}\right)^3 \geq 0 \quad \textbf{Equation 13-85}$$

Reconsolidation volumetric strain, $\varepsilon_v$, relationships for SPT and CPTu results in Figure 13-38 have been developed to be compatible by using the correlations for relative density from SPT and CPTu in Chapter 7. The $CSR^*_{eq}$, is computed based on Section 13.8.

The use of reconsolidation volumetric strain, $\varepsilon_v$, relationship based on Shamoto, et al. (1998), or Wu (2002) will require approval from the OES/GDS. If CPTu testing data are used with these relationships, the correlations for relative density from SPT and CPTu in Chapter 7 shall be used in order to maintain compatibility between testing methods.

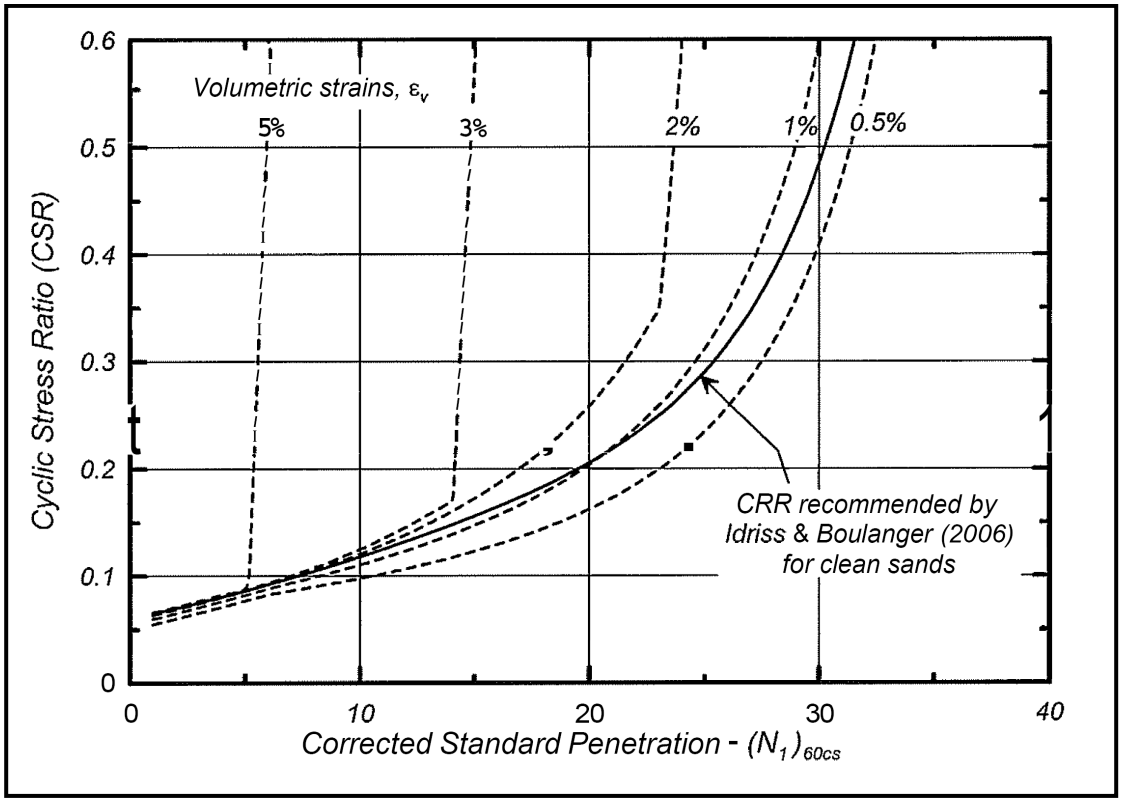


**(A) SPT Based Correlation ($N^*_{1,60,cs}$)**

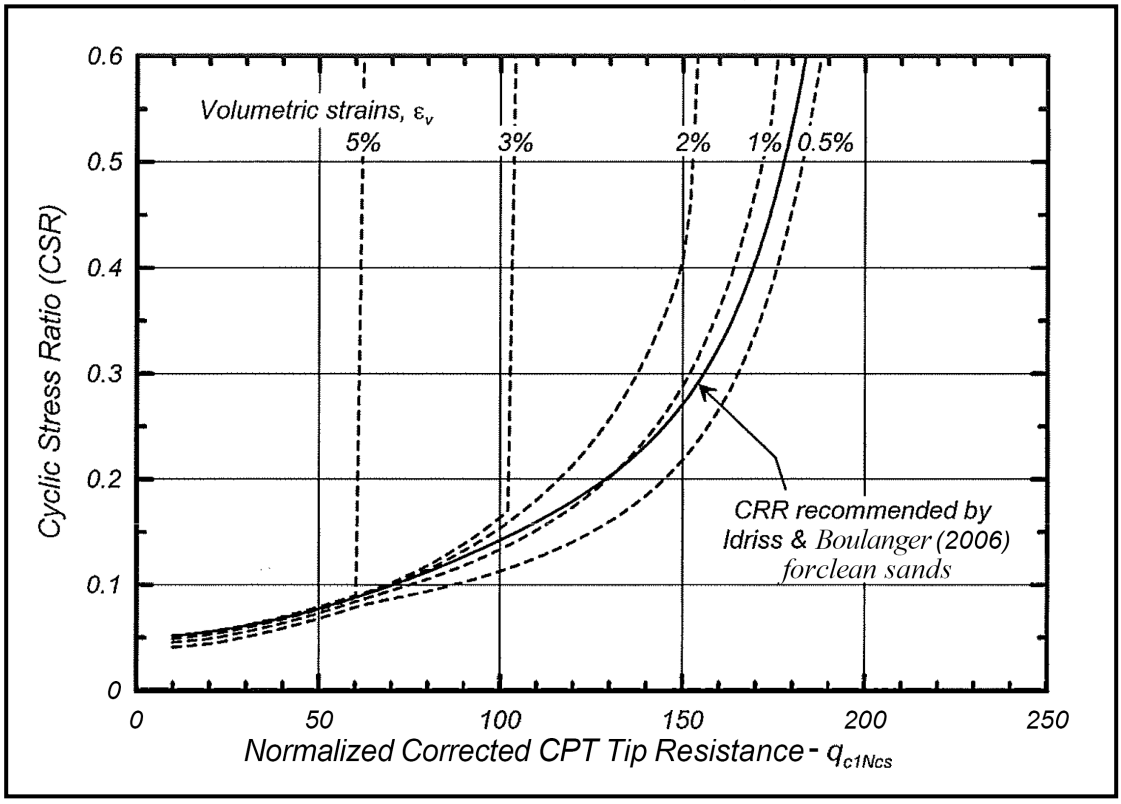


Note: $q_{c,1,N,CS} = q_{t,1,N,CS}$

**(B) CPT Based Correlation ($q_{t,1,N,cs}$)**

**Figure 13-40, Volumetric Strain Relationship - $M_w$=7.5; $\sigma'_{vc}$ = 1 atm (Ishihara and Yoshimine (1992); modified by Idriss and Boulanger (2008))**

When soils are stratified and potentially cyclic liquefiable layers are located between non-liquefiable soil layers, there is a possibility of under-predicting or over-predicting excess pore water developed depending on the location of the soil layers within the stratified system (Polito and Martin (2001)). Polito and Martin (2001) have shown that thin layers of dense sand (non-liquefiable soil) could liquefy if sandwiched between liquefiable soil layers. Ishihara (1985) proposed the method shown in Figure 13-39 to determine the thickness, $H_2$, of the liquefiable soil layer. $H_1$ is the thickness of the non-liquefiable soil layer above the liquefiable soil layer, $H_2$. The thickness of the liquefiable soil layer, $H_2$, is dependent on criteria indicated in Figure 13-39. In addition to the criteria indicated in Figure 13-39, the following criteria must also be satisfied:

**1.** Thickness of the non-liquefiable layer ($H_b$) is less than or equal to 5 feet ($H_b \leq 5$ feet).

**2.** Non-liquefiable soil layer "B" has a normalized and corrected SPT $N^*_{1,60,cs} < 30$ blows/foot or a normalized corrected CPT tip resistance $q_{1,c,N,cs} < 170$.

**3.** Non-liquefiable soil layer "B" is a sand or silty sand with FC $\leq 35$.

**4.** Moment magnitude of design seismic, $M_w \geq 7.0$.

This procedure to evaluate thickness, $H_2$, of liquefiable soil layers is used for all subsequent soil layers that have the potential to liquefy in the stratified soil system.

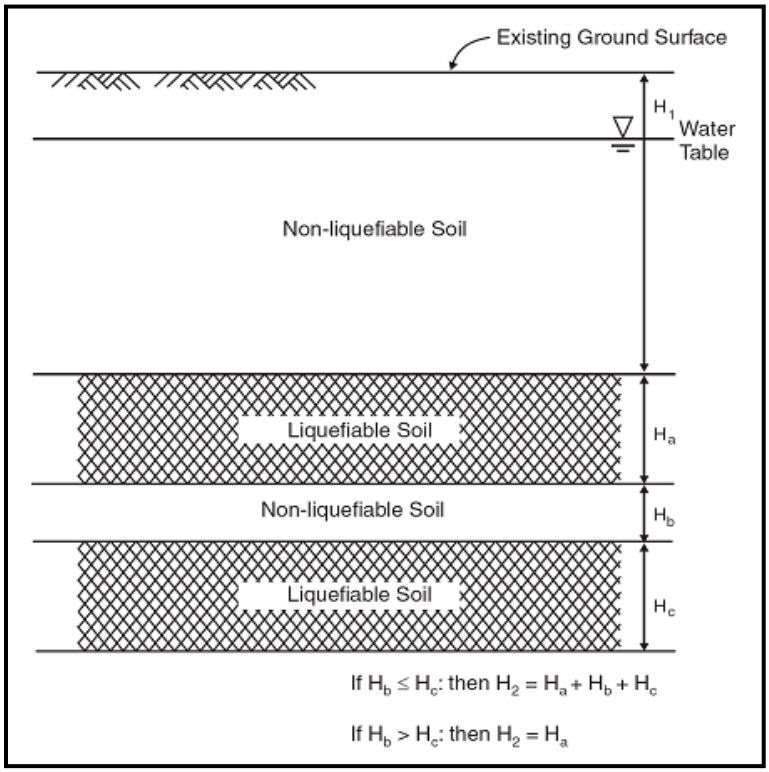


**Figure 13-41, Liquefiable Soil Layer Thickness in Stratified Soils (Ishihara (1985))**

## 13.17 SOFTWARE

Given the complexity of most of the analyses described in this Chapter, computer software is anticipated being used to solve these analyses. Appendix G contains a list of software used by SCDOT. SCDOT does not mandate the use nor advocate the use of the software listed in Appendix G. However, as part of a Pool Fund Study Research Project in conjunction with the Utah Department of Transportation as well as other state Departments of Transportation, Brigham Young University (BYU) has developed 2 software packages that may be used on SCDOT projects, "Simplified Performance-based Liquefaction Analysis Tool (SPLIQ)" and "Simplified Performance-based Liquefaction Analysis Tool (CPTLiq)". Both programs will evaluate the potential for liquefaction (SSL of Sand-Like soils), settlement and lateral spread. In addition, both programs will provide the probability of SSL occurring for Sand-Like soils. Both programs will provide the Factor of Safety against Liquefaction ($FS_L$) and the Probability of Liquefaction ($P_L$) occurring. Both $FS_L$ and $P_L$ shall be reported. However, $FS_L$ shall be converted to $\varphi_{SL}$ as described in Chapter 9 and compared to the $\varphi_{SL\text{-}SAND}$ found in Chapter 9. In addition, both programs are available on the SCDOT Website at:

https://www.scdot.org/business/geotech.aspx

### 13.17.1 SPLIQ

Details describing the procedures used in *SPLIQ* are contained in Franke, Ekstrom, Ulmer, Astorga and Error (2016) and a user's manual for the *SPLIQ* version 1.41 is found in Franke, Astorga and Error (2018). *SPLIQ* uses the Idriss and Boulanger (2008 and 2010) for determining $FS_L$ and uses Boulanger and Idriss (2012) to develop $P_L$. In addition, *SPLIQ* also determines settlement using the Ishihara and Yoshimine (1992) procedure for the Idriss and Boulanger (2008 and 2010). *SPLIQ* also uses the procedure developed by Cetin, et al. (2004 and 2009) $FS_L$ and $P_L$ to determine both liquefaction initiation and settlement. *SPLIQ* also provides the amount of lateral displacement using the procedure developed by Youd, Hansen and Bartlett (2002) as well as the amount of anticipated slope displacement developed by either Rathje or Saygili (2009) or Bray and Travasarou (2007). The results from the Idriss and Boulanger model shall be reported; however, the results from Cetin, et al. may also be reported.

### 13.17.2 CPTLIQ

Details describing the procedures used in *CPTLIQ* are contained in Franke, Coutu, Hatch and Arndt (2021), and Franke, He and Blonquist (2021) and a User's Manual for the *CPTLIQ* version 1.42 is found in Franke, He and Blonquist (2022). *CPTLIQ* uses the Idriss and Boulanger (2008 and 2010) for determining $FS_L$ and uses Boulanger and Idriss (2012 and 2014) to develop $P_L$. In addition, *CPTLIQ* also determines settlement using the Ishihara and Yoshimine (1992) procedure for the Idriss and Boulanger (2008 and 2010). *CPTLIQ* also uses the procedure developed by Ku, et al. (2012) $FS_L$ and $P_L$ to determine both liquefaction initiation and settlement. *CPTLIQ* also provides the amount of lateral displacement using the procedure developed by Zhang, Robertson and Brachman (2004). The results from the Idriss and Boulanger model shall be reported; however, the results from Ku, et al. may also be reported.

## 13.18 REFERENCES

American Association of State Highway and Transportation Officials, (2017), AASHTO LRFD Bridge Design Specifications Customary U.S. Units, 8th Edition, American Association of State Highway and Transportation Officials, Washington, D.C.

Anderson, D. G., Martin, G. R., Lam, I. and Wang, J. N., (2008), “Seismic Analysis and Design of Retaining Walls, Buried Structures, Slopes and Embankments”, NCHRP Report 611, Volumes 1 and 2, Transportation Research Board.

Bardet, J. P., Mace, N. and Tobita, T. (1999), "Liquefaction-induced Ground Deformation and Failure." Report to PEER/PG&E, Task 4A - Phase 1, University of Southern California, Los Angeles.

Bartlett, S.F. and Youd, T.L., (1992). "Empirical Analysis of Horizontal Ground Displacement Generated by Liquefaction Induced Lateral Spreads.” Technical Report NCEER 92-0021, National Center for Earthquake Engineering Research, University at Buffalo.

Bartlett, S.F. and Youd, T.L., (1995). "Empirical Prediction of Liquefaction-induced Lateral Spread.” Journal of Geotechnical Engineering, ASCE, v. 121, Issue 4.

Boulanger, R. W. (2003a). "High Overburden Stress Effects in Liquefaction Analyses." Journal of Geotechnical and Geoenvironmental Engineering, ASCE, v. 129, Issue 12, pp. 1071 - 1082.

Boulanger, R. W. (2003b), "Relating Ka to a Relative State Parameter Index", *Journal of Geotechnical and Geoenvironmental Engineering*, ASCE, v. 129, Issue 8, pp. 770 - 773.

Boulanger, R. W., and Idriss, I. M. (2004), “Evaluating the Potential for Liquefaction or Cyclic Failure of Silts and Clays”, Report UCD/CGM-04/01, Center for Geotechnical Modeling, University of California, Davis, California.

Boulanger, R. W., and Idriss, I. M. (2006), "Liquefaction Susceptibility Criteria for Silts and Clays", *Journal of Geotechnical and Geoenvironmental Engineering*, ASCE, v. 132, Issue 11, pp. 1413 - 1426.

Boulanger, R. W., and Idriss, I. M. (2007), "Evaluation of Cyclic Softening in Silts and Clays", *Journal of Geotechnical and Geoenvironmental Engineering*, ASCE, v. 133, Issue 6, pp. 641 - 652.

Boulanger, R. W., and Idriss, I. M., (2012), "Probabilistic Standard Penetration Test-Based Liquefaction Triggering Procedure", *Journal of Geotechnical and Geoenvironmental Engineering*, ASCE, v. 138, Issue 10, pp. 1185 - 1195.

Boulanger, R. W., and Idriss, I. M., (2014), “CPT and SPT Based Liquefaction Triggering Procedures”, Report UCD/CGM-14/01, Center for Geotechnical Modeling, University of California, Davis, California.

Bray, J. D., and Sancio R. B. (2006), "Assessment of the Liquefaction Susceptibility of Fine-Grained Soils", *Journal of Geotechnical and Geoenvironmental Engineering*, ASCE, v. 132, Issue 9 pp. 1165 - 1177.

Bray, J. D. and Travasarou, T. (2007). “Simplified Procedure for Estimating Earthquake-Induced Deviatoric Slope Displacements,” *Journal of Geotechnical and Geoenvironmental Engineering*, ASCE, Vol. 133, Issue 4, pp. 381–392.

Cetin, K. O., Seed, R. B., Der Kiureghian, A., Tokimatsu, K., Harder, L. F. Jr, Kayen, R. E., and Moss, R. E. S. (2004), “Standard Penetration Test-Based Probabilistic and Deterministic Assessment of Seismic Soil Liquefaction Potential”, *Journal of Geotechnical and Geoenvironmental Engineering*, ASCE, v. 130, Issue 12, pp. 1314 - 1340.

Cetin, K. O., Bilge, H. T., Wu, J., Kammerer, A. M., and Seed, R. B., (2009), “Probabilistic Model for the Assessment of Cyclically Induced Reconsolidation (Volumetric) Settlements”, *Journal of Geotechnical and Geoenvironmental Engineering*, ASCE, v. 135, Issue 3, pp. 387 – 398.

Darendeli M. B., (2001). "Development of a New Family of Normalized Modulus Reduction and Material Damping Curves", PhD Dissertation, Department of Civil Engineering, University of Texas, Austin, Texas.

Duncan, J. M., and Wright, S. G., (2005), Soil Strength and Slope Stability, John Wiley & Sons, Inc., Hoboken, New Jersey.

Ebeling, R. M., Chase, A., White, B. C., (2007), "Translational Response of Toe-Restrained Retaining Walls to Earthquake Ground Motions Using $C_{orps}W_{all}$Slip (CWSLIP)", Technical Report ERDC/ITL TR-07-01. Vicksburg, Mississippi: Corps of Engineers Waterways Experiment Station, June 2007.

Franke, K. W., (2018), “Simplified Standard Penetration Test Performance-Based Assessment of Liquefaction and Effects: Updated Liquefaction Parameter Mapping – Addendum Report”, UT-18.11, Brigham Young University, Provo, Utah.

Franke, K. W., Astorga, L., Error, B., (2018), “SPLIQ User’s Manual version 1.41”, UT-18.10, Brigham Young University, Provo, Utah.

Franke, K. W., Coutu, T. B., Hatch, M. S., and Arndt, A. M., (2021), “Simplified Cone Penetration Test Performance-Based Assessment of Liquefaction and Effects: Tasks 1, 2, 3, and 4”, Phase 1 of 2, UT-21.20, Brigham Young University, Provo, Utah.

Franke, K. W., Ekstrom, L. T., Ulmer, K. J., Astorga, L., and Error, B., (2016), “Simplified Standard Penetration Test Performance-Based Assessment of Liquefaction and Effects”, UT-16.16, Brigham Young University, Provo, Utah.

Franke, K. W., He. J., and Blonquist, J. L., (2021), “Simplified CPT Performance-Based Assessment of Liquefaction and Effects: Tasks 5, 6, 7, 8, 9, & 10”, Phase 2 of 2, UT-21.21, Brigham Young University, Provo, Utah.

Franke, K. W., He. J., and Blonquist, J. L., (2022), “CPTLIQ User’s Manual Version 1.42”, UT-22.02, Brigham Young University, Provo, Utah.

Golesorkhi, R. (1989), “Factors Influencing the Computational Determination of Earthquake-Induced Shear Stresses in Sandy Soils”, Ph. D. Thesis, University of California, Berkeley.

Goodman, R. E., and Seed, H. B. (1966), "Earthquake–induced Displacements in Sand Embankments”, *Journal of the Soil Mechanics and Foundations Division*, ASCE, v. 92, Issue 2, pp. 125 - 146.

Goulois, A. M., Whitman, R. V. and Hoeg, K., (1985), "Effects of Sustained Shear Stresses on the Cyclic Degradation of Clay", Strength Testing of Marine Sediments: Laboratory and In-Situ Strength Measurements, ASTM STP 883, R. C. Chaney and K. R. Demars, eds., ASTM, Philadelphia, pp. 336-351.

Harder, L. F., and Boulanger, R. W. (1997), "Application of K-alpha and K-sigma Correction Factors", Proceedings of the NCEER Workshop on Evaluation of Liquefaction Resistance of Soils, T. L. Youd and I. M. Idriss, editors, Technical Report NCEER-97-0022, pp. 167 – 190.

Hayati, H. and Andrus, R. D., (2008), “Liquefaction Potential Map of Charleston, South Carolina Based on the 1886 Earthquake”, *Journal of Geotechnical and Geoenvironmental Engineering*, ASCE, v. 134, Issue 6, pp. 815 - 828.

Hayati, H. and Andrus, R. D., (2009), “Updated Liquefaction Resistance Correction Factors for Aged Sands”, *Journal of Geotechnical and Geoenvironmental Engineering*, ASCE, v. 135, Issue 11, pp. 1683 - 1692.

Holtz, R. D., and Kovacs, W.D., (1981), An Introduction to Geotechnical Engineering, Prentice-Hall, Inc., Englewood Cliffs, New Jersey.

Houston, S. L., Houston, W. N., and Padilla, J. M. (1987), ‘‘Microcomputer-aided Evaluation of Earthquake-induced Permanent Slope Deformations’’, *Microcomputers in Civil Engineering*, Vol. 2, p. 207 - 222.

Hynes, M. E. and Franklin, A. G., (1984), "Rationalizing the Seismic Coefficient Method," Miscellaneous Paper GL-84-13, U.S. Army Waterways Experiment Station, Vicksburg, MS, July.

Idriss, I. M. (1999), “An Update to the Seed-Idriss Simplified Procedure for Evaluating Liquefaction Potential”, Proceedings, TRB Workshop on New Approaches to Liquefaction, (Publication No. FHWA-RD-99-165), FHWA, U.S. Department of Transportation.

Idriss, I. M. and Boulanger, R. W. (2003), “Estimating $K_\alpha$ for use in Evaluating Cyclic Resistance of Sloping Ground”, Proceedings, 8th U.S. – Japan Workshop on Earthquake Resistant Design of Lifeline Facilities and Countermeasures Against Liquefaction, M. Hamada, J.-P. Bardet and T. D. O’Rourke editors, MCEER.

Idriss, I. M. and Boulanger, R. W. (2006), “Semi-empirical Procedures for Evaluating Liquefaction Potential During Earthquakes,” Proceedings, 11th International Conference on Soil Dynamics and

Earthquake Engineering and 3rd International Conference on Earthquake Geotechnical Engineering, D. Doolin et. al., eds., Stallion Press, Vol. 1.

Idriss, I. M. and Boulanger, R. W., (2008), Soil Liquefaction During Earthquakes, Earthquake Engineering Research Institute (EERI), EERI Monograph MNO-12.

Idriss, I. M. and Boulanger, R. W., (2010), "SPT-Based Liquefaction Triggering Procedures", Report No. UCD/CGM-10/02, Center for Geotechnical Modeling, University of California, Davis, California.

Ishihara, K., (1985), "Stability of Natural Deposits During Earthquakes", Proceedings, 11th International Conference on Soil Mechanics and Foundation Engineering, San Francisco, CA, Volume 1.

Ishihara, K. and Yoshimine, M. (1992), "Evaluation of Settlements in Sand Deposits Following Liquefaction During Earthquakes", Soils and Foundations, 32 (1).

Iwasaki, T., Tatsuoka, F., and Takagi, Y. (1978), "Shear Moduli of Sands Under Cyclic Torsional Shear Loading", Soils and Foundations, 18 (1).

Jibson, R., (1994), "Predicting Earthquake-induced Landslide Displacement Using Newmark's Sliding Block Analysis", Transportation Research Record 1411, Transportation Research Board, Washington, D.C.

Kavazanjian, E., Wang, J-N. J., Martin, G. R., Shamsabadi, A., Lam, I., Dickenson, S. E., and Hung, C. E., (2012), LRFD Seismic Analysis and Design of Transportation Geotechnical Features and Structural Foundations, Engineering Circular No. 3, (Publication No. FHWA-NHI-11-032, August (Rev. 1)), US Department of Transportation, National Highway Institute, Federal Highway Administration, Washington, DC.

Kokushho, T. (2000), "Correlation of Pore-Pressure B-Value with P-Wave Velocity and Poisson's Ratio for Imperfectly Saturated Sand or Gravel", Soils and Foundations, Japanese Geotechnical Society, Vol. 40, No. 4., pp. 95 – 102.

Kramer, S. L. (1996), Geotechnical Earthquake Engineering, Prentice-Hall, Upper Saddle River, NJ

Kramer, S. L. and Elgamal, A.-W. (2001), "Modeling Soil Liquefaction Hazards for Performance-Based Earthquake Engineering," State-of-the-Art Report, Pacific Earthquake Engineering Research Center, in preparation.

Kramer, S. L. and Wang, C.-H., (2015), "Empirical Model for Estimation of the Residual Strength of Liquefied Soil", *Journal of Geotechnical and Geoenvironmental Engineering*, ASCE, published online May 6, 2015, ISSN 1090-0241/04015038(15).

Ku, C., Juang, C., Chang, C., and Ching, J., (2012), "Probabilistic Version of the Robertson and Wride Method for Liquefaction Evaluation: Development and Application," *Canadian Geotechnical Journal*, Volume 49, Number 1, pp. 27 – 44.

Ladd, C., and Foot. R. ,(1974), "New Design Procedure for Stability of Soft Clays", *Journal of the Geotechnical Engineering Division*, ASCE, v. 100, Issue 7, pp. 763 - 786.

Ladd, C. C., Foot, R., Ishihara, K., Schlosser, F., and Poulos, H. G. (1977), “Stress Deformation and Strength Characteristics”, Proceedings of 9th Int. Conf. on Soil Mech. and Found. Engrg., Vol. 2, Tokyo, Japan.

Leon, E., Gassman, S. L., and Talwani, P., (2006), "Accounting for Soil Aging When Assessing Liquefaction Potential”, *Journal of Geotechnical and Geoenvironmental Engineering*, ASCE, v. 132, Issue 3, pp. 363 - 377.

Lewis, M. R., Arango, I., and McHood, M. D., (2007), ‘‘Geotechnical Engineering at the Savannah River Site and Bechtel”, Report No. WSRC-STI-2007-00373, Contract No. DE-AC09--96SR18500, U. S. Department of Energy, July 17, 2007.

Makdisi, F. T., and Seed, H. B., (1978), “Simplified Procedure for Estimating Dam and Embankment Earthquake-Induced Deformations”, *Journal of Geotechnical Engineering*, ASCE, v. 104, Issue 7, 849 - 867.

Marcuson, W. F. III, Hynes, M. E., and Franklin, A. G. (1990), “Evaluation and Use of Residual Strength in Seismic Safety Analysis of Embankments”, Earthquake Spectra, Vol 6, No. 3, pp. 529 - 572.

Matasovic, N., Kavazanjian, E., and Giroud, J. P. (1998), “Newmark Seismic Deformation Analysis for Geosynthetic Covers”, Geosynthetics International, International Geosynthetics Society.

McGee W. J. , Sloan E., Manigault, G. E., Newcomb, S., Peters, K. E., and Herrmann, R. B. eds., (1986), "First-hand Observations of the Charleston Earthquake of August 31, 1886, and Other Earthquake Materials", Reports of Bulletin 41, South Carolina Geological Survey.

Newmark, N. M. (1965), ”Effects of Earthquakes on Dams and Embankments”, *Geotechnique*, v.5, no.2 London, England.

Olson, S. M., and Johnson, C. I., (2008), “Analyzing Liquefaction-Induced Lateral Spreads Using Strength Ratios,” *Journal of Geotechnical and Geoenvironmental Engineering*, ASCE, Volume 134, Issue 8, pp. 1035-1049.

Olson, S. M., and Stark, T. D., (2003), “Yield Strength Ratio and Liquefaction Analysis of Slopes and Embankments”, *Journal of Geotechnical and Geoenvironmental Engineering*, ASCE v. 129, Issue 8, pp. 727 - 737.

Polito, C. P., and Martin, J. R. (2001), "Effects of Nonplastic Fines on the Liquefaction Resistance of Sands", *Journal of Geotechnical and Geoenvironmental Engineering*, ASCE, v. 127, Issue 5, pp. 408 - 415.

Pyke, R., Seed, H.B., Chan, C.K. (1975), "Settlement of Sands Under Multi-directional Shearing", *Journal of Geotechnical Engineering*, ASCE, v. 101, Issue 4, pp. 379 - 398.

Rathje, E. M. and Saygili, G., (2009), "Probabilistic Assessment of Earthquake Induced Sliding Displacements of Natural Slopes", *Bulleting of the New Zealand Society for Earthquake Engineering*, v. 42, No. 1, March, pp. 18 – 27.

Richards, R. and Elms, D. G., (1979), "Seismic Behavior of Gravity Retaining Walls", *Journal of Geotechnical Engineering*, ASCE, v.105, Issue 4, pp. 449 - 464.

Robertson, P. K., and Wride, C. E. (1997), "Cyclic Liquefaction and its Evaluation Based on SPT and CPT", Proceedings NCEER Workshop on Evaluation of Liquefaction Resistance of Soils.

Schneider, J. A., and Mayne, P. W. (1999), "Soil Liquefaction Response in Mid-America Evaluated by Seismic Piezocone Tests", Report MAE-GT-3A, Mid America Earthquake Center, October, 253 pp.

Seed, H. B. (1986), "Design Problems in Soil Liquefaction", University of California, Earthquake Engineering Research Center (UCB/EERC), UBC/EERC-86/02, February.

Seed, H. B. (1987), "Design Problems in Soil Liquefaction", *Journal of Geotechnical Engineering*, ASCE, v.113, Issue 8, pp. 827 - 845.

Seed, R. B., Cetin, K. O., Moss, R. E. S., Kammerer, A., Wu, J., Pestana, J. and Riemer, M., Sancio, R. B., Bray, J. D., Kayen, R. E., and Faris, A. (2003), "Recent Advances in Soil Liquefaction Engineering: A Unified and Consistent Framework", EERC-2003–06, Earthquake Engineering Research Institute, Berkeley, Calif.

Seed, R. B. and Harder, L. F., Jr., (1990), "SPT-Based Analysis of Cyclic Pore Pressure Generation and Undrained Residual Strength", Proceedings, H. Bolton Seed Memorial Symposium, BiTech Publishers, Ltd.

Seed, H. B., and Idriss, I. M., (1971), "Simplified Procedure or Evaluating Soil Liquefaction Potential", *Journal of the Soil Mechanics and Foundations Division*, ASCE, v. 97, Number SM9, pp. 1249 - 1271.

Shamoto, Y., Zhang, J., and Tokimatsu, K. (1998), "New charts for predicting large residual post-liquefaction ground deformations", *Soil dynamics and earthquake engineering*, Vol. 17, Elsevier, New York.

Spencer, E. (1967), "A Method of Analysis of the Stability of Embankments Assuming Parallel Inter-Slice Forces," *Geotechnique*, v.17, no. 1, pp.11 – 26.

Stewart, J. P., Whang, D. H., Moyneur, M., and Duku, P. (2004), "Seismic Compaction of As-Compacted Fill Soils With Variable Levels of Fines Content and Fines Plasticity", Department of Civil and Environmental Engineering, University of California, Los Angeles, Consortium of Universities for Research in Earthquake Engineering (CUREE), CUREE Publication No. EDA-05, July 2004.

Talwani, P., and Schaeffer, W. T. (2001), "Recurrence rates of large earthquakes in the South Carolina Coastal Plain based on paleoliquefaction data", *Journal of Geophyiscal Research*, 106(B4), 6621–6642.

Terzaghi, K., Peck, R. B., and Mesri, G., (1996), Soil Mechanics in Engineering Practice, John Wiley & Sons, Inc., 605 Third Avenue, New York, NY.

Tokimatsu, K., and H. B. Seed. (1987), "Evaluation of Settlements in Sands Due to Earthquake Shaking", *Journal of Geotechnical Engineering*, ASCE, v. 113 Issue 8, pp. 861 - 878.

U.S. Geological Survey, http://earthquake.usgs.gov/hazards/qfaults/eusa/char.php.

Vucetic, M. and Dobry, R. (1991), "Effect of Soil Plasticity on Cyclic Response", *Journal of Geotechnical Engineering*, ASCE, v. 117 Issue 1, pp. 89 - 107.

Weems, R. E., Lemon, E. M., Jr., and Chirico, P. (1997), "Digital Geology and Topography of the Charleston Quadrangle, Charleston and Berkeley Counties, South Carolina", USGS Open-File Report Number 97-531, U.S. Geological Survey, Reston, Va.

Willoughby, R. H., Nystrom, P. J., Campbell, L. D., Katuna, M. P. (1999), "Cenozoic Stratigraphic Column of the Coastal Plain of South Carolina", South Carolina Department of Natural Resources, Geological Survey, Columbia, SC.

Wu, J. (2002), "Liquefaction triggering and Post-liquefaction Deformations of Monterey 0/30 Sand Under Uni-directional Cyclic Simple Shear Loading", Ph.D. Dissertation, University of California, Berkeley.

Yegian, M. K. Marciano, E., and Ghahraman, V.G. (1991), "Earthquake-Induced Permanent Deformations: Probabilistic Approach", *Journal of Geotechnical Engineering*, ASCE, v. 117 Issue 1, pp. 35 - 50.

Yoshimine, M., Nishizaki, H., Amano, K., and Hosono, Y., (2006), "Flow Deformation of Liquefied Sand under Constant Shear Load and its Application to Analysis of Flow Slide in Infinite Slope", Geomechanics, Geotechnical Special Publication (GSP) 143, ASCE.

Youd, T.L., (2018). "Application of MLR Procedure for Prediction of Liquefaction-Induced Lateral Spread Displacements." Journal of Geotechnical and Geoenvironmental Engineering, ASCE, v. 144, Issue 6.

Youd, T.L., Hansen, C.M., and Bartlett, S.F., (2002). "Revised Multilinear Repression Equations for Prediction of Lateral Spread Displacement." Journal of Geotechnical and Geoenvironmental Engineering, ASCE, v. 128, Issue 12.

Youd, T. L., and Idriss, I. M., eds. (1997), Technical Report NCEER-97-0022 Proceedings, *NCEER Workshop on Evaluation of Liquefaction Resistance of Soils*, National Center for Earthquake Engineering Research, State Univ. of New York at Buffalo.

Youd, T. L., Idriss, I. M., Andrus, R. D., Arango, I., Castro, G., Christian, J. T., Dobry, R., Finn, W. D. L., Harder, L. F., Jr., Hynes, M. E., Ishihara, K., Koester, J. P., Liao, S. S. C., Marcuson, W. F., III, Martin, G. R. Mitchell, J. K., Moriwaki, Y., Power, M. S., Robertson, P. K., Seed, R. B., and Stokoe, K. H., II, (2001), "Liquefaction resistance of soils: Summary Report from the 1996 NCEER and 1998 NCEER/NSF Workshops on Evaluation of Liquefaction Resistance of Soils," *Journal of Geotechnical and Geoenvironmental Engineering*, ASCE, v. 127, Issue 10, pp. 817 - 833.

Youd, T. L. and Perkins, D. M., (1978), "Mapping of Liquefaction-Induced Ground Failure Potential", *Journal of the Geotechnical Engineering Division*, ASCE, v. 104, Issue 4, pp. 433 - 446.

Zhang, G., Robertson, P. K., and Brachman, R. W. I., (2004), "Estimating Liquefaction-Induced Lateral Displacements Using the Standard Penetration Test or Cone Penetration Test," *Journal of Geotechnical and Geoenvironmental Engineering*, ASCE, v. 130, Issue 8, pp. 861 - 871.